UNIVERSITY OF CALIFORNIA, SAN DIEGO

Cell Context-Dependent Control of NF-kappaB Dimers

A dissertation submitted in partial satisfaction of the requirements for the degree of Doctor of Philosophy

in

Chemistry

by

Rachel Wei Tsui

Committee in charge:

Professor Alexander Hoffmann, Co-Chair
Professor Gourisankar Ghosh, Co-Char
Professor Jeff Hasty
Professor Elizabeth Komives
Professor Andrew McCammon

2014

The dissertation of Rachel Wei Tsui is approved, and it is acceptable in quality and form for publication on microfilm and electronically:

Co-Chair

Co-Chair

University of California, San Diego

2014

DEDICATION

I would like to dedicate this dissertation to everyone who inspired and helped me get into graduate school and persevere during the process. I would like to especially thank my family, specifically my parents, Stanley Tsui and Mirium Chiu, who have always supported my education and encouraged me to be the best that I could achieve. I would like to thank my teachers and professors, especially Professor John Caradonna from Boston University who let me work in the lab and inspired me to continue my education into graduate school. I would also like to dedicate this dissertation to all my friends, especially those who went through graduate school with me, who have encouraged me throughout the challenges that every graduate student faces.

TABLE OF CONTENTS

LIST OF ABBREVIATIONS

A:50 - RelA:p50 NFkB dimer

A:A - RelA:RelA NFkB dimer

ARD - ankyrin repeats domain

BAFF - B cell activating factor

BCR - B cell receptor

ChIP - chromatin immunoprecipitation

CpG - DNA motif (cytosine and guanine separated by a phosphate)

EMSA - electrophoretic mobility shift assay

IgM - Immunoglobulin M

IKK - IκB kinase

IL-6 - interleukin 6

IκB - inhibitor of NFκB

LPS - lipopolysaccharide

LTβ - lymphotoxin β

MEF - murine embryonic fibroblast

NEMO - NFκB essential modulator

NFκB - nuclear factor-κB

NIK - NFκB inducing kinase

ODE - ordinary differential equation

PBS - Phosphate buffered saline

TLRs - Toll-like receptors

TNF - tumor necrosis factor

TRAF - TNF receptor associated factor

WT - wild type

LIST OF FIGURES

LIST OF TABLES

LIST OF MODEL EQUATIONS

ACKNOWLEDGEMENTS

I would like to acknowledge Professor Alexander Hoffmann in his guidance and support throughout my graduate career. Despite the frustrations and the multiple drafts of several manuscripts, he has been able to motivate me in persevering through the Ph.D. process.

Chapter 2, in full, is a reprint of material being prepared for publication as “The Rel-NFκB dimer generation module: monomer competition and chaperone function by IκBβ” by Tsui R, Kearns JD, Lynch C, Vu D, Ngo K, Basak S, Ghosh G, and Hoffmann A. The dissertation author was the primary investigator and author of this material.

Chapter 3, in part, is a reprint of material as it appears in Alves BN, Tsui R, Almaden J, Shokhirev MN, Davis-Turak J, Fujimoto J, Birnbaum H, Ponomarenko J, Hoffmann A. “IκBε is a key regulator of B cell expansion by providing negative feedback in a stimulus-specific manner.” Journal of Immunology. 2014; 192(7):3121-32. The dissertation author was a primary investigator and author of this material. Bryce Alves performed the experimental data to demonstrate the phenotype in IκBε-deficient B cells and the experimental validation of anti-IgM and LPS stimulated B cells.

Chapter 4, in part, is a reprint of material being prepared for publication as “BAFF engages distinct NFκB effectors in maturing and proliferating B cells” by Almaden J, Tsui R, Birnbaum H, Shokhirev MN, Davis-Turak J, and Hoffmann A. Jon Almaden provided the experimental data supporting the

phenotype seen in co-stimulation of B cells and the experimental validation of computational model predictions for this chapter. The dissertation author was a primary investigator and author of this work.

Chapter 5, in full, is a reprint of material being prepared for publication as “Controlling the NFκB dimer repertoire in different cellular contexts” by Tsui R and Hoffmann A. The dissertation author was the primary investigator and author of this material.

VITA

Education

2009-2014	University of California San Diego, San Diego, CA Master of Science in Chemistry Doctor of Philosophy in Chemistry
2005-2009	Boston University, Boston, MA Bachelor of Arts in Chemistry with Distinction

Fellowships

2010-2013	National Science Foundation Graduate Research Fellowship
2010	Molecular Biophysics Training Grant

Publications

Alves B, **Tsui R**, Shokhirev M, Davis-Turak J, Almaden J, Fujimoto J, Birnbaum H, Hoffmann A. "IκBε is the key negative feedback regulator of cRel containing dimers in B-lymphocytes." The Journal of Immunology. 2014 April; 192(7): 3121-3132.

Shih VF, **Tsui R**, Caldwell A, Hoffmann A. "A single NFκB system for both canonical and non-canonical signaling." Cell Research. 2011 Jan; 21(1): 86-102.

Abstracts at Scientific Meetings

Tsui R, Kearns J, Lynch C, Vu D, Ngo K, Basak S, Ghosh G, Hoffmann, A. (2012) *IκBs have distinct functions in NFκB dimer generation and in regulating NFκB activity.* Annual NIH NIGMS National Centers for Systems Biology. Chicago, IL.

Kearns J, **Tsui R**, Lynch C, Vu D, Ngo K, Basak S, Ghosh G, Hoffmann, A. (2011) *IκBβ is a critical chaperone for the generation of specific NFκB dimers.* International Conference on Systems Biology of Human Disease. Boston, MA.

ABSTRACT OF THE DISSERTATION

Cell Context-Dependent Control of NF-kappaB Dimers

by

Rachel Wei Tsui

Doctor of Philosophy in Chemistry

University of California, San Diego, 2014

Professor Alexander Hoffmann, Co-Chair

Professor Gourisankar Ghosh, Co-Chair

The NFκB signaling network mediates numerous physiological functions such as growth and development, inflammatory responses, immune responses, and is implicated in several human diseases. While stimulus-

responsive NFκB activity mediated by the inhibitor of NFκB (IκB) degradation and feedback re-synthesis is mechanistically well understood, little is known about the mechanisms that control the formation of specific NFκB dimers. Indeed, different cell types have distinct repertoires of NFκB dimers, so studying the mechanisms that control specific NFκB dimer generation is critical for understanding the cell-type-specific functions of the NFκB signaling system. Two NFκB signaling pathways have been described: the canonical pathway that mediates transient inflammatory responses and the non-canonical pathway that mediates sustained developmental signaling. However, because there are numerous physical and functional interconnections, we consider here the two pathways as being mediated by a single signaling system. While regulatory interdependence has been described, the effectors of the two pathways do have distinct biological functions. An understanding of regulatory crosstalk within the NFκB signaling system is crucial for characterizing the specificity of cellular responses in various physiological states and their biological relationship.

My dissertation aims to understand the molecular mechanisms controlling NFkB dimer generation in different cellular contexts, and the potency and limitations of crosstalk between the canonical and non-canonical NFkB pathways. Biochemistry and mathematical modeling are used to explore how the formation of NFkB dimers in MEFs and the importance of the interaction of the NFkB signaling network in MEFs and B-lymphocytes. Taken

together, this work suggests that the cellular context, whether basally or undergoing stimulation, is critical in defining the NFκB dimer repertoire and its specific dimer activation. This specificity is important to consider when designing drugs to target a particular portion of the complex NFκB signaling network.

Chapter 1: General Introduction

Nuclear factor κB (NFκB) is a critical transcription factor involved in a broad range of biological processes, including immune responses, cell survival, stress responses, and maturation of various cell types. While NFκB activation is required to protect organisms from environmental effects and to allow for the proper development of cells and tissue, misregulated NFκB activity is often observed in various diseases including chronic inflammation and cancer. In fact, there are a variety of diseases that are a result of misregulation of NFκB, such as arthritis, asthma, osteoporosis, inflammatory bowel disease, and arteriosclerosis. These diseases are often caused by the hyper-activation of NFκB, resulting in super-induction of genes involved in these various diseases. Thus, the understanding of the regulation of NFκB signaling is important for maintaining human health.

The NFκB signaling system consists of five Rel homology domain (RHD) – containing polypeptides that can associate to potentially form 15 dimers that can act as transcription factors and their stoichiometric inhibitor proteins, IkBs. The RHD within the five monomers – RelA, RelB, cRel, p50, and p52 – mediates dimerization, DNA binding, interaction with IkBs, and nuclear translocation. RelA, RelB, and cRel all contain transcriptional activation domains, while p50 and p52 do not. However, the absence of a single NFκB monomer can result in various phenotypes. The absence of RelA causes embryonic lethality and liver degeneration due to apoptosis (Beg et al.,

1995). RelB deficiency results in the impaired formation of splenic marginal zone B-cells and the inability for these cells to form germinal centers (Weih et al., 2001). cRel deficiency causes immunodeficiences, and reduced B-cell proliferation and survival (Cariappa et al., 2000; Köntgen et al., 1995; Tumang et al., 1998). The absence of nfkb1/p50 causes inguinal lymph node defects while the loss of nfkb2/p52 can result in the loss of the dendritic cell network formation (Weih et al., 2001; Yilmaz et al., 2003). There are many different phenotypes that are caused from the loss of a single monomer, and the different NFκB dimeric complexes are expressed cell type- and stimulus-specifically. For example, RelA:p50 is the primary canonical NFκB dimer in fibrobalsts, while cRel:p50 is the primary canonical NFκB dimer found in B-cells. RelB:p52 is a primary non-canonical NFκB dimer and found in most cell types, while RelB:p50 has been found to be in high abundance in dendritic cells. Additionally, the p50:p50 NFκB dimer has been shown to bind DNA but because it does not contain a transcriptional activation domain, it does not act as a transcriptional activator. While we have an understanding of the requirement of NFkB on normal cell growth and development and on the inflammatory response, understanding the mechanism of NFκB dimer generation in a cell-type specific manner is still unclear.

The classical inhibitor proteins in the NFκB signaling system consist of the single polypeptide IκBs: IκBα, IκBβ, and IκBε. In resting cells, an IκB binds and sequesters an NFκB dimer and prevents DNA binding and transcriptional

activation. Stimulus-responsive activation of the IκB kinase (IKK) results in the degradation of the IκBs to release and activate NFκB. Synthesis of IκBs may be dependent on NFκB activity, and the inducible activation of IκBs results in negative feedback. Classical IκBs are characterized by their ankyrin repeats domain (ARD) that sequesters NFκB into a latent state. In addition to the classical IkBs, it has been found that p100, when present in a multimeric complex, may also mediate NFκB inhibition *in trans*; this activity was termed IκBδ (Basak et al., 2007). Moreover, size exclusion chromatography analyses suggest that IκBδ activity is mediated by a ~650kD high-molecular-weight complex, termed the IκBsome, which also contains IκBγ activity from p105 protein (Savinova et al., 2009). The pathways that govern IκBsome assembly and degradation are critical for regulating NFκB activity (Shih et al., 2009).

Activation of NFκB results in the induction of a variety of inflammatory, developmental, and survival genes. The rapid and reversible inflammatory and immune response typically occurs through the activation of the canonical pathway, while the slower and irreversible developmental response typically occurs through the non-canonical pathway. These two pathways are thought to be fundamentally distinct. While the canonical pathway is mediated through the activation of a NEMO (IKKγ)-dependent IκB kinase, the non-canonical pathway is classically defined as being mediated through the activation of a NEMO-independent kinase complex involving IKK1 and the NFκB inducing

kinase (NIK) (Scheidereit, 2006). In the canonical pathway, pre-existing, latent NFκB dimers are released from classical IκBs. In the non-canonical pathway, new synthesis p100 and RelB and the subsequent processing of p100 allows for generation of RelB:p52 which is insensitive to IκB control and thus localized to the nucleus.

The activation of the canonical pathway results in the expression of inflammatory and immune response genes. These signals must be transient and properly controlled, as prolonged NFκB activation can lead to aberrant gene expression, and the misregulation of NFκB activation has been implicated in pathologies including chronic inflammation and cancer. Hence it is not surprising that numerous mechanisms have evolved to provide for post-induction attenuation or termination of signaling.

The biological importance of the IκBs as negative feedback regulators in NFκB signaling has been established. Both IκBα and IκBε are inducibly expressed, and function as negative feedback regulators of NFκB. IκBs function as stoichiometric inhibitors that quickly sequester NFκB in the cytoplasm. A20, on the other hand, inhibits signaling upstream of IKK via its enzymatic function as a protease of signaling-associated K63-linked ubiquitin chains (Wertz et al., 2004). While both A20 and IκBα are inducible negative regulators, only IκBα functions as a dynamic negative feedback regulator (Werner et al., 2008). Instead, the evidence indicates that A20 may be thought

of as a tunable rheostat that determines IKK and NFκB responsiveness to subsaturating stimuli.

Not only does negative feedback limit the duration of stimulus-induced NFκB activity and the magnitude of the gene expression response, it may also mediate the transduction of stimulus-specific information via a “temporal signaling code” that determines which of the many possible target genes are activated in response to a specific stimulus. Stimulus-specific temporal control of NFκB is a result of the stimulus-specific temporal control of the canonical IKK activity (Werner et al., 2005). Stimulus-specific temporal profiles of IKK and NFκB are correlated with the expression of stimulus-specific genes. Although inactivation of the TNF autocrine loop provided a means to manipulate the LPS-specific IKK temporal profiles, this intervention may also affect a parallel pathway. Thus whether the stimulus-specific temporal profiles of NFκB activity encode information about the stimulus that is critical for stimulus-specific gene expression remains to be tested rigorously. Furthermore, it remains unknown how promoters of activated genes, or associated gene regulatory networks, distinguish between different temporal profiles. Understanding the mechanisms by which the temporal activity profile is decoded by target genes and what features of the temporal profile of NFκB activity carry stimulus-specific information remain pressing questions in the field (Behar et al., 2013).

Activation of the non-canonical NFκB is mediated through a NEMO-independent IKK1 kinase complex, which is a result of the developmental signaling (Claudio et al., 2002). Upon signaling, TRAF3 degradation is induced, allowing for the accumulation and activation of NIK protein (Liao et al., 2004). Previous work has shown that NIK activation results in IKK1 activation and p100 phosphorylation (Senftleben et al., 2001; Xiao et al., 2001). Activated IKK1 then further phosphorylates p100 which results in the signal induced partial degradation of the C-terminal ankryin repeats domain (ARD) of p100 by the 26S proteasome (Xiao et al., 2004). This non-canonical activity can also degrade IkBd through degradation of the ARD of p100 and release associated RelA:p50 and RelB:p50 NFkB dimers. Additionally, the processing of newly synthesized p100 results in activation of the RelB:p52 dimer, a major NFκB species that is involved in non-canonical activation. The molecular sequence of RelB:p52 dimer activation is poorly understood, and further studies are needed to reach a definitive conclusion if different NFκB dimers activated by the non-canonical pathway have specific or overlapping gene activation functions.

Though canonical and non-canonical pathways are generally thought to be distinct, recent studies have revealed numerous crosstalk mechanisms that connect them. This crosstalk involves expression control of NFκB monomers, interdependent proteolytic processing events of precursors, and the newly identified IκBδ activity that is inducibly expressed by one pathway and

inducibly degraded by another (Basak et al., 2008). In particular, RelA activity has been shown to be induced by non-canonical signals leading to enhanced inflammatory gene expression upon LT-βR signaling. This is due to sequestration of the RelA:p50 dimer by the IκBδ complex. Additionally, RelA:p50 activity is required for transcription of *relb* and *nfkb2*, both of which are important in the non-canonical pathway.

My dissertation aims to understand the molecular mechanisms of NFκB dimer generation and to delineate the functional interaction between the canonical and non-canonical NFκB pathways. Because of the complicated nature of the NFκB signaling network as a whole, I have implemented extensive mathematical models of the NFκB signaling network in order to supplement the biochemical observations throughout my dissertation.

Mathematical modeling allows for biologists to understand complex circuits and mechanisms that may not be easily inferred by biological data alone. The NFκB activation pathway is complex, and understanding the reaction networks within the NFκB pathway is often challenging. Using a mathematical model allows us to understand the interactions that may not be clear when solely relying on the interpretation of experimental data. However, not only does designing a model to understand the circuitry of NFκB activation require careful thought in the question to be answered, but it also requires careful thought in the experiments necessary to parameterize and test such a model.

Throughout my dissertation, I have used simple mathematical models representing biophysical relationships between protein association and dissociation in addition the more complex IKK-IkB-NFκB model. The IKK-IkB-NFκB model used in this dissertation is a mass-action ODE based model that includes NFkB monomer synthesis and degradation, NFκB dimer formation, IkB synthesis and degradation, and associations between IKK, IκB, and NFκB, and NFκB nuclear import and export. Several versions of this model are utilized throughout the dissertation, dependent on the cell type and experimental design of each project. One version of this model includes the non-canonical pathway and has the addition of NIK synthesis and degradation, p100 association to form IkBd, and the processing of p100 to form p52 NFkB dimers.

These models were used throughout the dissertation to further our understanding of the NFκB signaling network and the specific dimers that are activated in various cell types. The model first illustrated the lack of RelA:RelA homodimer formation in the absence of IκBβ. This work revealed the requirement for IκBβ in the formation of the RelA:RelA homodimer, revealing a function not specific to its classical inhibitory function. This model was then adapted to include cRel and illustrated the requirement of specific IkB:NFκB relationships for the stimulus-specific activation of RelA dimers vs. cRel dimers in B cells. The model was then subsequently adapted again to include the non-canonical pathway of NFκB activation and illustrated the proliferative role

of non-canonical NFκB signaling as an amplifier of canonical NFκB stimulation in B cells. With the mathematical models, I have been able to gain a deeper understanding of the NFκB signaling system during the course of my dissertation work.

Chapter 2: The Rel-NFκB dimer generation module: monomer competition and chaperone function by IκBβ

2.1 Abstract

The NFκB family of dimeric transcription factors mediates diverse biological functions in various cell types. While the dynamic regulation of NFκB dimer activity via the IκB-NFκB signaling module is well understood, there is little information on how cell type-specific dimer repertoires are generated from Rel family polypeptides. Here we report the iterative construction of a mathematical model of the Rel-NFκB generation module. Our study reveals that IκBβ, in contrast to IκBα and –ε (known key regulators of the IκB-NFκB signaling module), has essential functions within the Rel-NFκB generation module, specifically as a chaperone of RelA:RelA homodimers formation. Our findings revise the current dogma of three classical, functionally-related IκB proteins, but explain the phenotypes observed in IκB knockout mice and cells. More generally, our work points to a regulatory motif involving a positive 'licensing' factor (IκBβ) that determines cell type-specific responsiveness, relaying subsequent dynamic control to negative feedback regulators (IκBα and –ε) that determine the actual stimulus-specific cellular response.

2.2 Introduction

The NFκB family of dimeric transcription factors regulates a variety of biological responses in diverse cell types. Resting, unstimulated cells contain

a latent pool of NFκB dimers in the cytosol that are stoichiometrically associated with their inhibitors, IκBs (Ghosh and Hayden, 2008; Hoffmann et al., 2006). NFκB transcription factors are produced by homo- and heterodimerization from five Rel homology domain-containing proteins (RelA, RelB, cRel, p50, and p52). The IκB family comprises several isoforms including the classical IκBα, IκBβ, IκBε proteins and the IκBγ and IκBδ activities contained within the higher molecular weight IκBsome (Savinova et al., 2009). Combinatorial dimerization and IκB-NFκB interactions are hallmarks of the IκB-NFκB signaling system.

The coordinated functions of IκB proteins in controlling the dynamics of NFκB activity has been studied systematically using a combined experimental and mathematical modeling approach. Specifically, mathematical modeling recapitulates key events, such as how stimulus-responsive IκB kinase (IKK) phosphorylates IκBs, causing IκB degradation and release of nuclear NFκB DNA binding activity, as well as subsequent attenuation through several parallel and nested negative feedback regulators, such as IκBα, IκBε, A20, and IκBδ (Basak et al., 2012). Interestingly, these studies did not identify a critical function for IκBβ, and IκBβ-deficient mice and cells show attenuated, not increased inflammatory responses (Rao et al., 2010).

In contrast, little recent progress has been reported on how NFκB dimers are generated. Early studies led to an appreciation that the NFκB transcription factor family consists of up to 15 possible dimers, and that

different dimers are detectable in different cell types (Hoffmann et al., 2006). In fact, NFκB dimer repertoire changes dramatically during cell differentiation, as for example B-cell lines with early lineage markers contain primarily RelA:p50 and those with later lineage markers contain primarily cRel:p50 dimers (Liou et al., 1994). In murine embryonic fibroblasts, the RelA:p50 heterodimer and the RelA:RelA homodimer have been observed and shown to be responsible for the expression of distinct target genes (Hoffmann et al., 2003; Leung et al., 2004). However, surprisingly little is known about the mechanisms that control the formation of these distinct NFκB dimers that are critical for mediating diverse cell-type-specific functions. Indeed, we presently lack a quantitative understanding of the most fundamental processes of monomer synthesis and subsequent dimer formation.

Here, we have employed modeling and experimental approaches iteratively to study the mechanisms that control the dimer generation in tissue cells such as fibroblasts. Guided by a model based on first principles of protein–protein interactions, and using in vitro biophysical interaction measurement, we found that we can only account for in vivo observations of low affinity dimers when we considered potential chaperone proteins. Specifically, combined experimental and computational studies revealed that IκBβ functions as a positive regulator within the Rel-NFκB dimer generation module, essential for the formation of RelA:RelA homodimers. In contrast, IκBα is the key regulator of the dynamics of NFκB activity, not only of

RelA:p50 but also of RelA:RelA. We conclude that the classical IκBs actually fall into two classes; whereas IκBα and –ε primarily function within the IκB-NFκB signaling module that is responsive to inflammatory stimuli, IκBβ primarily functions within the Rel-NFκB dimer generation module. The resulting model explains the contrasting phenotypes of mice deficient for each of the classical IκBs.

2.2 Materials and Methods

Computational modeling

Four computational models were constructed for this study. Models 1-3 are simplified models that account for the generation of NFκB dimers from RelA and p50 NFκB monomers and the effect of the interactions with two IκB isoforms on their stabilities. These models are shown graphically in Fig. 1A, Fig. 2A, and Fig. 3A respectively. The model parameters are listed in Supplemental Tables 1-3, respectively. All species are given an initial concentration of zero nM and allowed to reach a steady state. The results shown in the figures are the final steady state concentrations.

Parameterization of the model required the exploration of the parameter space of variable IkB:NFkB affinities and determining the probabilities of such parameter predictions (see results Fig. 2E). Further parameterization of determining the correct IkB:NFkB affinities was determined using additional experimental data (Fig. 3) in order to eliminate parameter sets (see Supplemental Fig. 3C).

The fourth computational model appends the previously published IκB models with the reactions that govern RelA/NF-κB dimer generation. The input to this model is a numerical curve for IKK activity and the outputs are free, nuclear RelA:RelA homodimer and Rel:p50 heterodimer. The complete new model contains 40 species and 110 reactions governed by 65 parameters (Supplemental Table 4). Parameterization included the use of the basal

protein abundances as outputs from the model determined from protein standard curves determined in Supplemental Figure 4. IkB:NFkB affinities were determined based on a series of experimental data that had to be satisfied (see Supplemental Fig. 3C) and used subsequently in this model.

The ODEs were solved numerically using MATLAB version R2013a (The MathWorks, Inc.) with subroutine *ode15s*, a variable order, multi-step solver. Prior to stimulation, the system was allowed to equilibrate from starting conditions to a steady state, defined as showing no concentration changes greater than 1% over a period of 4000 minutes. Stimulus-induced perturbation from the steady state was accomplished by direct modulation of IKK activity via a numerical input curve representing TNF stimulation (adapted from Werner 2008). MATLAB models are available upon request.

Cell culture

Immortalized MEFs were prepared and cultured as previously described . Briefly, cells were grown to confluence in Dulbecco's Modified Eagle's Medium (DMEM) supplemented with 10% bovine calf serum, 1% penicillin-streptomycin, and 1% L-Glutamine. Stimulations were performed using 1ng/mL TNF (Roche). The cell lines used were: wild-type (Hoffmann *et al*, 2002), *iκbβ*$^{-/-}$ (Kearns *et al*, 2006), *iκbα*$^{-/-}$*iκbε*$^{-/-}$ (Hoffmann *et al*, 2002), *iκbα*$^{-/-}$ *iκbβ*$^{-/-}$*iκbε*$^{-/-}$ (O'Dea *et al*, 2007), *rela*$^{-/-}$ (Hoffmann *et al*, 2003), *rela*$^{-/-}$*crel*$^{-/-}$*nfkb1*$^{-/-}$ (O'Dea *et al*, 2007), *nfkb1*$^{-/-}$*nfkb2*$^{-/-}$ (Hoffmann *et al*, 2003). *Crel*$^{-/-}$*relb*$^{-/-}$*nfkb1*$^{-/-}$

nfkb2$^{-/-}$ knockouts were generated from E12.5-14.5 embryos and immortalized following the 3T3 protocol.

Biochemistry

EMSA (Hoffmann et al., 2002), deoxycholate (DOC) + EMSA (Basak *et al*, 2007), EMSA supershift (Basak *et al*, 2008), wild-type + mutant oligo competition EMSA (Hoffmann *et al*, 2003), immunodepletion, Rnase Protection Assay (Kearns *et al*, 2006), and Western blotting were performed as previously described. IκBα (sc-371), IκBβ (sc-946 for Western blot and sc-969 for immunodepletion), RelA (sc-372) antibodies were provided by Santa Cruz Biotechnology. P50 N-terminal antisera was a generous gift from Nancy Rice.

2.3 Results

NFκB dimerization affinities

To address the molecular basis for the generation of cell-type specific repertoires of NFκB dimers within the so-called 'Rel-NFκB dimer generation module', we first considered the fundamental principles regarding the generation of homo- and hetero-dimers from the classical NFκB proteins p50 and RelA (A), which are present in all differentiated human cells, and which show distinct gene-expression specificities (Hoffmann et al., 2003; Leung et al., 2004). Dimer abundance may be thought of as a function of monomer synthesis (m1, m2) and degradation (m-1, m-2), and combinatorial dimer association (d1, d2, d3) and dissociation (d-1, d-2, d-3) rate constants (Fig. 2.1A, Model 2.1, Table 2.1). As Rel proteins are obligate dimers, monomers are incompletely folded and more rapidly degraded in vivo than when dimerized (dd-1, dd-2, dd-3) (Fusco et al., 2008; Maine et al., 2007). As such, dimerization affinities are important regulators of cellular homo- and heterodimer abundances. Here we modeled the abundance of RelA:RelA (A:A) and RelA:p50 (A:50) dimers as a function of those dimer affinities keeping the p50:p50 dimer affinity constant at 30 nM (Fig. 2.1B), 3 nM and 300 nM (Fig. 2.2A). Whereas p50:p50 dimerization affinity did not affect A:A and A:50 abundances over that range, the simulations do illustrate an interdependence between A:A and A:50 formation, where p50 competes for RelA monomers and may thus inhibit A:A generation. To test whether

monomer competition occurs in cells, we compared nfkb1-/- (which lack p50) and wild type murine embryo fibroblasts (MEFs) and found an increase in the abundance of the A:A homodimers. These data confirm that the concept of monomer competition is physiologically relevant and tends to diminish the abundances of weak affinity dimers (Fig. 2.1C).

We next measured dimer affinities by biophysical techniques. Using purified recombinant RelA and p50 dimerization domains, we measured homo-dimer affinities by analytical ultracentrifugation (AUC) (Fig. 2.2B) and deduced the heterodimer affinity from quantitative gel filtration experiments that provided the ratios of dimer abundances (Fig. 2.2C-E). We found remarkably disparate affinities: whereas the interactions by p50 proteins were found within the expected range (5-40 nM), the A:A homodimer affinity was in the μM range (Fig. 2.1D). Although the weak A:A affinity would result in a lower abundance of A:A homodimers in the cell, we find that they are readily detectable in cells amounting to about a quarter of TNF-inducible NFκB activities (Fig. 2.1C, Fig. 2.1E); comparing simulations with experimental results shows that the simple model that includes the monomer competition of RelA and p50 in forming specific NFκB dimers parameterized by the biophysical data does not account for the observed abundance of the A:A dimer (Fig. 2.1E).

Interaction affinities between IκB isoforms and NFκB dimers

Given that IκBs associate along a large dimerization interface (Huxford et al., 1998), we considered the possibility that IκBs may stabilize RelA-

containing NFκB dimers. (Classical IκBs do not interact with p50:p50 (Ishikawa et al., 1998).) To test this idea, we extended the mathematical model by including IκB synthesis (i1) and degradation (i-1) and its interaction with A:A homodimers and A:50 heterodimers (di1, di-1, di2, di-2) (Fig. 2.3A, Model 2.2, Table 2.2). We used experimentally determined concentrations of various protein species as constraints in the model (Fig. 2.3B,C). In the resulting model, NFκB dimer abundances are then also a function of IκB abundances and the interaction affinities between NFκB dimers and IκB proteins. These interactions are thought to be tight (Bergqvist et al., 2009; O'Dea et al., 2007; Phelps et al., 2000), but systematic measurements using biophysical methods are hampered by the challenge of expressing and purifying full-length recombinant proteins that are not fully folded on the apo-form and have a tendency to aggregate.

Here, we developed an approach to derive in vivo IκB-NFκB affinities. The fact that IκBα, IκBβ, and IκBε protein abundances in MEFs deficient in classical NFκB dimers (rela-/-crel-/-nfkb1-/-) were much more reduced than their corresponding mRNA levels (Fig. 2.3B), indicated the degree to which the interaction with NFκB stabilized the half-life of the three classical IκBs (O'Dea et al., 2007; Pando and Verma, 2000). We reasoned that measurements of relative abundances of IκB proteins in mutant cells with alternate NFκB dimer repertoires could be used to infer in vivo IκB-NFκB dimer affinities.

To distinguish IκB interaction affinities for the A:50 and A:A dimers, we produced composite NFκB knockout MEFs (relb-/-nfkb2-/-nfkb1-/-crel-/-) in which RelA is the sole NFκB protein family member, and RelA-deficient MEFs, which do not contain A:A homodimers but contain the partially compensating cRel:p50 heterodimer in place of A:50 (Gapuzan et al., 2005; Hoffmann et al., 2003) (Fig. S3A, S3B). Using these cells, the experimentally determined IκBα / IκBβ abundance ratios in the context of other experimentally determined protein abundances (Fig. 2.3C) constrained the ranges of acceptable ranges of IκB-NFκB affinities via model parameter fitting procedures (Fig. 2.4). For example, in A:50-deficient cells, the IκBα abundance was reduced to 35 +/- 8% of that in wild type cells constraining the IκBα-A:A and IκBα-A:50 affinity to a narrow band within the two dimensional parameter space (top left panel). In contrast, IκBβ abundance was hardly affected (76% +/- 24% of the wild type cells) and provided less constraint on the acceptable affinities of IκBβ-A:A and IκBβ-A:50 interactions based on the particular parameter landscape (top right panel). Similarly, IκBα and IκBβ abundance measurements in A:A-deficient cells provided additional constraints (bottom panels). The overlap of these acceptable ranges for each IκB in both NFκB knockout conditions determined not a single parameter set but a narrower range of parameters that can account for all available experimental data.

Recognizing that the measurements may be associated with experimental error, we incorporated uncertaintly into our analysis by scanning over the probable dimer and IκB-dimer affinity spaces at two-fold about the mean. The ratios at each point were compared to the variance in the experimental data in order to determine the probability that the calculated affinity is correct (Fig. 2.5). Even allowing for substantial experimental error, IκBβ is predicted to have a clear preference for A:A over A:50 (>100 fold). To further test these parameter ranges in additional cell biological assays, we chose seven parameter sets representative of the probable and improbable regimes (Fig. 2.5, Table 2.5).

IκBβ promotes RelA:RelA dimer generation

Using the combination of probable and improbable parameter sets (Table 2.5) for IκB-NFκB dimer affinities within the experimentally determined ranges, we parameterized a mathematical model (for simplicity, IκBε and IκBα were treated identically) to account for the generation of distinct RelA dimers (Fig. 2.6, Model 2.3, Table 2.3). We developed three predictions that depend on high IκBβ preference for the RelA:A homodimer and tested them experimentally. First, we used the model to calculate the basal abundance of RelA protein in cells only containing RelA (relb-/-nfkb2-/-nfkb1-/-crel-/-) under two regimes, probable and improbable affinity predictions (Table 2.5). We found that most probable affinity sets predicted a lower decrease (~1.5-2 fold) in RelA protein levels than most improbable affinity sets (Fig. 3B). Indeed,

immunoblot analysis showed only a small decrease (~1.5 fold) in RelA protein (Fig. 2.7A,B).

Second, we used the model to simulate the steady state abundances of IκB-bound NFκB dimers in wild type cells; this resulted in the prediction that the majority of A:A homodimers are associated with IκBβ for the probable, but not improbable affinity sets (Fig. 2.7C). Further, the majority of A:50 dimers were predicted to be associated with IκBα but in some the primary interaction partner was IκBβ (Fig. 2.7C). To test this prediction we prepared cytoplasmic extracts from unstimulated MEFs, which contain latent IκB-NFκB complexes. The detergent deoxycholate is known to disrupt IκB-NFκB interactions, leaving the dimer intact and capable of binding DNA (Baeuerle and Baltimore, 1988), thereby revealing both latent RelA homo- and heterodimers (Fig. 2.7D, lane 2). By prior 22mmune-depleting IκBα or IκBβ, we found that IκBβ (>50%) is indeed the primary interaction partner for the A:A homodimer (lane 6), whereas IκBα depletion left the A:A homodimer largely intact (lane 4). Additionally, we found that IκBα is the primary interaction partner (>50%) for the A:50 heteromdimer (lane 4), although some A:50 is bound to IκBβ as well (lane 6). Based on these data, we were able to narrow the probably parameter range by excluded parameter sets that did not satisfy the experimentally determined IκB-NFκB interactions (Table 2.5).

Finally, we asked whether IκBβ is in fact required for A:A homodimer generation. Computational simulations with the probable affinity sets predicted

a dramatic decrease (<20% of wild type) in A:A homodimer abundance in IκBβ-deficient but not IκBα-deficient cells (Fig. 2.7E). Improbable parameter affinity sets yielded variable amounts of A:A homodimer abundance in the three genotypes. Our experimental analysis supported these probable affinity sets' predictions: IκBβ-deficient cells showed a dramatic drop (<2% of wild type) in the A:A homodimer abundance as revealed by deoxycholate treatment of cytoplasmic extracts, whereas IκBα-deficiency did not appear to alter the A:A homodimer repertoire (>97% of wild type) (Fig. 2.7F). We then determined which of the parameter sets passed the above three tests. Remarkably, none of the improbable parameters allowed for correct predictions, while two parameter sets from the initially determined probable range did (Table 2.5). These three model-directed experimental studies thus support the notion that a high affinity for the A:A homodimer endows IκBβ with chaperone function in A:A homodimer generation.

We probed this notion further in a mutant cell background that shows a higher abundance of homodimers than heterodimer; in p50-deficient cells, compensation by p52 is incomplete (Hoffmann et al., 2003), thus reducing monomer competition and allowing the majority of RelA to form A:A homodimers. We generated p50/IκBβ-doubly-deficient MEFs to investigate the effect of IκBβ deficiency on A:A homodimer formation. Interestingly, in this context IκBβ-deficiency again results in a severe reduction of A:A homodimer formation (~3-4 fold less), instead shunting RelA towards the RelA:p52

heterodimer (Fig. 2.8). These data provide a further illustration of the IκBβ-A:A model.

IκBα provides dynamic control for both RelA-containing dimer activities

The described mathematical model recapitulates the functions of the Rel-NFκB dimer generation module in generating the latent NFκB dimer repertoire in unstimulated fibroblasts. To study stimulus-induced dynamic regulation of the generation, activation and inactivation of RelA homo- and heterodimers, we connected this model with a well-tested model of the IκB-NFκB signaling module (Werner et al., 2008) (Fig. 2.9A, Fig. 2.10, Model 2.4, Table 2.4, Table 2.5).

A hallmark of NFκB signaling is negative feedback control mediated by IκBα that ensures post-induction repression of RelA:p50 activity following transient exposure to inflammatory cytokines (Hoffmann et al., 2002; Werner et al., 2008). To test whether the resulting model recapitulates the signaling dynamics of two NFκB dimers, we simulated TNF-induced signaling. Model simulations showed transient activation of both dimers in wild type cells. Post-induction repression was mediated by IκBα, as ikba-/- MEFs showed sustained activity in both computational (Fig. 2.9B) and experimental studies (Fig. 2.9C), not only of the A:50 heterodimer but also the A:A homodimer. The sustained A:A homodimer activity in ikba-/- MEFs is not due to an increase of IκBβ protein levels (Fig. 2.11A). While previous work has demonstrated the critical role of IκBα in the dynamic control of RelA:p50, our simulation and

experimental results show that IκBα plays a role in the dynamic control of RelA:RelA homodimer as well.

We asked how it is possible that IκBα is the key dynamic regulator of the A:A homodimer but does not contribute substantially to A:A dimer generation. We investigated these two roles as a function of the affinity between IκBα and the RelA:A homodimer. We simulated both the basal abundance of the A:A homodimer and the duration of A:A homodimer activity above the threshold of a 50% of maximum activity (Fig. 2.11B) as a function IκBα-A:A homodimer affinities over a thousand-fold range (Fig. 2.9D). We found that lowering the IκBα-A:A affinity would prolong A:A homodimer activity following transient stimulation, but have little impact on A:A abundance; however, increasing the affinity would increase the basal abundance of A:A homodimer. We thus conclude that the IκBα affinity for the A:A homodimer is tuned to be low enough that IκBα does not function within the Rel-NFκB dimer generation module, but high enough so that it functions within the IκB-NFκB signaling module to control the dynamics of A:A activity.

2.4 Discussion

The described work reveals a novel and specific function for IκBβ. IκBs are named "inhibitors of NFκB" because they are capable of inhibiting NFκB DNA binding activity in cell free *in vitro* assays (Baeuerle and Baltimore, 1988), and IκBβ was identified in that same manner (Zabel and Baeuerle, 1990). However, we show here that *in vivo* IκBβ functions as a positive regulator of NFκB dimer generation. Whereas the RelA:p50 dimers can readily form owing to a high dimerization affinity, RelA:RelA dimer formation requires IκBβ. These distinct functions of IκBβ and other IκBs explain the phenotypes observed in knockout mice.

Previous studies of the IκB-NFκB signaling module revealed that negative feedback by IκBα, IκBε, and IκBδ shape the dynamics of NFκB activity in response to stimuli (Basak et al., 2007; Hoffmann et al., 2002; Kearns et al., 2006; O'Dea et al., 2007; Shih et al., 2009; Werner et al., 2008). Indeed prolonged NFκB activity leads to a severe hyper-inflammatory phenotype in IκBα-deficient mice, and to hyper-proliferation in B-cells lacking IκBε (Alves et al., 2014) or IκBδ (J. Almaden and A.H., data not shown). However, IκBβ-deficient mice were recently reported to have hypo-inflammatory responses, reduced expression of TNF, and resistance to endotoxic shock and collagen-induced arthritis (Rao et al., 2010; Scheibel et al., 2010). We show here that IκBβ-deficient fibroblasts lack one member of

the NFκB dimer family, namely the homodimers of the potent activator RelA (Fig. 3). Similar RelA;RelA and RelA;cRel-deficiency was observed in macrophages (Rao et al., 2010).

Previously established mathematical models of the IκB-NFκB signaling module are unable to account for this phenotype. These models assume a constant amount of NFκB dimer as a given quantity, and calculated the control of its sub-cellular localization and DNA binding activity as a function of dynamically regulated IκB degradation and re-synthesis. Here, we have constructed a model for the Rel-NFκB dimer generation module and parameterized based on biophysical measurements of recombinant proteins and a series of iterative cycles of prediction and in vivo measurements. Our work reveals why IκBβ is critical for the formation of the NFκB RelA:RelA homodimers, whose spontaneous generation is challenged not only by poor intrinsic dimer affinities but also by competition by the high affinity heterodimerization partner p50.

A key feature of IκBβ function is an unusually high affinity for RelA:RelA homodimers (3.2 pM). As recombinant IκBβ is not mono-disperse in cell free systems this model-aided interpretation of cellular measurements cannot be tested directly. While sub-nano-molar dissociation constants have previously been reported for other protein-protein interactions (Salimi-Moosavi et al., 2012), we may reconsider the simplifying assumption of the coarse grained model formulation in which IκBβ interacts only with the pre-formed dimer.

Instead, IκBβ might be able to bind monomers sequentially (Fig. 2.12A). This change in association may more accurately reflect the chaperone effect of IκBβ on the RelA:RelA homodimer. Whereas the single step reaction scheme in the original model is $A + A \leftrightarrow A_2 + B \leftrightarrow A_2B$, defining dissociation constants as $Kd_1 = \frac{[A]^2}{[A_2]}, and\ Kd_2 = \frac{[A_2][B]}{[A_2B]}$, the two-step reaction scheme would be $A + B \leftrightarrow AB + A \leftrightarrow A_2B$, defining dissociation constants $Kd_3 = \frac{[A][B]}{[AB]}$, $Kd_4 = \frac{[AB][A]}{[A_2B]}$, and $Kd_4 = \frac{Kd_1Kd_2}{Kd_3}$. Whereas Kd_1 and Kd_2 were determined to be 800 nM and 3.2 x 10^{-3} nM respectively, in the two-step model Kd_3 are inversely proportional Kd_4 (Fig. 2.12B). Thus a two-step model would yield interaction constants in the micro- and nano-molar range that are more commonly observed within bi-molecular interactions. We note that within a two-step reaction scheme, IκBβ functions not only as a stabilizer of dimers but as a *bona fide* chaperone for dimer formation.

In addition to IκBβ's described role within the Rel-NFκB dimer generation module, a hypo-phosphorylated IκBβ has also been shown to have nuclear functions in macrophages in protecting promoter-bound NFκB from IκBα-mediated negative feedback (Suyang et al., 1996). Resistance to negative feedback may be imparted particularly to those NFκB dimers (e.g. A:A and RelA:cRel) that show high affinity for IκBβ (Rao et al., 2010; Scheibel et al., 2010). As such, both the proposed nuclear function and the here-described chaperone function are a consequence of the high affinity for

specific dimers revealed through our iterative experimental and computational study.

The parameterization of computational models is a recognized challenge of systems biology. Whereas strategies have been developed to parameterize mathematical synthesis and degradation expressions, and those describing enzymatic functions within cells, the interactions between proteins are rarely quantitatively addressed. *Ex vivo*, affinity and kinetic rate constants can be determined for the interaction of recombinant proteins, but the *in vivo* relevance of such constants is limited by the difficulties of producing recombinant full-length proteins with appropriate post-translational modifications. Here we exploited the fact the IκB abundance is a function of its interaction with NFκB (O'Dea et al., 2007) (Fig. 2B) and employed computational modeling in order to derive *in vivo* interaction affinities from immunoblot quantifications. Interestingly, it was previously observed that RelA deficiency results in IκBβ deficiency (Hertlein et al., 2005; Valovka and Hottiger, 2011), and such obligate interactions are not rare (Jones and Thornton, 1996; Mintseris and Weng, 2005), suggesting that our model parameterization strategy may be employed for other biological systems.

We described the Rel-NFκB dimer generation module and the IκB-NFκB signaling module as distinct but there are of course numerous interactions. At a minimum, we may consider that IκBβ within the Rel-NFκB dimer generation module functions as a 'licensing factor' for subsequent

dynamic control by IκBα. The distinct functions by these structurally homologous proteins are based on both their specific protein-interaction constants and their distinct dynamic degradation and synthesis control. Indeed, such ‘hand-off’ or ‘relay control’ network motifs based on kinetic differences between family members may be found in other regulatory systems.

2.5 Acknowledgements

Chapter 2, in full, is a reprint of material being prepared for publication as “The Rel-NFκB dimer generation module: monomer competition and chaperone function by IκBβ ” by Tsui R, Kearns JD, Lynch C, Vu D, Ngo K, Basak S, Ghosh G, and Hoffmann A. The dissertation author was the primary investigator and author of this material.

Model 2.1: RelA and p50 synthesis and dimerization

This model contains RelA and p50, which can form 3 NFκB dimers: RelA:A, ReA:p50, p50:p50. The parameter ID symbols in Model Supplemental Table 1 correspond to the rate constants in these equations.

$$\frac{dRelA}{dt} = m_1 - m_{-1}\,(RelA) - 2d_1(RelA)(RelA) + 2d_{-1}(RelA{:}\,A) - d_2(RelA)(p50) + d_{-2}(RelA{:}\,p50)$$

$$\frac{dp50}{dt} = m_2 - m_{-2}\,(p50) - 2d_3(p50)(p50) + 2d_{-3}(p50{:}\,p50) - d_2(RelA)(p50) + d_{-2}(RelA{:}\,p50)$$

$$\frac{dRelA{:}\,A}{dt} = d_1(RelA)(RelA) - d_{-1}(RelA{:}\,A) - dd_1(RelA{:}\,A)$$

$$\frac{dRelA{:}\,p50}{dt} = d_2(RelA)(p50) - d_{-2}(RelA{:}\,p50) - dd_2(RelA{:}\,p50)$$

$$\frac{dp50{:}\,p50}{dt} = d_3(p50)(p50) - d_{-3}(p50{:}\,p50) - dd_3(p50{:}\,p50)$$

Model 2.2: Interactions between a generic IκB with RelA and p50 NFκB dimers

This model contains RelA and p50, which can form 3 NFκB dimers: RelA:A, RelA:p50, p50:p50. A generic IκB can complex with RelA:A and RelA:p50. The p50:p50 dimer has not been demonstrated to bind to IκB, so that interaction is excluded from this model. The IκB-NFκB complex is also stable, and so there is no degradation of the complex, it either dissociates or IκB gets degraded and releases the NFκB dimer. The parameter ID symbols in Model Supplemental Table 2 correspond to the rate constants in these equations.

$$\frac{dRelA}{dt} = m_1 - m_{-1}\,(RelA) - 2d_1(RelA)(RelA) + 2d_{-1}(RelA{:}\,A) - d_2(RelA)(p50) + d_{-2}(RelA{:}\,p50)$$

$$\frac{dp50}{dt} = m_2 - m_{-2}\,(p50) - 2d_3(p50)(p50) + 2d_{-3}(p50{:}\,p50) - d_2(RelA)(p50) + d_{-2}(RelA{:}\,p50)$$

$$\frac{dIkB}{dt} = i_1 - i_{-1}\,(IkB) - di_1(IkB)(RelA{:}\,A) + di_{-1}(IkB\_RelA{:}\,A) - di_2(IkB)(RelA{:}\,p50) + di_{-2}(IkB\_RelA{:}\,p50)$$

$$\frac{dRelA{:}\,A}{dt} = d_1(RelA)(RelA) - d_{-1}(RelA{:}\,A) - dd_1(RelA{:}\,A) - di_1(IkB)(RelA{:}\,A) + di_{-1}(IkB\_RelA{:}\,A) + did_1(IkB\_RelA{:}\,A)$$

$$\frac{dRelA{:}\,p50}{dt} = d_2(RelA)(p50) - d_{-2}(RelA{:}\,p50) - dd_2(RelA{:}\,p50) - di_2(IkB)(RelA{:}\,p50) + di_{-2}(IkB\_RelA{:}\,p50) + did_2(IkB\_Relp50{:}\,A)$$

$$\frac{dp50{:}\,p50}{dt} = d_3(p50)(p50) - d_{-3}(p50{:}\,p50) - dd_3(p50{:}\,p50)$$

$$\frac{dIkB\_RelA{:}\,A}{dt} = di_1(IkB)(RelA{:}\,A) - di_{-1}(IkB\_RelA{:}\,A) - did_1(IkB\_RelA{:}\,A)$$

$$\frac{dIkB\_RelA{:}\,p50}{dt} = di_2(IkB)(RelA{:}\,p50) - di_{-2}(IkB\_RelA{:}\,p50) - did_2(IkB\_RelA{:}\,p50)$$

Model 2.3: Interactions of IκBα/ε and IκBβ with RelA and p50 NFκB dimers

This model contains RelA and p50, which can form 3 NFκB dimers: RelA:A, RelA:p50, p50:p50. IκBα/ε and IκBβ are the specific IκBs in the model, which can complex with RelA:A and RelA:p50. IκBε is assumed to behave the same as IκBα in this simplified model. The p50:p50 dimer has not been demonstrated to bind to IκB, so that interaction is excluded from this model. The IκB-NFκB complex is also stable, and so there is no degradation of the complex, it either dissociates or IκB gets degraded and releases the NFκB dimer. The parameter ID symbols in the Model Supplemental Table 3 correspond to the rate constants in these equations.

$$\frac{dRelA}{dt} = m_1 - m_{-1}\,(RelA) - 2d_1(RelA)(RelA) + 2d_{-1}(RelA{:}A) - d_2(RelA)(p50) + d_{-2}(RelA{:}p50)$$

$$\frac{dp50}{dt} = m_2 - m_{-2}\,(p50) - 2d_3(p50)(p50) + 2d_{-3}(p50{:}p50) - d_2(RelA)(p50) + d_{-2}(RelA{:}p50)$$

$$\frac{dIkBa/e}{dt} = i_1 - i_{-1}\,(IkBa/e) - di_1(IkBa/e)(RelA{:}A) + di_{-1}(IkBa/e\_RelA{:}A) - di_2(IkBa/e)(RelA{:}p50) + di_{-2}(IkBa/e\_RelA{:}p50)$$

$$\frac{dIkBb}{dt} = i_2 - i_{-2}\,(IkBb) - di_3(IkBb)(RelA{:}A) + di_{-3}(IkBb\_RelA{:}A) - di_4(IkBb)(RelA{:}p50) + di_{-4}(IkBb\_RelA{:}p50)$$

$$\frac{dRelA{:}A}{dt} = d_1(RelA)(RelA) - d_{-1}(RelA{:}A) - dd_1(RelA{:}A) - di_1(IkBa/e)(RelA{:}A) + di_{-1}(IkBa/e\_RelA{:}A) + did_1(IkBa/e\_RelA{:}A) - di_3(IkBb)(RelA{:}A) + di_{-3}(IkBb\_RelA{:}A) + did_3(IkBb\_RelA{:}A)$$

$$\frac{dRelA{:}p50}{dt} = d_2(RelA)(p50) - d_{-2}(RelA{:}p50) - dd_2(RelA{:}p50) - di_2(IkBa/e)(RelA{:}p50) + di_{-2}(IkBa/e\_RelA{:}p50) + did_2(IkBa/e\_RelA{:}p50) - di_4(IkBb)(RelA{:}p50) + di_{-4}(IkBb\_RelA{:}p50) + did_4(IkBb\_RelA{:}p50)$$

$$\frac{dp50{:}p50}{dt} = d_3(p50)(p50) - d_{-3}(p50{:}p50) - dd_3(p50{:}p50)$$

Model 2.3: Interactions of IκBα/ε and IκBβ with RelA and p50 NFκB dimers, Continued

$$\frac{dIkBa/e\_RelA{:}\,A}{dt} = di_1(IkBa/e)(RelA{:}\,A) - di_{-1}(IkBa/e\_RelA{:}\,A) - did_1(IkBa/e\_RelA{:}\,A)$$

$$\frac{dIkBb\_RelA{:}\,A}{dt} = di_2(IkBb)(RelA{:}\,A) - di_{-2}(IkBb\_RelA{:}\,A) - did_2(IkBb\_RelA{:}\,A(t))$$

$$\frac{dIkBa/e\_RelA{:}\,p50}{dt} = di_3(IkBa/e)(RelA{:}\,p50) - di_{-3}(IkBa/e\_RelA{:}\,p50) - did_3(IkBa/e\_RelA{:}\,p50)$$

$$\frac{dIkBb\_RelA{:}\,p50}{dt} = di_4(IkBb)(RelA{:}\,p50) - di_{-4}(IkBb\_RelA{:}\,p50) - did_4(IkBb\_RelA{:}\,p50)$$

Model 2.4: An integrated model of NFκB dimer generation, IκB-NFκB interactions, and IKK-dependent signaling

This model is adapted from previously published IκB-NFκB signaling models (Shih et al. 2012, Shih et al. 2009) but with three specific NFκB dimers are present in this new model: RelA:A, RelA:p50, and p50:p50. There are also three IκBs in this model: IκBα, IκBβ, and IκBε, all which interact with RelA:A and RelA:p50. The IKK signaling input is represented as a multiplier on the degradation rate constant of IKK induced IκB degradation, since IKK activity results in phosphorylation and subsequent degradation of IκBs, allowing for the release of NFκB dimers.

The model also allows the translocation of species between the cytoplasm and the nucleus, so transport rates are included in this model as well. The IκB:NFκB affinities were determined from the previous models and in this work (Fig. 2E).

All transcriptional activation reactions used the following Hill equation:

$$kt = \frac{ktc\left(1 + \sum w\left(\frac{[d]}{Kd}\right)^3\right)}{\left(1 + \sum\left(\frac{[d]}{Kd}\right)^3\right)}$$

ktc = constitutive basal mRNA synthesis rate
w = inducible multiplier
d = NFκB dimer concentration
Kd = Hill Kd (NFκB induced)

Table 2.1: Parameter Table for Model 2.1

Reaction	Category	Param ID no	Param ID symbol	Parameter Value	Source
NFκB reactions					
=> RelA	NFκB Syn.	1	m1	1.6e-2 nM sec^{-1}	Fit to measured protein abundance levels
=> p50	NFκB Syn.	2	m2	1.6e-2 nM sec^{-1}	
RelA =>	NFκB Deg.	3	m-1	3.85e-4 sec^{-1}	Based on estimated 30 min half-life of NFκB monomers
p50 =>	NFκB Deg.	4	m-2	3.85e-4 sec^{-1}	
RelA + RelA => RelA:A	NFκB Association	5	d1	1e-5 nM^{-1} sec^{-1}	Based on affinity determined from AUC (800 nM) with an association rate constant that is estimated from a diffusion limited rate constant set to a high affinity of 0.1 nM
RelA + p50 => RelA:p50	NFκB Association	6	d2	3.16e-5 nM^{-1} sec^{-1}	Based on affinity determined from AUC and gel filtration (10 nM) with an association rate constant that is estimated from a diffusion limited rate constant set to a high affinity of 0.1 nM
p50 + p50 => p50:p50	NFκB Association	7	d3	3e-5 nM^{-1} sec^{-1}	Based on affinity determined from AUC (30 nM) with an association rate constant that is estimated from a diffusion limited rate constant set to a high affinity of 0.1 nM
RelA:A => RelA + RelA	NFκB Dissociation	8	d-1	8e-3 sec^{-1}	Calculated from affinity determined from AUC (800 nM) and the association rate constant
RelA:p50 => RelA + p50	NFκB Dissociation	9	d-2	3.16e-4 sec^{-1}	Calculated from affinity determined from AUC and gel filtration (10 nM) and the association rate constant
p50:p50 => p50 + p50	NFκB Dissociation	10	d-3	9e-4 sec^{-1}	Calculated from affinity determined from AUC (30 nM) and the association rate constant
NFκB =>	NFκB Deg.	11	dd	4e-6 sec^{-1}	Based on estimated 48 hour half-life

Table 2.2: Parameter Table for Model 2.2

Reaction	Category	Param ID no	Param ID symbol	Parameter Value	Source
IκB reactions					
=> IκB	IκB Syn.	1	i1	1.6e-2 nM sec^{-1}	Fit to measured protein abundance levels
IκB =>	IκB Deg.	2	i-1	2e-3 sec^{-1}	Basak et al, 2007, O'Dea et al, 2007
NFκB reactions					
=> RelA	NFκB Syn.	3	m1	1.6e-2 nM sec^{-1}	Fit to measured protein abundance levels
=> p50	NFκB Syn.	4	m2	1.6e-2 nM sec^{-1}	
RelA =>	NFκB Deg.	5	m-1	3.85e-4 sec^{-1}	Based on estimated 30 min half-life of NFκB monomers
p50 =>	NFκB Deg.	6	m-2	3.85e-4 sec^{-1}	
RelA + RelA => RelA:A	NFκB Association	7	d1	1e-5 nM^{-1} sec^{-1}	From Model 1
RelA + p50 => RelA:p50	NFκB Association	8	d2	3.16e-5 nM^{-1} sec^{-1}	From Model 1
p50 + p50 => p50:p50	NFκB Association	9	d3	3e-5 nM^{-1} sec^{-1}	From Model 1
RelA:A => RelA + RelA	NFκB Dissociation	10	d-1	8e-3 sec^{-1}	From Model 1
RelA:p50 => RelA + p50	NFκB Dissociation	11	d-2	3.16e-4 sec^{-1}	From Model 1
p50:p50 => p50 + p50	NFκB Dissociation	12	d-3	9e-4 sec^{-1}	From Model 1
NFκB =>	NFκB Deg.	13	dd	4e-6 sec^{-1}	Based on estimated 48 hour half-life
IκB-NFκB interactions					
IκB + RelA:A => IκB-RelA:A	IκB-NFκB inter	14	di1	1e-3 nM^{-1} sec^{-1}	Adapted from Shih et al. 2012
IκB + RelA:p50 => IκB-RelA:p50	IκB-NFκB inter	15	di2	1e-3 nM^{-1} sec^{-1}	Adapted from Shih et al. 2012
IκB-RelA:A => IκB + RelA:A	IκB-NFκB inter	16	di-1	variable sec^{-1}	Variable with association rate constant set (Kd = 0.001-1000 nM)
IκB-RelA:p50 => IκB + RelA:p50	IκB-NFκB inter	17	di-2	variable sec^{-1}	Variable with association rate constant set (Kd = 0.001-1000 nM)
IκB-NFκB =>NFκB	IκB Deg.	18	did	6e-5 sec^{-1}	Basak et al, 2007, O'Dea et al, 2007

Table 2.3: Parameter Table for Model 2.3

Reaction	Category	Param ID no	Param ID symbol	Parameter Value	Source
IκB reactions					
=> IκBα	IκB Syn.	1	i1	1.6e-2 nM sec^{-1}	Fit to measured protein abundance levels
=> IκBβ	IκB Syn.	2	i2	1.6e-2 nM sec^{-1}	
IκBα =>	IκB Deg.	3	i-1	2e-3 sec^{-1}	Basak et al, 2007, O'Dea et al, 2007
IκBβ =>	IκB Deg.	4	i-2	3e-3 sec^{-1}	
NFκB reactions					
=> RelA	NFκB Syn.	5	m1	1.6e-2 nM sec^{-1}	Fit to measured protein abundance levels
=> p50	NFκB Syn.	6	m2	1.6e-2 nM sec^{-1}	
RelA =>	NFκB Deg.	7	m-1	3.85e-4 sec^{-1}	Based on estimated 30 min half-life of NFκB monomers
p50 =>	NFκB Deg.	8	m-2	3.85e-4 sec^{-1}	
RelA + RelA => RelA:A	NFκB Association	9	d1	1e-5 nM^{-1} sec^{-1}	From Model 1
RelA + p50 => RelA:p50	NFκB Association	10	d2	3.16e-5 nM^{-1} sec^{-1}	From Model 1
p50 + p50 => p50:p50	NFκB Association	11	d3	3e-5 nM^{-1} sec^{-1}	From Model 1
RelA:A => RelA + RelA	NFκB Dissociation	12	d-1	8e-3 sec^{-1}	From Model 1
RelA:p50 => RelA + p50	NFκB Dissociation	13	d-2	3.16e-4 sec^{-1}	From Model 1
p50:p50 => p50 + p50	NFκB Dissociation	14	d-3	9e-4 sec^{-1}	From Model 1
NFκB =>	NFκB Deg.	15	dd	4e-6 sec^{-1}	Based on estimated 48 hour half-life
IκB-NFκB interactions					
IκBα + RelA:A => IκBα-RelA:A	IκB-NFκB inter	16	di1	1e-3 nM^{-1} sec^{-1}	Adapted from Shih et al. 2012
IκBβ + RelA:A =>IκBβ-RelA:A	IκB-NFκB inter	17	di3	1e-3 nM^{-1} sec^{-1}	Adapted from Shih et al. 2012
IκBα + RelA:p50 => IκBα-RelA:p50	IκB-NFκB inter	18	di2	1e-3 nM^{-1} sec^{-1}	Adapted from Shih et al. 2012
IκBβ + RelA:p50 =>IκBβ-RelA:p50	IκB-NFκB inter	19	di4	1e-3 nM^{-1} sec^{-1}	Adapted from Shih et al. 2012
IκBα-RelA:A => IκBα + RelA:A	IκB-NFκB inter	20	di-1	See Supp. Fig. 3C sec^{-1}	Predicted from Fig. 2E
IκBβ-RelA:A => IκBβ + RelA:A	IκB-NFκB inter	21	di-3	See Supp. Fig. 3C sec^{-1}	Predicted from Fig. 2E
IκBα-RelA:p50 => IκBα + RelA:p50	IκB-NFκB inter	22	di-2	See Supp. Fig. 3C sec^{-1}	Predicted from Fig. 2E
IκBβ-RelA:p50 =>IκBβ + RelA:p50	IκB-NFκB inter	23	di-4	See Supp. Fig. 3C sec^{-1}	Predicted from Fig. 2E
IκBα-NFκB =>NFκB	IκB Deg.	24	did	6e-5 sec^{-1}	Basak et al, 2007, O'Dea et al, 2007
IκBβ-NFκB =>NFκB	IκB Deg.	25	did	6e-5 sec^{-1}	

Table 2.4: Parameter Table for Model 2.4

Reaction	Category	Location	Param ID no	Parameter Value	Source
Reaction rates determined by transcripts and protein levels					
=> tIκBα (basal)	IκB Synth.	Nucleus	1	2.2e-4 nM sec^{-1}	Set to fit measured mRNA and protein expression profiles (Werner et al., 2008) and a Hill function where Hill coefficient =3
=> tIκBβ (basal)	IκB Synth.	Nucleus	2	1e-5 nM sec^{-1}	*Refer to #1*
=> tIκBε (basal)	IκB Synth.	Nucleus	3	1.33e-6 nM sec^{-1}	*Refer to #1*
=> tRelA (basal)	NFκB Synth.	Nucleus	4	1.2e-6 nM sec^{-1}	*Refer to #1*
=> tp50 (basal)	NFκB Synth.	Nucleus	5	1.2e-6 nM sec^{-1}	*Refer to #1*
IκB Reactions					
mRNA => mRNA + protein	Translation	Nuc - > Cyt	6	0.2 proteins/ mRNA sec^{-1}	Based on elongation rate of the ribosome and corrected for the nucleotide spacing between adjacent ribosomes on the same transcript: 30 nt sec-1 / 150 nt = 0.2 sec-1
.=> tIκBα (RelAp50-induced)	IκB Synth.	Nucleus	7	25 fold over constitutive	*Refer to #1*
Hill K_d (RelAp50-induced)	IκB Synth.	Nucleus	8	150 nM	*Refer to #1*
.=> tIκBβ (A50-induced, 45 min. delay)	IκB Synth.	Nucleus	9	1 fold over constitutive	*Refer to #1*
Hill K_d (RelAp50-induced)	IκB Synth.	Nucleus	10	150 nM	*Refer to #1*
.=> tIκBε (A50-induced, 45 min. delay)	IκB Synth.	Nucleus	11	125 fold over constitutive	*Refer to #1*
Hill K_d (RelAp50-induced)	IκB Synth.	Nucleus	12	150 nM	*Refer to #1*
IκBα© => IκBα(n)	Transport	Cyt -> Nuc	13	1e-2 sec^{-1}	Adapted from (Shih et al., 2009)
IκBβ© => IκBβ(n)	Transport	Cyt -> Nuc	14	1.5e-4 sec^{-1}	(Shih et al., 2009)
IκBε© => IκBε(n)	Transport	Cyt -> Nuc	15	7.5e-4 sec^{-1}	(Shih et al., 2009)
IκBα(n) => IκBα©	Transport	Nuc - > Cyt	16	2e-3 sec^{-1}	(Shih et al., 2009)
IκB[β/ε](n) => IκB[β/ε]©	Transport	Nuc - > Cyt	17	2e-4 sec^{-1}	(Shih et al., 2009)
tIκBα =>	IκB Deg.	Nucleus	18	7.3e-4 sec^{-1}	(Shih et al., 2009)
tIκBβ =>	IκB Deg.	Nucleus	19	4.8e-5 sec^{-1}	(Shih et al., 2009)
tIκBε =>	IκB Deg.	Nucleus	20	6.4e-5 sec^{-1}	(Shih et al., 2009)
IκBα =>	IκB Deg.	Cyt, Nuc	21	2e-3 sec^{-1}	(Shih et al., 2009)
IκBβ =>	IκB Deg.	Cyt, Nuc	22	2e-3 sec^{-1}	(Shih et al., 2009)

Table 2.4: Parameter Table for Model 2.4, Continued

Reaction	Category	Location	Param ID no	Parameter Value	Source
IκB[α/β/ε]-NFκB => NFκB	IκB Deg.	Cyt, Nuc	24	4e-6 sec^{-1}	Basak et al, 2007, O'Dea et al, 2007
IκBα => (NEMO-mediated)	IκB Deg.	Cytoplasm	25	2.25e-5 nM^{-1} sec^{-1}	O'Dea et al, 2007
IκBα-NFκB => NFκB (NEMO-mediated)	IκB Deg.	Cytoplasm	25	2.25e-5 nM^{-1} sec^{-1}	
IκBβ => (NEMO-mediated)	IκB Deg.	Cytoplasm	26	7.5e-6 nM^{-1} sec^{-1}	*Refer to # 25*
IκBβ-NFκB => NFκB (NEMO-mediated)	IκB Deg.	Cytoplasm	26	7.5e-6 nM^{-1} sec^{-1}	*Refer to # 25*
IκBε => (NEMO-mediated)	IκB Deg.	Cytoplasm	27	1.5e-5 nM^{-1} sec^{-1}	*Refer to # 25*
IκBε-NFκB => NFκB (NEMO-mediated)	IκB Deg.	Cytoplasm	27	1.5e-5 nM^{-1} sec^{-1}	*Refer to # 25*
NFκB reactions					
tRelA =>	NFκB Deg.	Nucleus	28	4.8e-5 sec^{-1}	(Shih et al., 2009)
tp50 =>	NFκB Deg.	Nucleus	29	4.8e-5 sec^{-1}	(Shih et al., 2009)
RelA =>	NFκB Deg.	Cyt, Nuc	30	3.85e-4 sec^{-1}	Based on estimated 30 min half-life of NFκB monomers
p50 =>	NFκB Deg.	Cyt, Nuc	31	3.85e-4 sec^{-1}	
RelA + RelA => RelA:A	NFκB Synth.	Nucleus	32	1e-5 nM^{-1} sec^{-1}	This study (Fig. 1B,1C)
RelA + p50 => RelA:p50	NFκB Synth.	Nucleus	33	3.16e-5 nM^{-1} sec^{-1}	
p50 + p50 => p50:p50	NFκB Synth.	Nucleus	34	3e-5 nM^{-1} sec^{-1}	
RelA + RelA => RelA:A	NFκB Synth.	Cytoplasm	35	1e-5 nM^{-1} sec^{-1}	This study (Fig. 1B,1C)
RelA + p50 => RelA:p50	NFκB Synth.	Cytoplasm	36	3.16e-5 nM^{-1} sec^{-1}	
p50 + p50 => p50:p50	NFκB Synth.	Cytoplasm	37	3e-5 nM^{-1} sec^{-1}	
RelA:A => RelA + RelA	NFκB Synth.	Nucleus	38	8e-4 sec^{-1}	This study (Fig. 1B,1C)
RelA:p50 => RelA + p50	NFκB Synth.	Nucleus	39	3.16e-5 sec^{-1}	
p50:p50 => p50 + p50	NFκB Synth.	Nucleus	40	9e-5 sec^{-1}	
RelA:A => RelA + RelA	NFκB Synth.	Cytoplasm	41	8e-3 sec^{-1}	This study (Fig. 1B,1C)
RelA:p50 => RelA + p50	NFκB Synth.	Cytoplasm	42	3.16e-4 sec^{-1}	
p50:p50 => p50 + p50	NFκB Synth.	Cytoplasm	43	9e-4 sec^{-1}	
NFκB© => NFκB(n)	Transport	Cyt -> Nuc	44	9e-2 sec^{-1}	(Shih et al., 2009)
NFκB(n) => NFκB©	Transport	Nuc -> Cyt	45	8e-5 sec^{-1}	(Shih et al., 2009)
NFκB =>	NFκB Deg.	Cyt, Nuc	46	4e-6 sec^{-1}	Based on estimated 48 hour half-life
IκB[α/β/ε]-NFκB => IκB[α/β/ε]	NFκB Deg.	Cyt, Nuc	47	4e-6 sec^{-1}	*Refer to #24*
IκB-NFκB interactions					
IκBα + RelA:A => IκBα-RelA:A	IκB-NFκB inter	Cyt, Nuc	48	1e-3 nM^{-1} sec^{-1}	Adapted from Shih et al. 2012
IκBβ + RelA:A => IκBβ-RelA:A	IκB-NFκB inter	Cyt, Nuc	49	1e-3 nM^{-1} sec^{-1}	
IκBε + RelA:A => IκBε-RelA:A	IκB-NFκB inter	Cyt, Nuc	50	1e-3 nM^{-1} sec^{-1}	
IκBα + RelA:p50 => IκBα-RelA:p50	IκB-NFκB inter	Cyt, Nuc	51	1e-3 nM^{-1} sec^{-1}	Adapted from Shih et al. 2012
IκBβ + RelA:p50 => IκBβ-RelA:p50	IκB-NFκB inter	Cyt, Nuc	52	1e-3 nM^{-1} sec^{-1}	

Table 2.4: Parameter Table for Model 2.4, Continued

Reaction	Category	Location	Param ID no	Parameter Value	Source
IκBε + RelA:p50 => IκBε-RelA:p50	IκB-NFκB inter	Cyt, Nuc	53	1e-3 nM^{-1} sec^{-1}	
IκBα-RelA:A => IκBα + RelA:A	IκB-NFκB inter	Cyt, Nuc	54	1e-4 sec^{-1}	This study (Fig. 2E)
IκBβ-RelA:A => IκBβ + RelA:A	IκB-NFκB inter	Cyt, Nuc	55	3.2e-6 sec^{-1}	
IκBε-RelA:A => IκBε + RelA:A	IκB-NFκB inter	Cyt, Nuc	56	1e-4 sec^{-1}	
IκBα-RelA:p50 => IκBα + RelA:p50	IκB-NFκB inter	Cyt, Nuc	57	2.51e-6 sec^{-1}	This study (Fig. 2E)
IκBβ-RelA:p50 => IκBβ + RelA:p50	IκB-NFκB inter	Cyt, Nuc	58	2.51e-1 sec^{-1}	
IκBε-RelA:p50 => IκBε + RelA:p50	IκB-NFκB inter	Cyt, Nuc	59	2.51e-6 sec^{-1}	
IκBα-NFκB© => IκBα-NFκB(n)	Transport	Cyt -> Nuc	60	4.6e-3 sec^{-1}	(Shih et al., 2009)
IκBβ-NFκB© => IκBβ-NFκB(n)	Transport	Cyt -> Nuc	61	4.6e-4 sec^{-1}	(Shih et al., 2009)
IκBε-NFκB© => IκBε-NFκB(n)	Transport	Cyt -> Nuc	62	2.6e-3 sec^{-1}	(Shih et al., 2009)
IκBα-NFκB(n) => IκBα-NFκB©	Transport	Nuc -> Cyt	63	1.4e-2 sec^{-1}	(Shih et al., 2009)
IκBβ-NFκB(n) => IκBβ-NFκB©	Transport	Nuc -> Cyt	64	7e-3 sec^{-1}	(Shih et al., 2009)
IκBε-NFκB(n) => IκBε-NFκB©	Transport	Nuc -> Cyt	65	7e-3 sec^{-1}	(Shih et al., 2009)

Table 2.5: Probable and improbable parameter sets

Combination of Points		Kd (nM)	Kd (nM)		Kd (nM)	Kd (nM)					
ikba	ikbb	IκBα - A:A	IκBα - A:50		IκBβ -A:A	IκBβ - A:50		Fig. 3B/C	Fig. 3D/E	Fig. 3F/G	pass
1	A	1.58	251	probable	0.0032	251	probable	1	0	1	0
1	B	1.58	251	probable	0.0032	7.94	probable	1	0	0	0
1	C	1.58	251	probable	0.0501	251	probable	1	0	0	0
1	D	1.58	251	probable	0.0501	7.94	probable	1	0	0	0
1	E	1.58	251	probable	79.4	251	improbable	0	0	0	0
1	F	1.58	251	probable	7.94	0.794	improbable	0	0	0	0
1	G	1.58	251	probable	0.0032	0.0079	improbable	1	0	0	0
2	A	0.251	0.794	probable	0.0032	251	probable	1	1	0	0
2	B	0.251	0.794	probable	0.0032	7.94	probable	1	1	0	0
2	C	0.251	0.794	probable	0.0501	251	probable	0	1	0	0
2	D	0.251	0.794	probable	0.0501	7.94	probable	0	1	0	0
2	E	0.251	0.794	probable	79.4	251	improbable	0	0	0	0
2	F	0.251	0.794	probable	7.94	0.794	improbable	0	0	0	0
2	G	0.251	0.794	probable	0.0032	0.0079	improbable	0	0	0	0
3	A	0.1	0.0025	probable	0.0032	251	probable	1	1	1	1
3	B	0.1	0.0025	probable	0.0032	7.94	probable	1	1	1	1
3	C	0.1	0.0025	probable	0.0501	251	probable	1	1	0	0
3	D	0.1	0.0025	probable	0.0501	7.94	probable	1	1	0	0
3	E	0.1	0.0025	probable	79.4	251	improbable	1	0	0	0
3	F	0.1	0.0025	probable	7.94	0.794	improbable	1	0	0	0
3	G	0.1	0.0025	probable	0.0032	0.0079	improbable	1	0	0	0
4	A	0.0251	251	improbable	0.0032	251	probable	1	0	0	0
4	B	0.0251	251	improbable	0.0032	7.94	probable	1	0	0	0
4	C	0.0251	251	improbable	0.0501	251	probable	1	0	0	0
4	D	0.0251	251	improbable	0.0501	7.94	probable	1	0	0	0
4	E	0.0251	251	improbable	79.4	251	improbable	1	0	0	0
4	F	0.0251	251	improbable	7.94	0.794	improbable	1	0	0	0
4	G	0.0251	251	improbable	0.0032	0.0079	improbable	1	0	0	0
5	A	0.0025	25.1	improbable	0.0032	251	probable	1	0	0	0
5	B	0.0025	25.1	improbable	0.0032	7.94	probable	1	0	0	0
5	C	0.0025	25.1	improbable	0.0501	251	probable	1	0	0	0
5	D	0.0025	25.1	improbable	0.0501	7.94	probable	1	0	0	0

Table 2.5: Probable and Improbable Parameter Sets, Continued

Combination of Points		Kd (nM)	Kd (nM)		Kd (nM)	Kd (nM)					
5	E	0.0025	25.1	improbable	79.4	251	improbable	1	0	0	0
5	F	0.0025	25.1	improbable	7.94	0.794	improbable	1	0	0	0
5	G	0.0025	25.1	improbable	0.0032	0.0079	improbable	1	0	0	0
6	A	0.0351	0.794	improbable	0.0032	251	probable	1	1	0	0
6	B	0.0351	0.794	improbable	0.0032	7.94	probable	1	1	0	0
6	C	0.0351	0.794	improbable	0.0501	251	probable	1	1	0	0
6	D	0.0351	0.794	improbable	0.0501	7.94	probable	1	1	0	0
6	E	0.0351	0.794	improbable	79.4	251	improbable	1	0	0	0
6	F	0.0351	0.794	improbable	7.94	0.794	improbable	1	0	0	0
6	G	0.0351	0.794	improbable	0.0032	0.0079	improbable	1	0	0	0
7	A	79.4	251	improbable	0.0032	251	probable	1	0	1	0
7	B	79.4	251	improbable	0.0032	7.94	probable	1	0	1	0
7	C	79.4	251	improbable	0.0501	251	probable	1	0	1	0
7	D	79.4	251	improbable	0.0501	7.94	probable	1	0	1	0
7	E	79.4	251	improbable	79.4	251	improbable	0	0	0	0
7	F	79.4	251	improbable	7.94	0.794	improbable	0	0	0	0
7	G	79.4	251	improbable	0.0032	0.0079	improbable	1	0	0	0

Combinations of the probable and improbable parameter sets chosen from Fig. 2E and whether they pass each test in Fig. 3 individually.

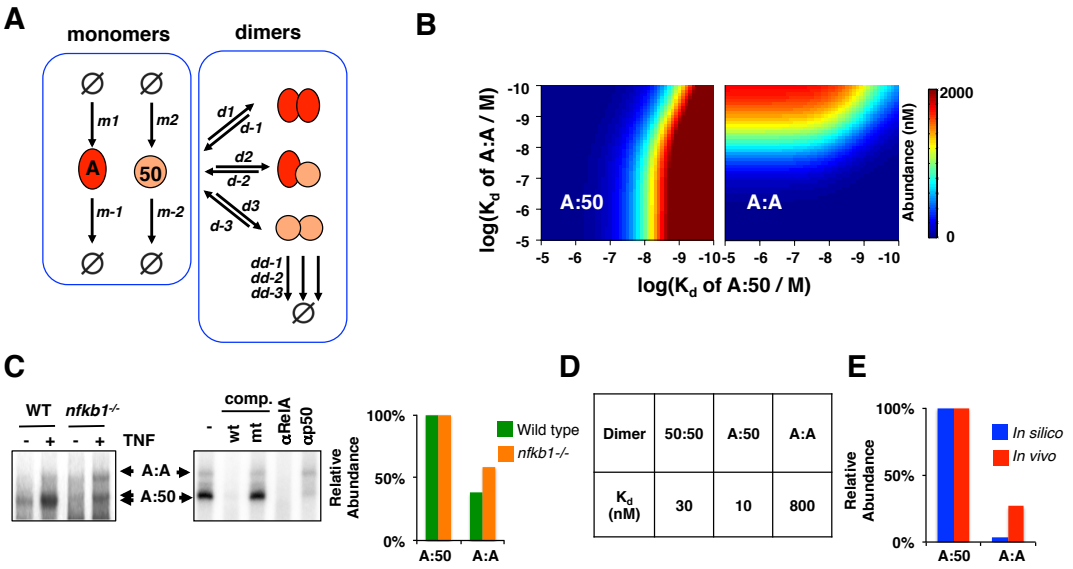

Figure 2.1: Biophysical measurements do not account for in vivo NFκB dimer repertoire

A. A schematic of a simple model depicting the dimerization of NFκB RelA and p50 polypeptides. *m1* and *m2* are synthesis rate constants, *m-1* and *m-2* are degradation rate constants. *d1, d2*, and *d3* are dimer association rate constants, while *d-1, d-2,* and *d-3* are dimer dissociation rate constants. *dd-1*, *dd-2*, and *dd-3* are dimer degradation rate constants. B. Heat maps of protein abundances of A:A and A:50 dimers computationally simulated as a function of the dimer affinities (Kd). These were generated by the model schematized in (A). C. Electrophoretic mobility shift assays (EMSA) with nuclear extracts prepared from TNF-stimulated (30 min) mouse embryo fibroblasts (MEFs) of indicated genotype (left panel). The right panel confirms the identity of the indicated DNA-protein complexes using competition (comp.) with a 100-fold excess of unlabeled probe that either contains the wild type (wt) or mutant (mt) κB site sequence. The RelA and p50 antibody (a-RelA and a-p50) are used in shift-ablation studies to confirm that the identity of the A:A-DNA and A:50-DNA complexes. D. Summary table of dimer affinities as measured by analytical ultracentrifugation (AUC) and quantitative gel-filtration analysis of purified recombinant proteins (Supplemental Fig. 1B-E). The A:A homodimer affinity is lower than those of p50-containing dimers. E. Both bar graphs are quantitations from Fig. 1C. The top panel is a bar graph comparison of wild type (green) and *nfkb1-/-* (orange) abundances of A:A and A:50 dimers. The bottom panel is a bar graph comparison of model predicted (blue) and experimentally measured (red) abundances of A:A and A:50 dimers.

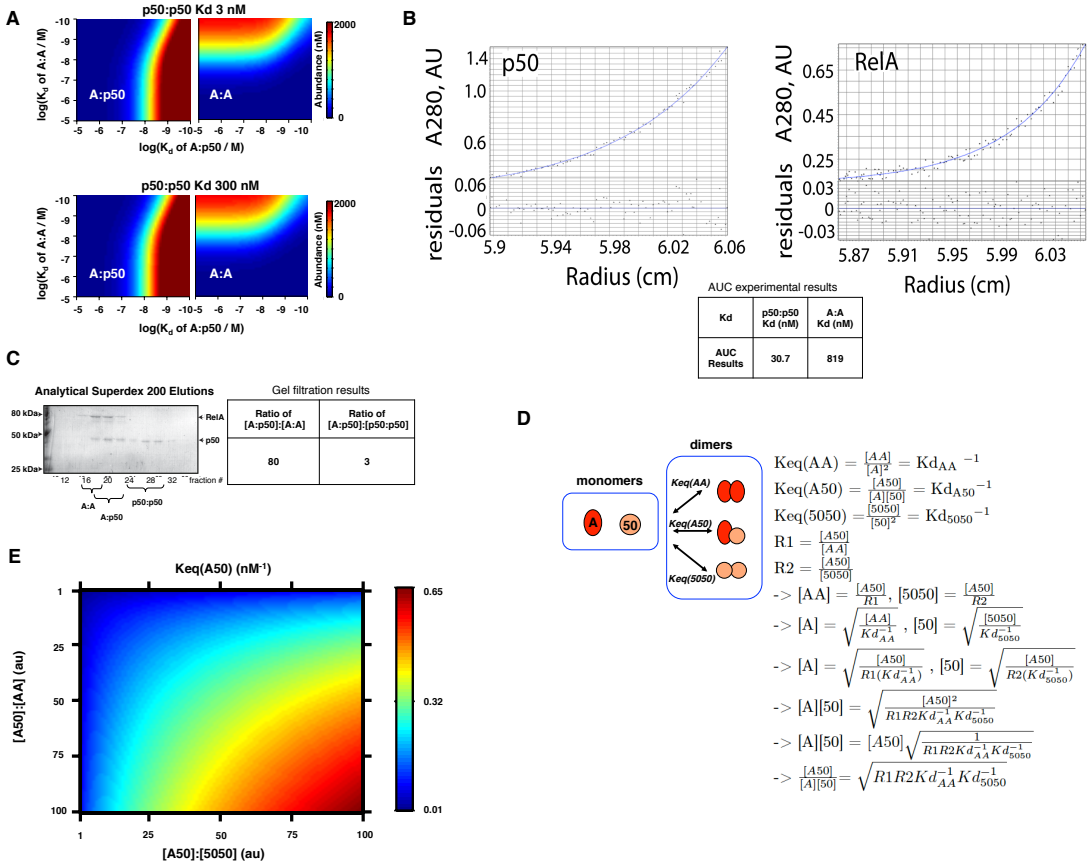

Figure 2.2: Biophysical measurements to determine NFκB dimer affinities

A. A:A and A:p50 abundances were calculated from Model 1 as in Fig. 1B through variation of the A:A and A:p50 dimer affinities but using a 10 fold less than and 10 fold greater than the wild type p50:p50 affinity. B. Analytical ultra-centrifugation analysis of the RelA and p50 dimerization domains and the summary of the results, resulting in an affinity of ~30 nM for p50:p50 and ~800 nM for A:A. C. Gel filtration of RelA and p50 dimerization domain samples were done to determine the ratio of the A:p50 heterodimer to the A:A homodimer or the p50 homodimer. D. Using basic equilibrium equations, the affinity of the A:p50 heterodimer can be calculated using the ratios of the A:p50 heterodimer to each homodimer (Supplmentary Fig. 1C) is known and the affinities of each homodimer (Supplementary Fig. 1B). E. The range of affinities that the equation predicts over a range of the ratios of the concentration of A:p50 to each homodimer, A:A and p50:p50.

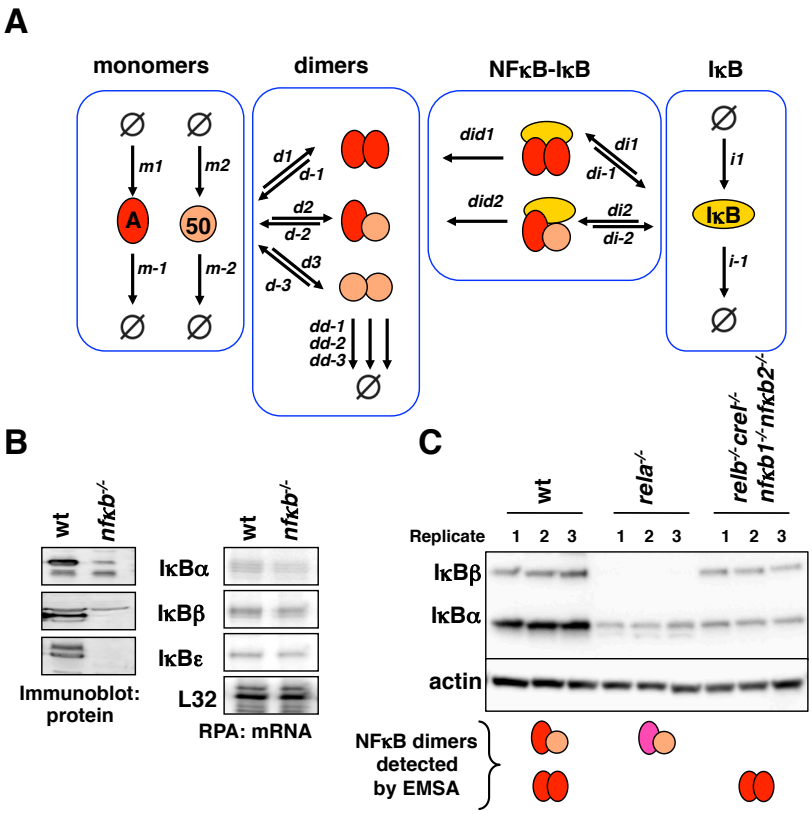

Figure 2.3: Deriving IκB-NFκB affinities
A. A schematic of the dimerization model of RelA and p50 NFκB polypeptides with the addition of the inhibitor of NFkB (IkB). *m1* and *m2* are RelA and p50 synthesis rate constants, *m-1* and *m-2* are RelA and p50 degradation rate constants. *d1, d2*, and *d3* are dimer association rate constants, while *d-1, d-2,* and *d-3* are A:A, A:p50, and p50:p50 dimer dissociation rate constants. *dd-1*, *dd-2*, and *dd-3* are A:A, A:p50, and p50:p50 dimer degradation rate constants. *i1* is the IkB synthesis rate constant, *i-1* is the IkB degradation rate constant. *di1* and di2 are the IkB-NFkB association rate constants. *di-1* and *di-2* are the IkB-NFkB dissociation rate constants. *did1* and *did2* are the IkB-NFkB degradation rate constants of IkB to release NFkB. B. Whole cell extracts of wild type MEFs and MEFs deficient in canonical NFκB genes (RelA, cRel, and p50) show an absence of canonical IkB proteins, without a significant decrease in mRNA abundance. C. IκB protein abundance could be measured in different NFκB dimer composite MEFs as compared to wild type MEFs. MEFs containing only A:A homodimers have approximately equal levels of IκBβ, but lower levels of IκBα, while MEFs containing the cRel:p50 heterodimer has undetectable levels of IκBβ and lowered levels of IκBα.

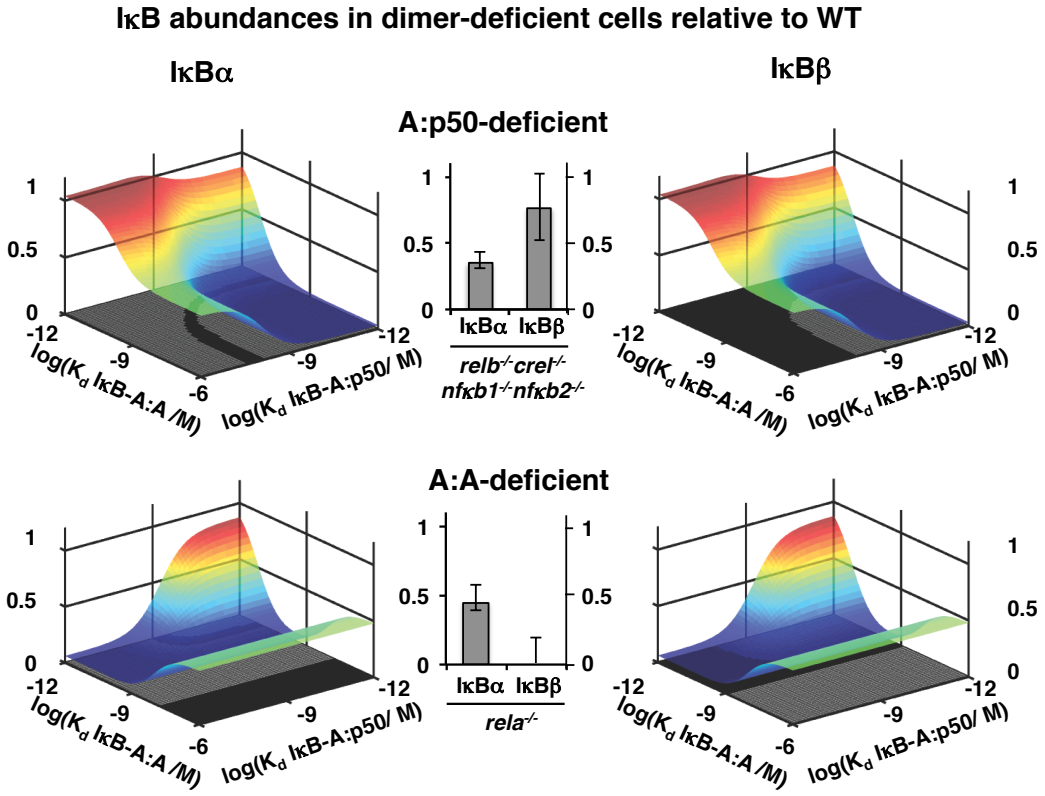

Figure 2.4: Deriving IκB-NFκB affinities via relative abundances
The basal abundance of IκB in different genotypes (WT, RelA:A homodimer-deficient and RelA:p50 heterodimer-deficient) was predicted using the model from Fig. 2A over a range of varying IκB-NFκB affinities, and the ratio of the IκB abundances in the specific NFκB dimer deficient cells to WT cells was determined from Fig. 2C and indicated by the surface. These abundances were used to constrain the allowable range of allowable IkB–NFκB affinities, indicated by the darker shadows on the xy-plane.

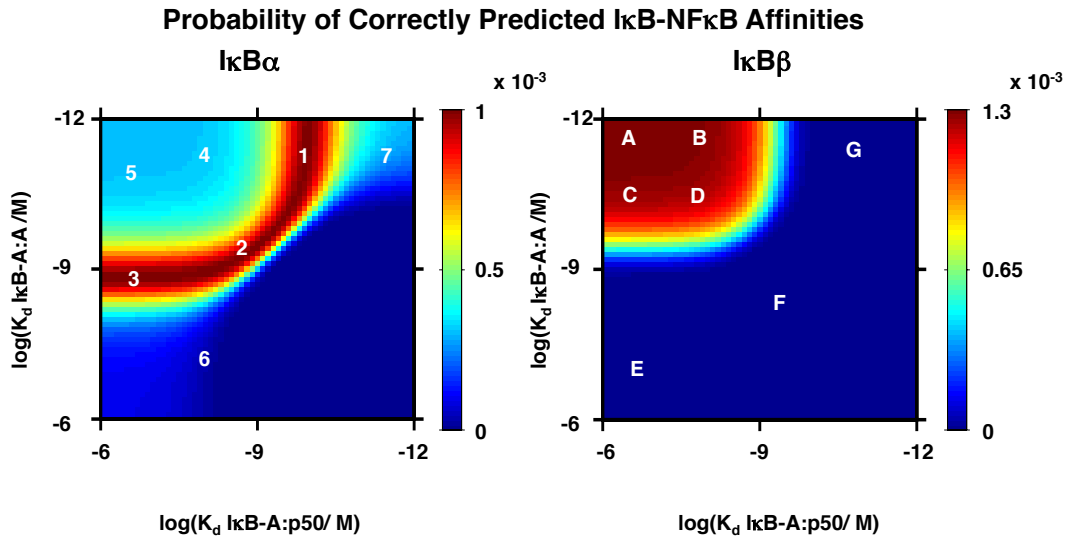

Figure 2.5: Probable IκB-NFκB affinities
The predicted affinities from Fig. 2D is used with assumed A:A, A:p50, and p50:p50 dimer affinities from the AUC data in Fig 1B. These probabilities of the model's fit for the given predicted affinities from the observed experimental value were calculated using the normal distribution of the model's prediction at a particular point with the variance of the experimental data. The most probable IkB-NFκB affinities are in red, while the least probable affinities are in dark blue. Specific probable and improbable parameters were used for model predictions in Fig. 3 and are listed in the Supplementary Fig. 3C.

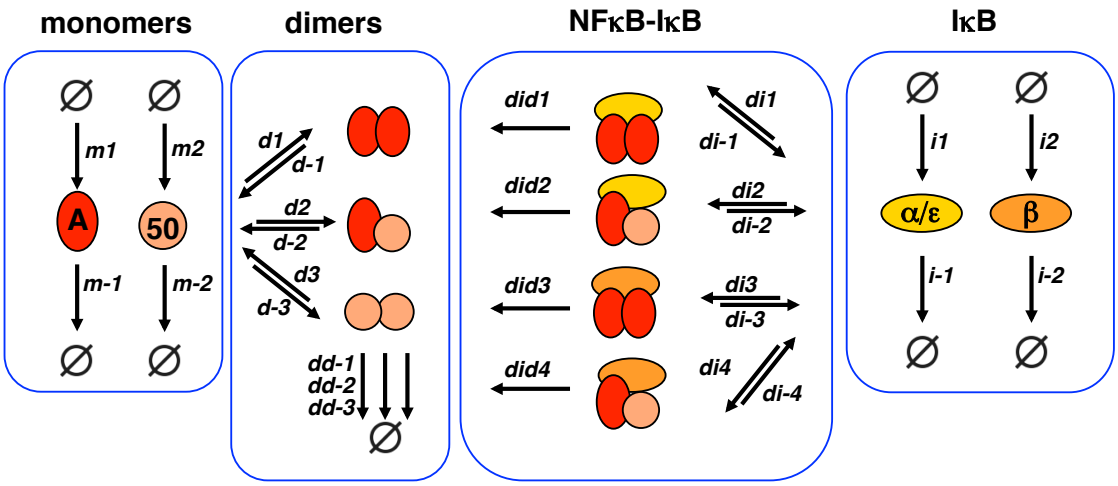

Figure 2.6: Model schematic of Rel-NFκB including specific IκBs
A schematic of the dimerization model of RelA and p50 NFκB polypeptides with the addition of specific inhibitors of NFkB, IκBα and IκBβ. *m1* and *m2* are RelA and p50 synthesis rate constants, *m-1* and *m-2* are RelA and p50 degradation rate constants. *d1, d2*, and *d3* are dimer association rate constants, while *d-1, d-2,* and *d-3* are A:A, A:p50, and p50:p50 dimer dissociation rate constants. *dd-1*, *dd-2*, and *dd-3* are A:A, A:p50, and p50:p50 dimer degradation rate constants. *i1* and *i2* are the IkB synthesis rate constants, *i-1* and *i-2* are the IkB degradation rate constants. *di1,di2*, *di3*, and *di4* are the IkB-NFkB association rate constants. *di-1*, *di-2, di-3,* and *di-4* are the IkB-NFkB dissociation rate constants. *did1, did2, did3,* and *did4* are the IkB-NFkB degradation rate constants of IkB to release NFkB.

Figure 2.7: Iterative testing and refinement of IκBβ-RelA:RelA preference model

A. Using the model from Fig. 3A and the combination of IkB-NFkB affinities from Supplementary Fig. 3C, different levels of total RelA protein abundance in the RelA:p50 deficient cells relative to wild type cells were predicted, where probable affinities are depicted in red and improbable affinities are predicted in blue. B. There is >0.5 fold RelA abundance in RelA:p50 deficient MEFs as compared to WT MEFs. C. Using the model from Fig. 3A and the combination of IkB-NFkB affinities from Supplementary Fig. 3C, the abundances of IkB bound NFkB were predicted. The probable affinities (red) consistently predict more IkBb than IkBa bound to A:A homodimer. The improbable affinities (blue) predict variable binding of the A:A homodimer to the two IkBs. Both probable and improbable parameter sets predict variable binding of the A:p50 heterodimer to the two IkBs. D. Deoxycholate (DOC) treated cellular extracts result in the separation of NFκB dimers from their IkB-bound form and can be run on an electrophoretic mobility shift assay to determine the amount of NFkB dimers at the basal state. Pre-immunodepletion of the extracts by antibodies to IkBa or IkBb result in the depletion of IkB-bound NFκB dimer binding to the DNA probe after treatment with DOC and run on an. This indicated that there is more IκBβ (>0.5) than IκBα bound to the RelA:A homodimer and more IkBa (>0.5) than IkBb bound to the RelA:p50 heterodimer. E. Using the model from Fig. 3A and the combination of IkB-NFkB affinities from Supplementary Fig. 3C, the basal abundance of the RelA:A homodimer in IκBβ-deficient cells is predicted to be lower than in WT, while the RelA:A homodimer abundance of IκBα-deficient cells is similar to WT cells in the model with probable affinities (red). Improbable affinities predict variable levels of basal RelA:A homodimer abundance in the three genotypes. F. DOC treated cellular extracts show that there is a significant loss of RelA:A homodimer formation in IκBβ-deficient cells (<0.2x of WT) while IκBα-deficient cells have similar levels of RelA:A homodimer formation (>0.97x) as WT cells.

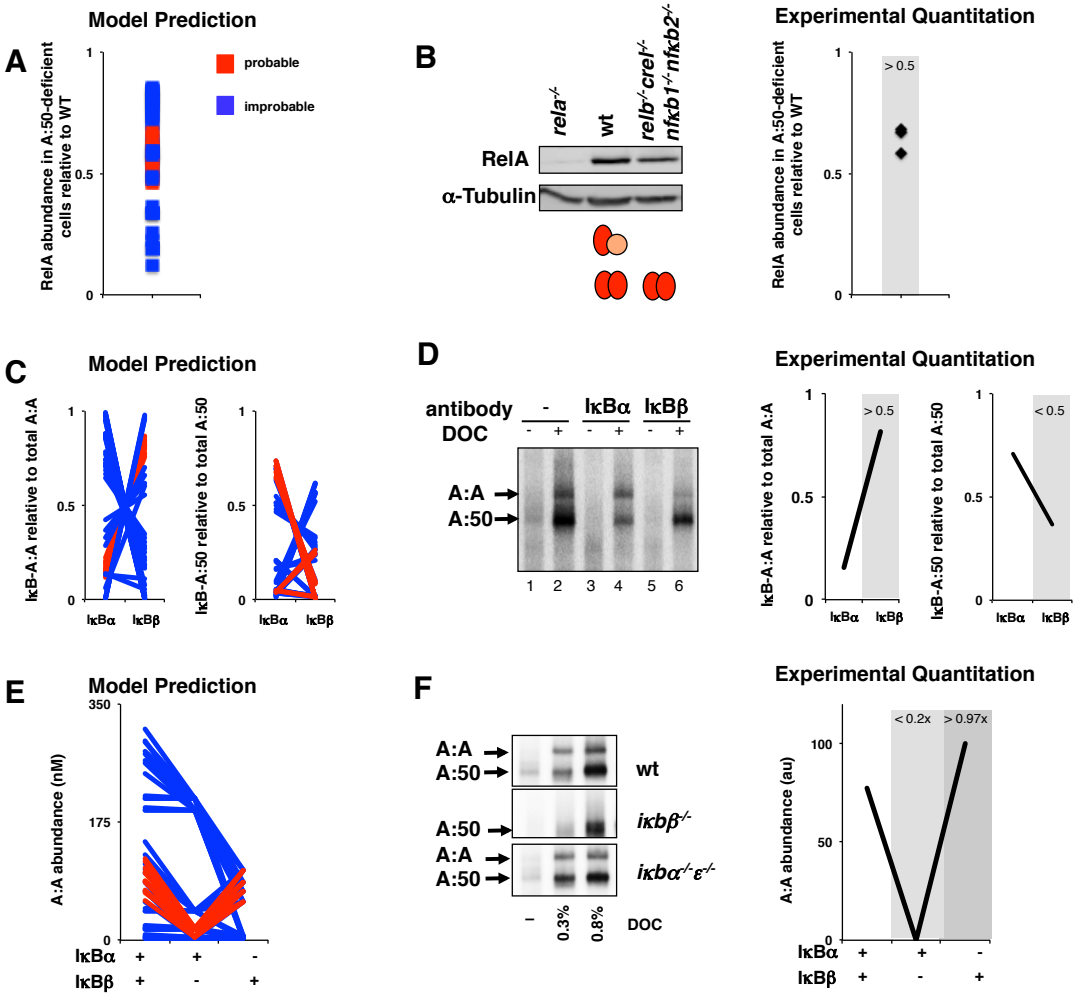
A
Model Prediction
RelA abundance in A:50-deficient cells relative to WT
probable
improbable
B
rela-/-
wt
relb-/-crel-/-
nfkb1-/-nfkb2-/-
RelA
α-Tubulin
Experimental Quantitation
RelA abundance in A:50-deficient cells relative to WT
> 0.5
C
Model Prediction
IκB-A:A relative to total A:A
IκB-A:50 relative to total A:50
IκBα
IκBβ
D
antibody
DOC
IκBα
IκBβ
A:A
A:50
1 2 3 4 5 6
Experimental Quantitation
IκB-A:A relative to total A:A
IκB-A:50 relative to total A:50
> 0.5
< 0.5
E
Model Prediction
A:A abundance (nM)
350
175
IκBα + + -
IκBβ + - +
F
A:A
A:50
wt
iκbβ-/-
iκbα-/-ε-/-
–
0.3%
0.8%
DOC
Experimental Quantitation
A:A abundance (au)
< 0.2x
> 0.97x
IκBα + + -
IκBβ + - +

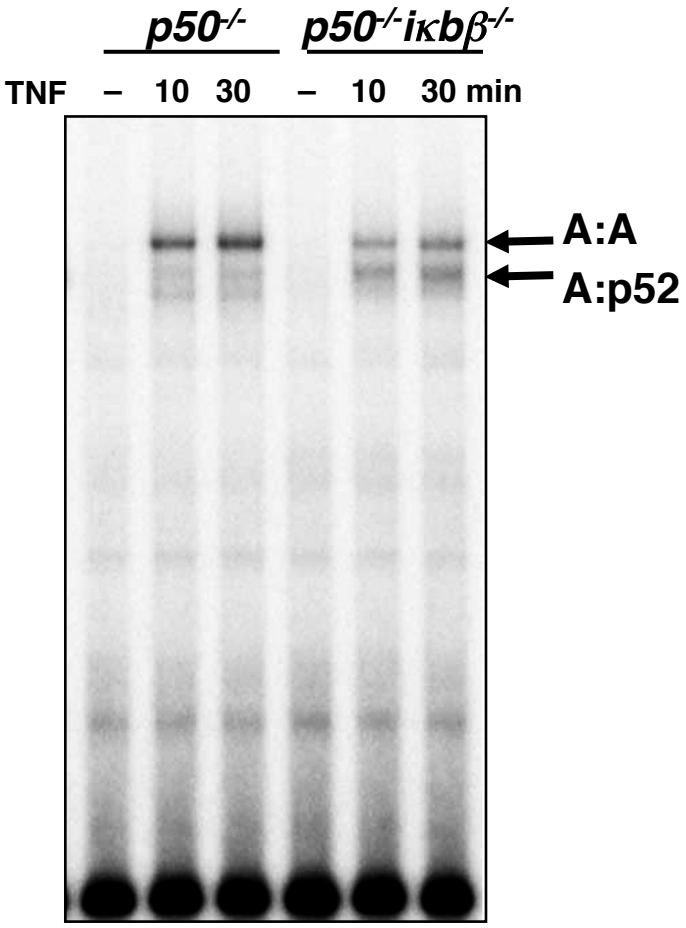

Figure 2.8: IκBβ is important in RelA:RelA homodimer formation
Electrophoretic shift mobility assay of nuclear extracts of p50- deficient and p50/IkBb-deficient MEFs treated with TNF at 10 and 30 minutes. A:A homodimers are readily detectable in p50-deficient MEFs, but upon additional IκBβ-deficiency, A:p52 dimers form and less A:A homodimers are formed.

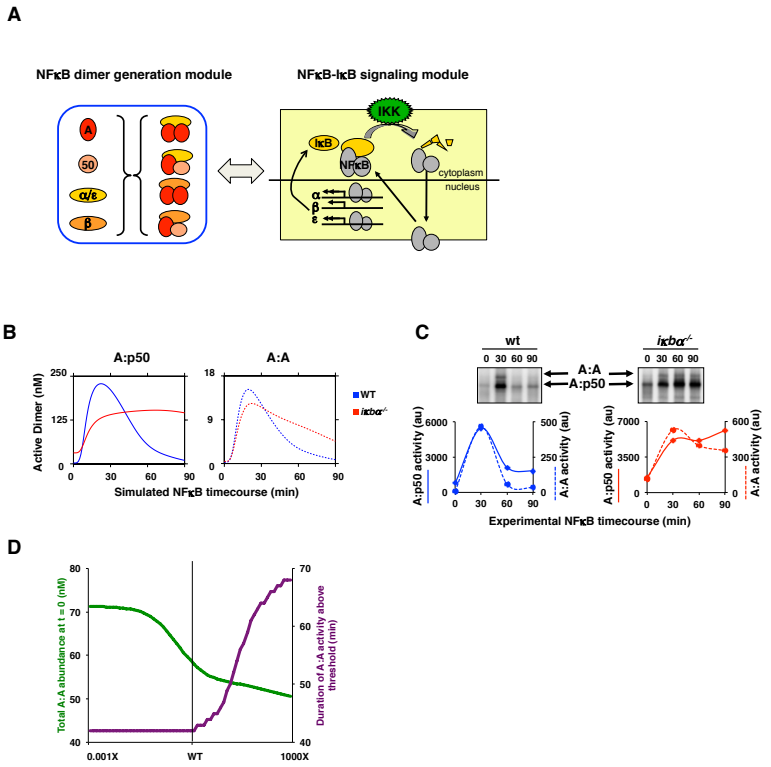

Figure 2.9: Whereas IκBβ is an indispensible regulator in the Rel-NFκB dimer generation module, IκBα is a key regulator of the IκB-NFκB signaling module.

A. The IκB-NFκB interaction module was incorporated into a signaling module including stimulus-induced activation of NFκB. The RelA and p50 monomers were explicitly added into an adaptation of the previously published Werner 2008 model, with A:A, A:p50, and p50:p50 dimers. IκBα, IκBβ, and IκBe have interactions with the A:A and A:p50 dimers, and their affinities were predicted from the previous tests in Fig. 3 from the combinations from Supplementary Fig. 3C. A full schematic is depicted in Supplementary Fig. 5A. B. Model simulations of TNF stimulated NFκB dimer activity predicted that in IκBα-deficient cells, both the A:p50 heterodimer and the A:A homodimer would have prolonged activation as compared to wild-type MEFs. C. Nuclear extracts of wild-type and IkBa-deficient MEFs were prepared from TNF stimulated cells at 30, 60 and 90 minutes. Quantitation of the A:A and A:50 NFkB dimers show prolonged activation as compared to wild-type MEFs. D. Changing the affinity between IκBα and the RelA:A homodimer in the model illustrates that the duration of RelA:A homodimer activity is dependent on affinity, but the total abundance of RelA:A homodimer stays unchanged and only increases at very high affinities between IκBα and the RelA:A homodimer.

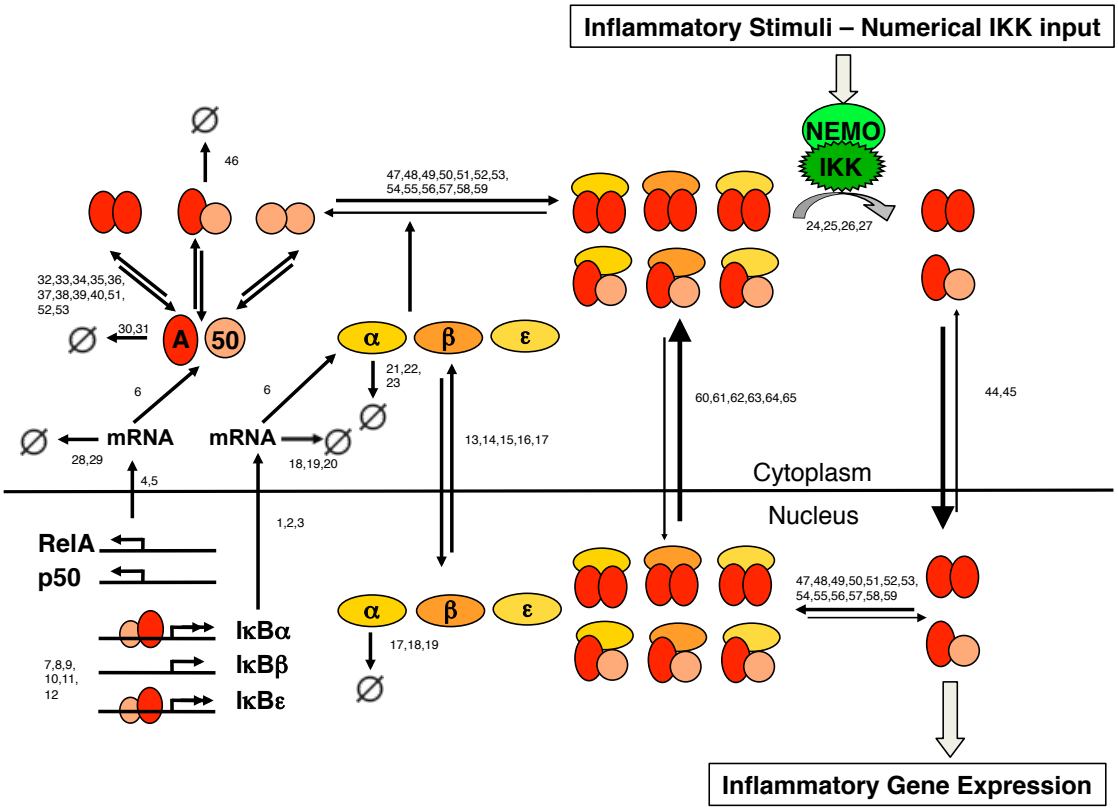

Figure 2.10: Multi-dimer model of NFκB signaling
A schematic of the full multi-dimer model with TNF-induced signaling that integrates the Rel-NFκB dimer generation module with the IκB-NFκB signaling module. Parameters are from Model 4 and Table 2.4.

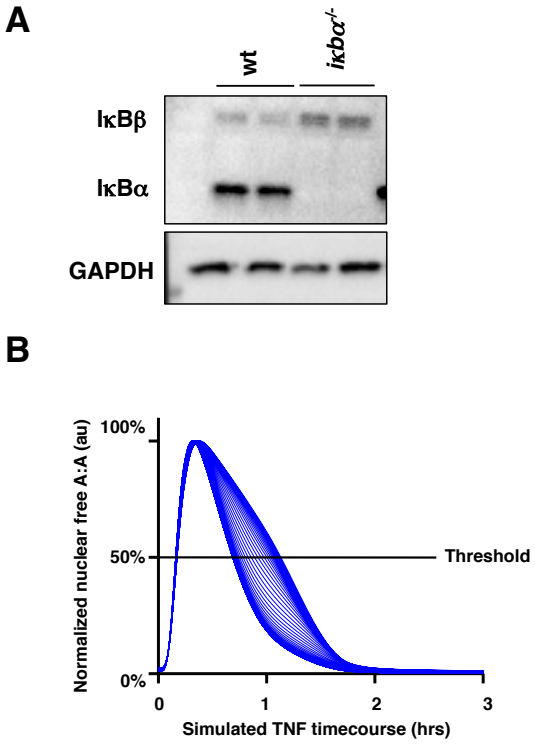

Figure 2.11: Analysis of IκBα-A:A interaction affinity
A. Immunoblot for the indicated proteins of whole cell extracts of wild-type and IκBα-deficient MEFs. B. Computational prediction using the model depicted by Fig. 2.10, where the IκBα-A:A interaction affinity was varied, and the duration of NFκB activity is defined as the amount of time greater than 50% of the maximum free A:A in the nucleus.

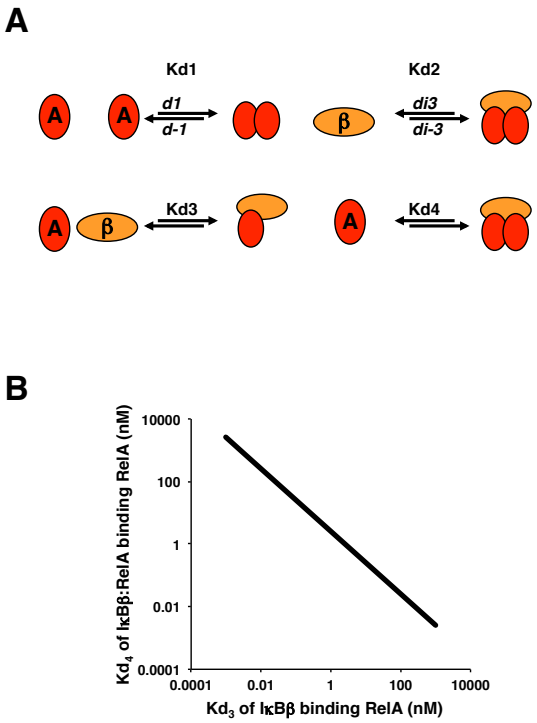

Figure 2.12: A 2-step IκBβ-A:A interaction model
A. A schematic of the comparison of the original model (top) shown in Fig. 3A to a 2-step model (bottom), in which IκBβ binds one RelA monomer before binding another RelA monomer. *d1* is the A:A dimer association rate constant and *d-1* is the A:A dimer dissociation rate constant, where Kd1 is the dimer dissociation constant (~800 nM). *di3* is the IκBβ-A:A association rate constant and *di-3* is the IκBβ-A:A dissociation rate constant, where Kd2 is the IκBβ-A:A dissociation constant (3.2 pM). Kd3 is the dissociation constant between IκBβ and a RelA monomer, and Kd4 is the dissociation constant between IκBβ:A and a second RelA monomer. B. A graph depicting the relationship between the Kd3 and Kd4 of the 2-step model (panel A) given known affinities of A:A dimerization (Kd = 800 nM) and IκBβ-A:A interaction (Kd = 3.2 pM).

Chpater 3: IκBε is a key negative feedback regulator of cRel containing NFκB dimers in B-lymphocytes

3.1 Introduction

In Chapter 2 we established the novel role of IκBβ's function as a chaperone in for the A:A homodimer in fibroblasts. We also demonstrated the importance of monomer competition that occurs in NFκB generation in fibroblasts. Here, we look at the role of IκBε as a key negative feedback regulator of cRel containing NFκB dimers in B-lymphocytes. While major insights into the mechanism of NFκB control have largely been derived from cell lines such as fibroblasts and HeLa cells, much of NFκB's major physiological functions lie in B cells, where NFκB plays an important role in regulating both proliferation and survival in adaptive immune responses (Doi et al., 1997; Gerondakis et al., 1998, 2006; Ghosh and Hayden, 2008; Grumont and Gerondakis, 1994; Grumont et al., 1998; Köntgen et al., 1995; Sha et al., 1995; Sriskantharajah et al., 2009). When activated by antigenic or pathogenic stimulation, B cells have been shown to have an increase in the nuclear DNA binding activity from both RelA:p50 and cRel:p50 dimers. However, the majority of previous studies have suggested that cRel and p50 are the critical NFκB monomers in controlling B cell proliferation, not RelA (Gerondakis et al., 1998, 2006; Grumont et al., 1998).

There are various NFκB dimers in different cell types, and the cRel:p50 dimer is known to play a critical role in B cell proliferation and survival. However, it is still unclear how cRel:p50 activity in B cells is controlled. While IκBα is known to control A:A and A:50 dimers in fibroblasts, IκBε only plays a secondary role in controlling the activity of NFκB in fibroblasts, as IκBε can compensate for an IκBα deficiency but there is no phenotype in IκBε deficiency (Kearns et al., 2006). Additionally, IkBa binds preferentially to A:50 dimers while IκBε can associate with RelA- and cRel- containing dimers (Li and Nabel, 1997; Simeonidis et al., 1997; Whiteside et al., 1997). These differences suggest that IκBα and IκBε have specific and distinct roles in the control of NFκB dimers.

In this study, we find that there is a stimulus specific effect on the increase of late NFκB activity in IkBe deficient B cells. This work was done in collaboration with a previous member of the lab, and we used a combined mathematical modeling and biochemical analysis of B cells in order to demonstrate the importance of IκBε in limiting B cell expansion through negative feedback. The mathematical model generated for this chapter showed that the critical role of IκBε's negative feedback is dimer-specific through differential kinetics.

3.2 Materials and Methods

Cell isolation and culture

Spleens were harvested from C57Bl6 mice wild-type (Jackson Labs, Bar Harbor, MN), and C57Bl6 IkBe$^{-/-}$ mice. The collected spleens were homogenized using frosted glass slide grinding. For B cell isolation, homogenized splenocytes were incubated with anti-CD43 (Ly-48) microbeads for 15 minutes at room temperature. Following this incubation, the cells were washed with Hanks Buffered salt solution (HBSS) (Gibco 14170) containing 1% FCS, 10mM HEPES (Gibco 15630) and 1% FCS (Sigma F2442) and separated over a magnetic column (LS column Miltenyi Biotec 130-042-401). For B cells, purity was determined by flow cytometry using PE anti-B220 (ebioscience 12-0452-83), FITC anti-CD3 (ebioscience 11-0031-82), APC anti-CD4 (ebioscience 17-0041-83) and PerCP anti-CD8 (ebioscience 46-0081-82). Purity was consistently found to be between 92% and 95% (data not shown). For experiments where separation of marginal zone (MZ) B cell and follicular B cell was performed, anti-CD43 magnetically separated B cells were stained with APC anti-CD9 (ebioscience 17-0091-82) and B cell population separation was performed using a FACS-ARIA II cell sorter (BD bioscience). Complete media consisting of RPMI-1640 (Gibco 11875), 10 mM HEPES (Gibco 15630), 1 mM Sodium Pyruvate (Gibco 11360), 1 mM non-essential amino acids (Gibco 11140), .055 mM β-mercaptoethanol (Gibco 21985), 100 units Penicillin/Streptomycin (Gibco 10378016) and .3 mg/ml glutamine was

used to culture either B cells. B cells were stimulated with either 10 mg/ml anti-IgM (Jackson laboratories 115-006-020) or 10 ug/ml LPS (Sigma L2630).

Flow cytometry analysis of cell proliferation and survival

Purified B cells were stained with 5 mM CFSE (invitrogen C1157) and culture in complete media with previously mentioned stimuli (see above). At various time points B cells were collected and stained with 7AAD (invitrogen A1310). The B cells were analyzed for proliferation and survival using a C6 accuri flow cytometer (BD biosciences). Differences in cell proliferation was measured using FlowJo (Tree star inc.).

EMSA and Supershifts

Nuclear extracts were generated from B cells using high salt extraction. In brief, purified B cells were incubated with a low salt buffer (10mM HEPEs pH 7.9 (Gibco), 10mM KCl (Thermo Fisher Scientific P217), .1mM EGTA (Sigma E-4378), .1mM EDTA (Thermo Fisher Scientific S312), 1mM DTT (Thermo Fisher Scientific BP172-5), 1mM PMSF (Sigma P7626), 5 mg/ml apoprotein (Sigma A1153), 5 mg/ml leupeptin (Sigma L2884), 1 mM pepstatin A (Sigma P5318)) for 10 minutes on ice. Following this incubation, the cells were disrupted through the addition of NP-40 (US Biological N3500) to a final concentration of .5% and votexing for 15 seconds. Nuclei were pelleted away from the cytoplasmic fraction by centrifugation at 15,000 rpm for 1 minute and the cytoplasmic fraction was pipetted into a separate tube. The remaining nuclei were disrupted by a 20 minute incubation at 4^{o}C in a high salt

buffer (20mM HEPES pH 7.9 (Gibco), 400mM NaCl (Thermo Fisher Scientific S671), 1mM EGTA (Thermo Fisher Scientific), 1mM EDTA (Thermo Fisher Scientific), 20% Glycerol (Thermo Fisher Scientific), 1mM DTT (Thermo Fisher Scientific), 1mM PMSF(Sigma)). The nuclear fraction was collected following centrifugation at 15,000 rpm for 5 minutes. Equal amounts of nuclear extracts (1 ug) were pre-incubated for 20 minutes on ice in the presence or absence of antibodies specific for RelA (Santa Cruz Biotechnology sc-372), RelB (Santa Cruz Biotechnology sc-226), cRel (Santa Cruz Biotechnologies sc-71) or in combinations as follows; RelA/RelB, RelA/cRel and RelB/cRel. Following the pre-incubation with antibodies, [g-^{32}P] ATP (GE health) radio-labeled probe derived from HIV-kB sequence: 5'-GCTACAAGGGACTTTCCGCTGGGGACTTTCCAGGGAGG-3' was added and incubated at room temperature for an additional 15 minutes. The resulting DNA/protein/antibody complexes were resolved by electrophoresis on a 5% non-denaturing polyacrylamide gel and exposed to storage phosphor screen (GE healthcare) overnight before image development on at Typhoon 9200 Variable Mode Imager (GE Healthcare). Images were analyzed and quantitated using ImageQuant™ (GE Healthcare).

Computational modeling of NFkB dimer activity

The computational model appends the previously published IκB models with the reactions that govern RelA/NFκB dimer generation. The input to this model is a numerical curve for IKK activity and the outputs are free, nuclear

RelA:A homodimer, Rel:p50 heterodimer, and cRel:p50 heterodimer. The model contains 51 species and 117 reactions governed by 87 parameters (Model 3.1, Table 3.1). The ODEs were solved numerically using MATLAB version R2012b (The MathWorks, Inc.) with subroutine ode15s, a variable order, multi-step solver. Prior to stimulation, the system was allowed to equilibrate from starting conditions to a steady state, defined as showing no concentration changes greater than 1% over a period of 4000 minutes. Stimulus-induced perturbation from the steady state was accomplished by direct modulation of IKK activity via a numerical input curve representing IgM or LPS stimulation (adapted from Werner 2008). MATLAB model codes are available upon request.

Animal use.

The animal protocols for this study were approved by the University of California, San Diego Animal Care and Use Committee.

3.3 Results

IκBε deficiency results in B cell expansion due to an increase in late NFκB activity

Upon examination of both wild type and IkBe deficient B cells, we found that both an antigenic stimulation (anti-IgM) and a pathogenic stimulation (LPS) result in an increase in B-cell proliferation and survival in IkBe deficient B cells (Fig. 3.1). Because IkBe is a player in the NFkB signaling system, we wanted to determine how IkBe deficiency affects NFkB dimer activity. Analysis of the nuclear extracts of the NFkB showed that there is a stimulus specific increase in late RelA dimer activity and late cRel dimer activity. The anti-IgM stimulus showed an increase in late cRel dimer activity, while LPS stimulation resulted in an increase in both late RelA and late cRel dimer activity (Fig 3.5). These activity results suggest that IkBe plays an important role in providing negative feedback of late cRel and RelA dimer activity in B cells and that this negative feedback is stimulus specific.

A mathematical model of RelA and cRel dynamics suggests a kinetic basis for IκBε's stimulus-specific functions

The observation that the signaling phenotypes are stimulus specific may suggest that there are underlying stimulus-specific biochemical mechanisms, such as a co-stimulatory signaling pathway, that are activated by one stimulus but not another. An alternative, more parsimonious explanation is that differential-signaling kinetics may account for the stimulus-specific

phenotypes. Using a mathematical modeling approach, we sought to test the latter hypothesis. To begin, we summarized the known relative relationships between the two potential negative-feedback regulators IκBα and IκBε in terms of their interactions with RelA- and cRel-containing dimers, their differential responsiveness to IKK-induced degradation, and the stimulus-specific dynamics of IKK activity (Model 3.1, Table 3.1). Interestingly, we found that, although NF-κB–responsive IκBα gene expression required RelA, NFκB–responsive IκBε gene expression could be mediated by either RelA or cRel. Next, we constructed a mathematical model with these parameters by adapting a previously established mathematical model to include the cRel dimers and to recapitulate B cell–specific dynamic control of RelA- and cRel-containing dimers (Werner et al., 2008) (Fig 3.2, Fig. 3.3). Simulations of this model with the IgM-induced transient IKK activity showed that RelA:p50 dimer is barely affected by IκBε deficiency; however, in response to LPS-induced long-lasting IKK activity, RelA:p50 remains hyperactivated at late time points (Fig. 3.4A). In contrast, cRel:p50 was hyperactivated under both conditions. By quantitating the time course at 24 h, the stimulus-agnostic effect on cRel and stimulus-specific effect on RelA are readily appreciated; in fact, this graph closely resembles the experimental results obtained biochemically (Fig. 3.4B, Fig. 3.5).

These simulation results demonstrate that the kinetic argument is a sufficient explanation for the stimulus-specific phenotype seen in IκBε-deficient

B cells. We can summarize the kinetic argument as follows: in response to transient IKK signals, IkBα is capable of providing post-induction repression on its high-affinity target RelA:p50 but less effectively on its low-affinity target cRel:p50, which requires IkBε for complete suppression. However, IkBα's responsiveness to long-lasting IKK signals renders it effectively neutralized; thus, under these conditions, IkBε, which has lower responsiveness, plays an important role for its high-affinity target cRel:p50 and for its low-affinity target RelA:p50. Interestingly, the single specificity of the IkBα negative-feedback loop for RelA:p50 and the dual specificity of the IkBε negative-feedback loop for RelA:p50 and cRel:p50 are reflected in the dimer requirements for IkBα and IkBε inducible expression. We note that, although reported kinetic relationships are consistent with this sufficiency argument, we cannot rule out that a stimulus-specific signaling pathway also plays a role in the described phenotype.

3.4 Discussion

In this study, we identified IκBε as a key negative-feedback regulator of cRel-containing NFκB dimers in B cells, which limits B cell proliferation in response to mitogenic stimulation. In contrast to our understanding based on fibroblast studies, we found that IκBε also plays a nonredundant role in limiting the ubiquitous RelA-containing NFκB, albeit in a stimulus-specific manner. This result led to two insights: first from a physiological perspective we found that limiting RelA activation is relevant for controlling B cell expansion, because neutralizing the expression of the RelA target gene IL-6 mitigated the IκBε-deficient phenotype. Second, considering the NFκB system as a dynamic one, we conclude that the stimulus-specific functions of IκBε negative feedback are based on kinetics rather than the engagement of a stimulus-specific mechanism or pathway.

In fact, we were able to utilize a mathematical modeling approach in order to demonstrate how the stimulus specific phenotype in NFκB activation can occur. The observation of the kinetic parameters show that there is a requirement of specific IκB:NFκB relationships for the stimulus-specific activation of RelA dimers versus cRel dimers in B cells. In fact, this stimulus-specific control is based on kinetic differences in the molecular interactions and stimulus-induced kinase activities.

3.5 Acknowledgements

Chapter 3, in part, is a reprint of material as it appears in Alves BN, Tsui R, Almaden J, Shokhirev MN, Davis-Turak J, Fujimoto J, Birnbaum H, Ponomarenko J, Hoffmann A. “IκBε is a key regulator of B cell expansion by providing negative feedback in a stimulus-specific manner.” Journal of Immunology. 2014; 192(7):3121-32. The dissertation author was a primary investigator and author of this material. Bryce Alves performed the experimental data to demonstrate the phenotype in IkBe-deficient B cells and the experimental validation of anti-IgM and LPS stimulated B cells.

Model 3.1: A B-cell model containing NFκB dimer generation, IκB:NFκB interactions, and IKK dependent signaling

This model is adapted from previously published IκB-NFκB signaling models but three specific NFκB dimers are present in this new model: RelA:p50, cRel:p50 and p50:p50. There are also three IκBs in this model: IκBα, IκBβ, and IκBε, which interact with RelA:p50 and cRel:p50. The IKK signaling input is represented as a multiplier on the degradation rate constant of IKK induced IκB degradation, since IKK activity results in phosphorylation and subsequent degradation of IκBs, allowing for the release of NFκB dimers.
The model also allows the translocation of species between the cytoplasm and the nucleus, so transport rates are included in this model as well. The parameter ID symbols in the model supplement tables correspond to the rate constants in these equations.

NFκB monomer and IκB transcript reactions

$$\frac{dtRelA}{dt} = kt - trdeg(RelA(t))$$
$$\frac{dtcRel}{dt} = kt - trdeg(cRel(t))$$
$$\frac{dtp50}{dt} = kt - trdeg(p50(t))$$
$$\frac{dtIkBa}{dt} = kt - trdeg(tIkBa(t))$$
$$\frac{dtIkBb}{dt} = kt - trdeg(tIkBb(t))$$
$$\frac{dtIkBe}{dt} = kt - trdeg(tIkBe(t))$$

$$kt = \frac{ktc\left(1 + \sum w\left(\frac{[d]}{Kd}\right)^3\right)}{\left(1 + \sum\left(\frac{[d]}{Kd}\right)^3\right)}$$

ktc = constitutive basal mRNA synthesis rate
w = inducible multiplier
d = NFκB dimer concentration
Kd = Hill Kd (NFκB induced)

Model 3.1: A B-cell model containing NFκB dimer generation, IκB:NFκB interactions, and IKK dependent signaling, Continued

NFκB monomer reactions

Cytoplasmic Reactions

$$\frac{dRelA}{dt} = tr(tRelA(t)) - ka(RelA(t))(p50(t)) + kd(RelA{:}\,p50(t)) - \deg(RelA(t))$$

$$\frac{dcRel}{dt} = tr(tcRel(t)) - ka(cRel(t))(p50(t)) + kd(cRel{:}\,p50(t)) - \deg(cRel(t))$$

$$\frac{dp50}{dt} = tr(tp50(t)) - ka(RelA(t))(p50(t)) - ka(p50(t))(p50(t)) + kd(p50{:}\,p50(t)) + kd(RelA{:}\,p50(t)) - \deg(p50(t))$$

Nuclear Reactions

$$\frac{dRelA}{dt} = tr(tRelA(t)) - ka(RelA(t))(p50(t)) + kd(RelA{:}\,p50(t)) - \deg(RelA(t))$$

$$\frac{dcRel}{dt} = tr(tcRel(t)) - ka(cRel(t))(p50(t)) + kd(cRel{:}\,p50(t)) - \deg(cRel(t))$$

$$\frac{dp50}{dt} = tr(tp50(t)) - ka(RelA(t))(p50(t)) - ka(p50(t))(p50(t)) + kd(p50{:}\,p50(t)) + kd(RelA{:}\,p50(t)) - \deg(p50(t))$$

IκB reactions

Cytoplasmic Reactions

$$\frac{dIkBa}{dt} = tr(tIkBa(t)) - ikkdeg(IkBa(t))(IKK) - ideg(IkBa(t)) - imp(IkBa(t)) + \exp(IkBa(t)) - ka(RelA{:}\,p50(t))(IkBa(t)) - ka(cRel{:}\,p50(t))(IkBa(t)) + kd(IkBa\_RelA{:}\,p50(t)) + kd(IkBa\_cRel{:}\,p50(t)) + ndeg(IkBa\_RelA{:}\,p50(t)) + ndeg(IkBa\_cRel{:}\,p50(t))$$

Model 3.1: A B-cell model containing NFκB dimer generation, IκB:NFκB interactions, and IKK dependent signaling, Continued

$$\frac{dIkBb}{dt} = tr(tIkBb(t)) - ikkdeg(IkBb(t))(IKK) - ideg(IkBb(t)) - imp(IkBb(t)) + \exp(IkBb(t)) - ka(RelA{:}p50(t))(IkBb(t)) - ka(cRel{:}p50(t))(IkBb(t)) + kd(IkBb\_RelA{:}p50(t)) + kd(IkBb\_cRel{:}p50(t)) + ndeg(IkBb\_RelA{:}p50(t)) + ndeg(IkBb\_cRel{:}p50(t))$$

$$\frac{dIkBe}{dt} = tr(tIkBe(t)) - ikkdeg(IkBe(t))(IKK) - ideg(IkBe(t)) - imp(IkBe(t)) + \exp(IkBe(t)) - ka(RelA{:}p50(t))(IkBe(t)) - ka(cRel{:}p50(t))(IkBe(t)) + kd(IkBe\_RelA{:}p50(t)) + kd(IkBe\_cRel{:}p50(t)) + ndeg(IkBe\_RelA{:}p50(t)) + ndeg(IkBb\_cRel{:}p50(t))$$

Nuclear Reactions

$$\frac{dIkBa}{dt} = tr(tIkBa(t)) - ikkdeg(IkBa(t))(IKK) - ideg(IkBa(t)) + imp(IkBa(t)) - \exp(IkBa(t)) - ka(RelA{:}p50(t))(IkBa(t)) - ka(cRel{:}p50(t))(IkBa(t)) + kd(IkBa\_RelA{:}p50(t)) + kd(IkBa\_cRel{:}p50(t)) + ndeg(IkBa\_RelA{:}p50(t)) + ndeg(IkBa\_cRel{:}p50(t))$$

$$\frac{dIkBb}{dt} = tr(tIkBb(t)) - ikkdeg(IkBb(t))(IKK) - ideg(IkBb(t)) + imp(IkBb(t)) - \exp(IkBb(t)) - ka(RelA{:}p50(t))(IkBb(t)) - ka(cRel{:}p50(t))(IkBb(t)) + kd(IkBb\_RelA{:}p50(t)) + kd(IkBb\_cRel{:}p50(t)) + ndeg(IkBb\_RelA{:}p50(t)) + ndeg(IkBb\_cRel{:}p50(t))$$

$$\frac{dIkBe}{dt} = tr(tIkBe(t)) - ikkdeg(IkBe(t))(IKK) - ideg(IkBe(t)) + imp(IkBe(t)) - \exp(IkBe(t)) - ka(RelA{:}p50(t))(IkBe(t)) - ka(cRel{:}p50(t))(IkBe(t)) + kd(IkBe\_RelA{:}p50(t)) + kd(IkBe\_cRel{:}p50(t)) + ndeg(IkBe\_RelA{:}p50(t)) + ndeg(IkBb\_cRel{:}p50(t))$$

Model 3.1: A B-cell model containing NFκB dimer generation, IκB:NFκB interactions, and IKK dependent signaling, Continued

NFκB dimer reactions

Cytoplasmic Reactions

$$\frac{dRelA{:}\,p50}{dt} = ka\big(RelA(t)\big)\big(p50(t)\big) - kd\big(RelA{:}\,p50(t)\big) - imp\big(RelA{:}\,p50(t)\big) + \exp\big(RelA{:}\,p50(t)\big) - \deg\big(RelA{:}\,p50(t)\big) - ka\big(RelA{:}\,p50(t)\big)\big(IkBa(t)\big) - ka\big(RelA{:}\,p50(t)\big)\big(IkBb(t)\big) - ka(RelA{:}\,p50(t))(IkBe(t)) + kd\big(IkBa\_RelA{:}\,p50(t)\big) + kd\big(IkBb\_RelA{:}\,p50(t)\big) + kd\big(IkBe\_RelA{:}\,p50(t)\big) + bideg\big(IkBa\_RelA{:}\,p50(t)\big) + bideg\big(IkBb\_RelA{:}\,p50(t)\big) + bideg\big(IkBe\_RelA{:}\,p50(t)\big) + bikkdeg\big(IkBa\_RelA{:}\,p50(t)\big)(IKK) + bikkdeg\big(IkBb\_RelA{:}\,p50(t)\big)(IKK) + bikkdeg(IkBe\_RelA{:}\,p50(t))(IKK)$$

$$\frac{dcRel{:}\,p50}{dt} = ka\big(cRel(t)\big)\big(p50(t)\big) - kd\big(cRel{:}\,p50(t)\big) - imp\big(cRel{:}\,p50(t)\big) + \exp\big(cRel{:}\,p50(t)\big) - \deg\big(cRel{:}\,p50(t)\big) - ka\big(cRel{:}\,p50(t)\big)\big(IkBa(t)\big) - ka\big(cRel{:}\,p50(t)\big)\big(IkBb(t)\big) - ka(cRel{:}\,p50(t))(IkBe(t)) + kd\big(IkBa\_cRel{:}\,p50(t)\big) + kd\big(IkBb\_cRel{:}\,p50(t)\big) + kd\big(IkBe\_cRel{:}\,p50(t)\big) + bideg\big(IkBa\_cRel{:}\,p50(t)\big) + bideg\big(IkBb\_cRel{:}\,p50(t)\big) + bideg\big(IkBe\_cRel{:}\,p50(t)\big) + bikkdeg\big(IkBa\_cRel{:}\,p50(t)\big)(IKK) + bikkdeg\big(IkBb\_cRel{:}\,p50(t)\big)(IKK) + bikkdeg(IkBe\_cRel{:}\,p50(t))(IKK)$$

$$\frac{dp50{:}\,p50}{dt} = ka\big(p50(t)\big)\big(p50(t)\big) - kd\big(p50{:}\,p50(t)\big) - imp\big(p50{:}\,p50(t)\big) + \exp\big(p50{:}\,p50(t)\big) - \deg\big(p50{:}\,p50(t)\big)$$

Nuclear Reactions

$$\frac{dRelA{:}\,p50}{dt} = ka\big(RelA(t)\big)\big(p50(t)\big) - kd\big(RelA{:}\,p50(t)\big) + imp\big(RelA{:}\,p50(t)\big) - \exp\big(RelA{:}\,p50(t)\big) - \deg\big(RelA{:}\,p50(t)\big) - ka\big(RelA{:}\,p50(t)\big)\big(IkBa(t)\big) - ka\big(RelA{:}\,p50(t)\big)\big(IkBb(t)\big) - ka(RelA{:}\,p50(t))(IkBe(t)) + kd\big(IkBa\_RelA{:}\,p50(t)\big) + kd\big(IkBb\_RelA{:}\,p50(t)\big) + kd\big(IkBe\_RelA{:}\,p50(t)\big) + bideg\big(IkBa\_RelA{:}\,p50(t)\big) + bideg\big(IkBb\_RelA{:}\,p50(t)\big) + bideg\big(IkBe\_RelA{:}\,p50(t)\big) + bikkdeg\big(IkBa\_RelA{:}\,p50(t)\big)(IKK) + bikkdeg\big(IkBb\_RelA{:}\,p50(t)\big)(IKK) + bikkdeg(IkBe\_RelA{:}\,p50(t))(IKK)$$

$$\frac{dcRel{:}\,p50}{dt} = ka\big(cRel(t)\big)\big(p50(t)\big) - kd\big(cRel{:}\,p50(t)\big) + imp\big(cRel{:}\,p50(t)\big) - \exp\big(cRel{:}\,p50(t)\big) - \deg\big(cRel{:}\,p50(t)\big) - ka\big(cRel{:}\,p50(t)\big)\big(IkBa(t)\big) - ka\big(cRel{:}\,p50(t)\big)\big(IkBb(t)\big) - ka(cRel{:}\,p50(t))(IkBe(t)) + kd\big(IkBa\_cRel{:}\,p50(t)\big) + kd\big(IkBb\_cRel{:}\,p50(t)\big) + kd\big(IkBe\_cRel{:}\,p50(t)\big) + bideg\big(IkBa\_cRel{:}\,p50(t)\big) + bideg\big(IkBb\_cRel{:}\,p50(t)\big) + bideg\big(IkBe\_cRel{:}\,p50(t)\big) + bikkdeg\big(IkBa\_cRel{:}\,p50(t)\big)(IKK) + bikkdeg\big(IkBb\_cRel{:}\,p50(t)\big)(IKK) + bikkdeg(IkBe\_cRel{:}\,p50(t))(IKK)$$

$$\frac{dp50{:}\,p50}{dt} = ka\big(p50(t)\big)\big(p50(t)\big) - kd\big(p50{:}\,p50(t)\big) + imp\big(p50{:}\,p50(t)\big) - \exp\big(p50{:}\,p50(t)\big) - \deg\big(p50{:}\,p50(t)\big)$$

IκB-NFκB reactions

Cytoplasmic reactions

$$\frac{dIkBa\_RelA{:}\,p50}{dt} = ka\big(RelA{:}\,p50(t)\big)\big(IkBa(t)\big) - kd\big(IkBa\_RelA{:}\,p50(t)\big) - imp\big(IkBa\_RelA{:}\,p50(t)\big) + \exp\big(IkBa\_RelA{:}\,p50(t)\big) - bikkdeg\big(IkBa\_RelA{:}\,p50(t)\big)(IKK) - bideg\big(IkBa\_RelA{:}\,p50(t)\big) - \deg\,(IkBa\_RelA{:}\,p50(t))$$

$$\frac{dIkBb\_RelA{:}\,p50}{dt} = ka\big(RelA{:}\,p50(t)\big)\big(IkBb(t)\big) - kd\big(IkBb\_RelA{:}\,p50(t)\big) - imp\big(IkBb\_RelA{:}\,p50(t)\big) + \exp\big(IkBb\_RelA{:}\,p50(t)\big) - bikkdeg\big(IkBb\_RelA{:}\,p50(t)\big)(IKK) - bideg\big(IkBb\_RelA{:}\,p50(t)\big) - \deg\,(IkBb\_RelA{:}\,p50(t))$$

$$\frac{dIkBe\_RelA{:}\,p50}{dt} = ka\big(RelA{:}\,p50(t)\big)\big(IkBe(t)\big) - kd\big(IkBe\_RelA{:}\,p50(t)\big) - imp\big(IkBe\_RelA{:}\,p50(t)\big) + \exp\big(IkBe\_RelA{:}\,p50(t)\big) - bikkdeg\big(IkBe\_RelA{:}\,p50(t)\big)(IKK) - bideg\big(IkBe\_RelA{:}\,p50(t)\big) - \deg\,(IkBe\_RelA{:}\,p50(t))$$

$$\frac{dIkBa\_cRel{:}\,p50}{dt} = ka\big(cRel{:}\,p50(t)\big)\big(IkBa(t)\big) - kd\big(IkBa\_cRel{:}\,p50(t)\big) - imp\big(IkBa\_cRel{:}\,p50(t)\big) + \exp\big(IkBa\_cRel{:}\,p50(t)\big) - bikkdeg\big(IkBa\_cRel{:}\,p50(t)\big)(IKK) - bideg\big(IkBa\_cRel{:}\,p50(t)\big) - \deg\,(IkBa\_cRel{:}\,p50(t))$$

$$\frac{dIkBb\_cRel:p50}{dt} = ka(cRel:p50(t))(IkBb(t)) - kd(IkBb\_cRel:p50(t)) - imp(IkBb\_cRel:p50(t)) + \exp(IkBb\_cRel:p50(t)) - bikkdeg(IkBb\_cRel:p50(t))(IKK) - bideg(IkBb\_cRel:p50(t)) - \deg(IkBb\_cRel:p50(t))$$

$$\frac{dIkBe\_cRel:p50}{dt} = ka(cRel:p50(t))(IkBe(t)) - kd(IkBe\_cRel:p50(t)) - imp(IkBe\_cRel:p50(t)) + \exp(IkBe\_cRel:p50(t)) - bikkdeg(IkBe\_cRel:p50(t))(IKK) - bideg(IkBe\_cRel:p50(t)) - \deg(IkBe\_cRel:p50(t))$$

Nuclear Reactions

$$\frac{dIkBa\_RelA:p50}{dt} = ka(RelA:p50(t))(IkBa(t)) - kd(IkBa\_RelA:p50(t)) + imp(IkBa\_RelA:p50(t)) - \exp(IkBa\_RelA:p50(t)) - bikkdeg(IkBa\_RelA:p50(t))(IKK) - bideg(IkBa\_RelA:p50(t)) - \deg(IkBa\_RelA:p50(t))$$

$$\frac{dIkBb\_RelA:p50}{dt} = ka(RelA:p50(t))(IkBb(t)) - kd(IkBb\_RelA:p50(t)) + imp(IkBb\_RelA:p50(t)) - \exp(IkBb\_RelA:p50(t)) - bikkdeg(IkBb\_RelA:p50(t))(IKK) - bideg(IkBb\_RelA:p50(t)) - \deg(IkBb\_RelA:p50(t))$$

$$\frac{dIkBe\_RelA:p50}{dt} = ka(RelA:p50(t))(IkBe(t)) - kd(IkBe\_RelA:p50(t)) + imp(IkBe\_RelA:p50(t)) - \exp(IkBe\_RelA:p50(t)) - bikkdeg(IkBe\_RelA:p50(t))(IKK) - bideg(IkBe\_RelA:p50(t)) - \deg(IkBe\_RelA:p50(t))$$

$$\frac{dIkBa\_cRel:p50}{dt} = ka(cRel:p50(t))(IkBa(t)) - kd(IkBa\_cRel:p50(t)) + imp(IkBa\_cRel:p50(t)) - \exp(IkBa\_cRel:p50(t)) - bikkdeg(IkBa\_cRel:p50(t))(IKK) - bideg(IkBa\_cRel:p50(t)) - \deg(IkBa\_cRel:p50(t))$$

$$\frac{dIkBb\_cRel:p50}{dt} = ka(cRel:p50(t))(IkBb(t)) - kd(IkBb\_cRel:p50(t)) +$$

$$imp\big(IkBb\_cRel{:}\,p50(t)\big) - \exp\big(IkBb\_cRel{:}\,p50(t)\big) - bikkdeg\big(IkBb\_cRel{:}\,p50(t)\big)(IKK) - bideg\big(IkBb\_cRel{:}\,p50(t)\big) - \deg\left(IkBb\_cRel{:}\,p50(t)\right)$$

$$\frac{dIkBe\_cRel{:}\,p50}{dt} = ka\big(cRel{:}\,p50(t)\big)\big(IkBe(t)\big) - kd\big(IkBe\_cRel{:}\,p50(t)\big) + imp\big(IkBe\_cRel{:}\,p50(t)\big) - \exp\big(IkBe\_cRel{:}\,p50(t)\big) - bikkdeg\big(IkBe\_cRel{:}\,p50(t)\big)(IKK) - bideg\big(IkBe\_cRel{:}\,p50(t)\big) - \deg\left(IkBe\_cRel{:}\,p50(t)\right)$$

Table 3.1: Parameter Table for Model 3.1

Reaction	Category	Location	Param ID no	Parameter Value	Source
Reaction rates determined by transcripts and protein levels					
=> tIκBα (basal)	IκB Synth.	Nucleus	1	1.5e-5 nM sec^{-1}	Set to fit measured mRNA and protein expression profiles (Werner et al., 2008) and a Hill function where Hill coefficient =1.1
=> tIκBβ (basal)	IκB Synth.	Nucleus	2	1e-5 nM sec^{-1}	*As in #1*
=> tIκBε (basal)	IκB Synth.	Nucleus	3	1.2e-6 nM sec^{-1}	*As in #1*
=> tRelA (basal)	NFκB Synth.	Nucleus	4	1.2e-6 nM sec^{-1}	*As in #1*
=> cRel (basal)	NFκB Synth.	Nucleus	5	1.2e-6 nM sec^{-1}	*As in #1*
=> tp50 (basal)	NFκB Synth.	Nucleus	6	1.2e-6 nM sec^{-1}	*As in #1*
IκB Reactions					
mRNA => mRNA + protein	Translation	Nuc - > Cyt	7	0.2 proteins/ mRNA sec^{-1}	Derived from the elongation rate of the ribosome and corrected for the nucleotide spacing between adjacent ribosomes on the same transcript: 30 nt sec-1 / 150 nt = 0.2 sec-1
=> tIκBα (A50-induced)	IκB Synth.	Nucleus	8	100 fold over constitutive	*As in #1*
=> tIκBβ (A50-induced, 45 min. delay)	IκB Synth.	Nucleus	9	1 fold over constitutive	*As in #1*
=> tIκBε (A50-induced, 45 min. delay)	IκB Synth.	Nucleus	10	25 fold over constitutive	*As in #1*
=> tIκBα (C50-induced)	IκB Synth.	Nucleus	11	1 fold over constitutive	*As in #1*
=> tIκBβ (C50-induced, 45 min. delay)	IκB Synth.	Nucleus	12	1 fold over constitutive	this study (adapted from Tsui et al. in preparation)
=> tIκBε (C50-induced, 45 min. delay)	IκB Synth.	Nucleus	13	125 fold over constitutive	this study (adapted from Tsui et al. in preparation)
IκBα Hill K_d (NFκB-induced)	IκB Synth.	Nucleus	14	150 nM	*As in #1*
IκBβ Hill K_d (NFκB-induced)	IκB Synth.	Nucleus	15	150 nM	*As in #1*
IκBε Hill K_d (NFκB-induced)	IκB Synth.	Nucleus	16	150 nM	*As in #1*
Hill Coefficient for inducible txn of tIkB by NFκB	IκB Synth	Nucleus	17	1.1	this study (adapted from Tsui et al. in preparation)
IκBα(c) => IκBα(n)	Transport	Cyt -> Nuc	18	1e-3 sec^{-1}	(Shih et al., 2009)
IκBβ(c) => IκBβ(n)	Transport	Cyt -> Nuc	19	1.5e-4 sec^{-1}	As in #21

Table 3.1: Parameter Table for Model 3.1, Continued

Reaction	Category	Location	Param ID no	Parameter Value	Source
IκBε(c) => IκBε(n)	Transport	Cyt -> Nuc	20	7.5e-4 sec^{-1}	As in #21
IκB[α/β/ε](n) => IκB[α/β/ε](c)	Transport	Nuc - > Cyt	21	2e-4 sec^{-1}	As in #21
tIκBα =>	IκB Deg.	Cyt, Nuc	22	7.3e-4 sec^{-1}	As in #21
tIκBβ =>	IκB Deg.	Cyt, Nuc	23	4.8e-5 sec^{-1}	As in #21
tIκBε =>	IκB Deg.	Cyt,Nuc	24	6.4e-5 sec^{-1}	As in #21
IκBα =>	IκB Deg.	Cyt, Nuc	25	2e-3 sec^{-1}	As in #21
IκBβ =>	IκB Deg.	Cyt, Nuc	26	2e-3 sec^{-1}	As in #21
IκBε =>	IκB Deg.	Cyt, Nuc	27	1.925e-4 sec^{-1}	Schuerenberg and Hoffmann unpublished results
IκB[α/β/ε]-NFκB => NFκB	IκB Deg.	Cyt, Nuc	28	4e-6 sec^{-1}	Based on estimated 48 hour half-life
IκBα => (NEMO-mediated)	IκB Deg.	Cytoplasm	29	2.25e-5 nM^{-1} sec^{-1}	Based on measured IκB degradation timecourses given numerical input curves
IκBα-NFκB => NFκB (NEMO-mediated)	IκB Deg.	Cytoplasm	30	2.25e-5 nM^{-1} sec^{-1}	
IκBβ => (NEMO-mediated)	IκB Deg.	Cytoplasm	31	7.5e-6 nM^{-1} sec^{-1}	As in #21
IκBβ-NFκB => NFκB (NEMO-mediated)	IκB Deg.	Cytoplasm	32	7.5e-6 nM^{-1} sec^{-1}	As in #21
IκBε => (NEMO-mediated)	IκB Deg.	Cytoplasm	33	1.5e-5 nM^{-1} sec^{-1}	As in #21
IκBε-NFκB => NFκB (NEMO-mediated)	IκB Deg.	Cytoplasm	34	1.5e-5 nM^{-1} sec^{-1}	As in #21
NFκB reactions					
tRelA =>	NFκB Deg.	Nucleus	35	4.8e-5 sec^{-1}	As in #21
tp50 =>	NFκB Deg.	Nucleus	36	4.8e-5 sec^{-1}	As in #21
tcRel =>	NFκB Deg.	Nucleus	37	4.8e-5 sec^{-1}	Based on Shih et al. 2009
RelA =>	NFκB Deg.	Cyt, Nuc	38	3.85e-4 sec^{-1}	Based on estimated 30 min half-life of NFκB monomers
p50 =>	NFκB Deg.	Cyt, Nuc	39	3.85e-4 sec^{-1}	
cRel =>	NFκB Deg.	Cyt, Nuc	40	3.85e-4 sec^{-1}	
RelA + p50 => RelA:p50	NFκB Synth.	Nucleus	41	3.16e-5 nM^{-1} sec^{-1}	Tsui et al. in preparation
p50 + p50 => p50:p50	NFκB Synth.	Nucleus	42	3e-5 nM^{-1} sec^{-1}	
cRel + p50 => cRel:p50	NFκB Synth.	Nucleus	43	3.16e-5 nM^{-1} sec^{-1}	this study (adapted from Tsui et al. in preparation)
RelA + p50 => RelA:p50	NFκB Synth.	Cytoplasm	44	3.16e-5 nM^{-1} sec^{-1}	*As in #44*
p50 + p50 => p50:p50	NFκB Synth.	Cytoplasm	45	3e-5 nM^{-1} sec^{-1}	
cRel + p50 => cRel:p50	NFκB Synth.	Cytoplasm	46	3.16e-5 nM^{-1} sec^{-1}	*As in #47*
RelA:p50 => RelA + p50	NFκB Synth.	Nucleus	47	3.16e-5 sec^{-1}	*As in #44*
p50:p50 => p50 + p50	NFκB Synth.	Nucleus	48	9e-5 sec^{-1}	
cRel:p50 => cRel +p50	NFκB Synth.	Nucleus	49	3.16e-5 nM^{-1} sec^{-1}	*As in #47*
RelA:p50 => RelA + p50	NFκB Synth.	Cytoplasm	50	3.16e-4 sec^{-1}	*As in #44*

Table 3.1: Parameter Table for Model 3.1, Continued

Reaction	Category	Location	Param ID no	Parameter Value	Source
p50:p50 => p50 + p50	NFκB Synth.	Cytoplasm	51	9e-4 sec^{-1}	*As in #44*
cRel:p50 => cRel +p50	NFκB Synth.	Cytoplasm	52	3.16e-5 nM^{-1} sec^{-1}	*As in #47*
NFκB(c) => NFκB(n)	Transport	Cyt -> Nuc	53	9e-2 sec^{-1}	(Shih et al., 2009)
NFκB(n) => NFκB(c)	Transport	Nuc -> Cyt	54	8e-5 sec^{-1}	(Shih et al., 2009)
NFκB =>	NFκB Deg.	Cyt, Nuc	55	4e-6 sec^{-1}	Based on estimated 48 hour half-life
IκB[α/β/ε]-NFκB => IκB[α/β/ε]	NFκB Deg.	Cyt, Nuc	56	4e-6 sec^{-1}	*As in #31*
IκB-NFκB interactions					
IκBα + RelA:p50 => IκBα-RelA:p50	IκB-NFκB inter	Cyt, Nuc	57	8.01e-5 nM^{-1} sec^{-1}	*As in #44*
IκBβ + RelA:p50 => IκBβ-RelA:p50	IκB-NFκB inter	Cyt, Nuc	58	3.55e-6 nM^{-1} sec^{-1}	
IκBε + RelA:p50 => IκBε-RelA:p50	IκB-NFκB inter	Cyt, Nuc	59	2.24e-5 nM^{-1} sec^{-1}	
IκBα + cRel:p50 => IκBα-cRel:p50	IκB-NFκB inter	Cyt, Nuc	60	5.01e-5 nM^{-1} sec^{-1}	*As in #47*
IκBβ + cRel:p50 => IκBβ-cRel:p50	IκB-NFκB inter	Cyt, Nuc	61	3.55e-6 nM^{-1} sec^{-1}	
IκBε + cRel:p50 => IκBε-cRel:p50	IκB-NFκB inter	Cyt, Nuc	62	2.24e-5 nM^{-1} sec^{-1}	
IκBα-RelA:p50 => IκBα + RelA:p50	IκB-NFκB inter	Cyt, Nuc	63	1e-5 sec^{-1}	*As in #44*
IκBβ-RelA:p50 => IκBβ + RelA:p50	IκB-NFκB inter	Cyt, Nuc	64	2.82e-4 sec^{-1}	
IκBε-RelA:p50 => IκBε + RelA:p50	IκB-NFκB inter	Cyt, Nuc	65	1e-4 sec^{-1}	
IκBα-cRel:p50 => IκBα + cRel:p50	IκB-NFκB inter	Cyt, Nuc	66	8e-5 sec^{-1}	*As in #47*
IκBβ-cRel:p50 => IκBβ + cRel:p50	IκB-NFκB inter	Cyt, Nuc	67	2.82e-4 sec^{-1}	
IκBε-cRel:p50 => IκBε + cRel:p50	IκB-NFκB inter	Cyt, Nuc	68	4.47e-8 sec^{-1}	
IκBα-NFκB(c) => IκBα-NFκB(n)	Transport	Cyt -> Nuc	69	4.6e-3 sec^{-1}	(Shih et al., 2009)
IκBβ-NFκB(c) => IκBβ-NFκB(n)	Transport	Cyt -> Nuc	70	4.6e-4 sec^{-1}	(Shih et al., 2009)
IκBε-NFκB(c) => IκBε-NFκB(n)	Transport	Cyt -> Nuc	71	2.3e-3 sec^{-1}	(Shih et al., 2009)
IκBα-NFκB(n) => IκBα-NFκB(c)	Transport	Nuc -> Cyt	72	1.4e-2 sec^{-1}	(Shih et al., 2009)
IκBβ-NFκB(n) => IκBβ-NFκB(c)	Transport	Nuc -> Cyt	73	7e-3 sec^{-1}	(Shih et al., 2009)
IκBε-NFκB(n) => IκBε-NFκB(c)	Transport	Nuc -> Cyt	74	7e-3 sec^{-1}	(Shih et al., 2009)

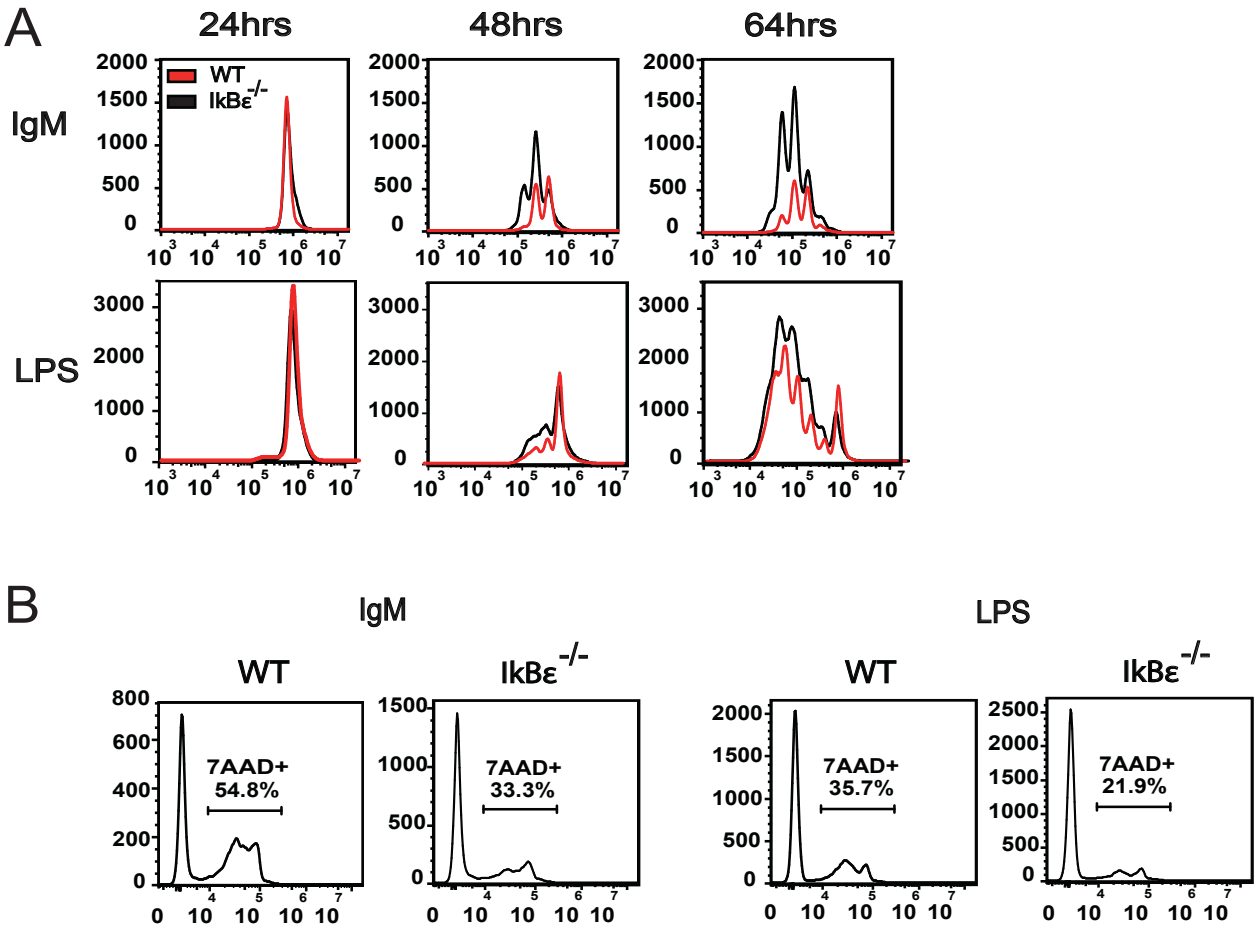

Figure 3.1: IkBe deficient B cells have increased proliferation and survival

A. B cells from IkBe-/- mice displayed increase in proliferation at in response to both IgM and LPS at each time point. B. 7-AAD measurements of B cell death show an increased percentage of B cells in the WT population undergo apoptotic death compared with IkBe-/- B cells.

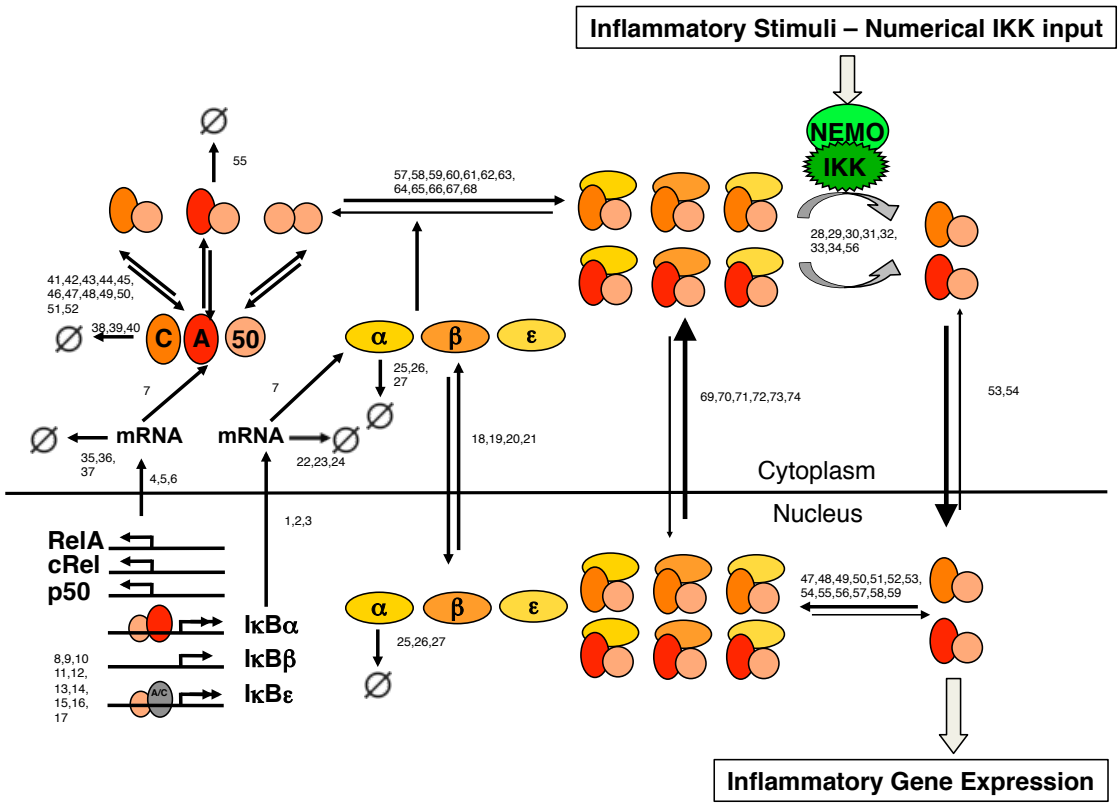

Figure 3.2: Model schematic of B cell NFκB signaling system
Wiring diagram of the full multi-dimer model containing RelA, p50, and cRel monomers forming indicated RelA:p50, cRel:p50, and p50:p50 dimers, and corresponding complexes with IκBα, -β, and -ε. Based on our data, this model allows for RelA:p50-responsive induction of IkBa, and RelA:p50 and cRel:p50-responsive induction of IkBe. The model calculates the activity dynamics of NFκB dimers RelA:p50 and cRel:p50 in response to experimentally determined IKK activities following IgM and LPS stimulation of B cells.

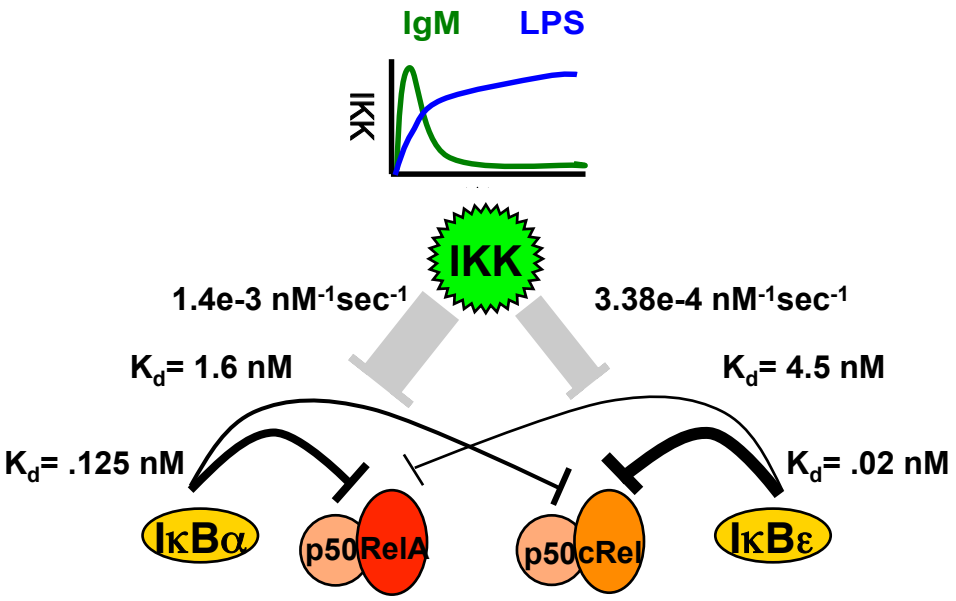

Figure 3.3: Specific IκB:NFκB affinity relationships result in stimulus specific NFκB activity in B cells
IgM and LPS stimulation results in two different IKK-activity profiles; IgM stimulation causes a transient profile while LPS provides lasting IKK activity. Activation of IKK results in degradation of IkBs and release of NFkB dimers into the nucleus. We infer that IκBε has a very strong affinity for cRel:p50, while IκBα has a strong affinity for RelA:p50, although weaker than IκBε-cRel:p50. IkBe has a low affinity for RelA:p50, while IκBα has a weak affinity for cRel:p50, although the affinity between IκBα-RelA:p50 is stronger than IκBε-cRel:p50.

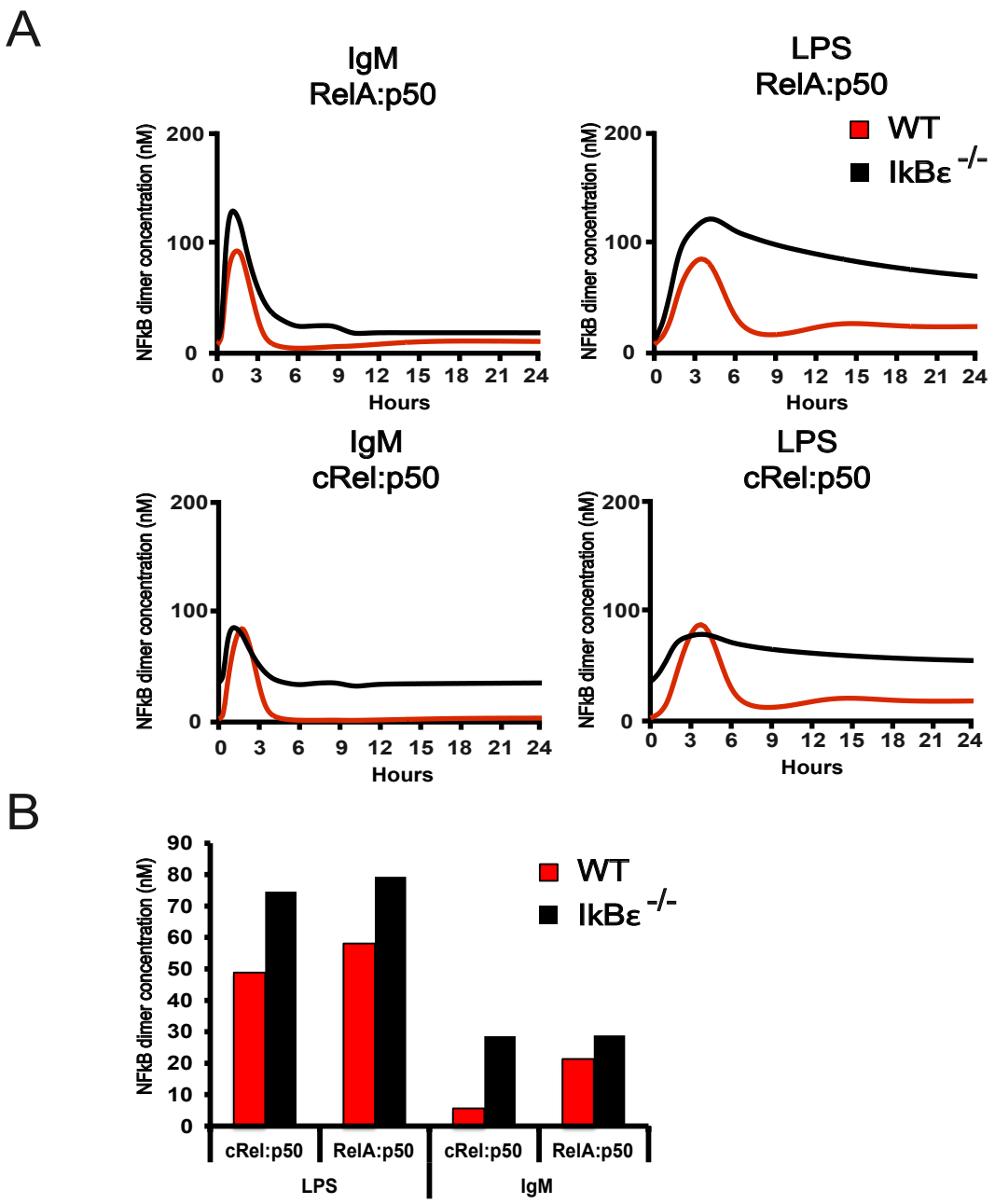

Figure 3.4: Model simulation results of IgM and LPS stimulated B cells
A. Data from the computational model illustrate the NFkB activity profiles for both WT and IkBe-deficient B cells under IgM and LPS stimulation. B. The model is able to recapitulate the experimental late time points, in which IkBe-deficient B cells have elevated cRel:p50 after both LPS and IgM stimulation. However, RelA:p50 is only elevated after LPS stimulation in IkBe-deficient B cells.

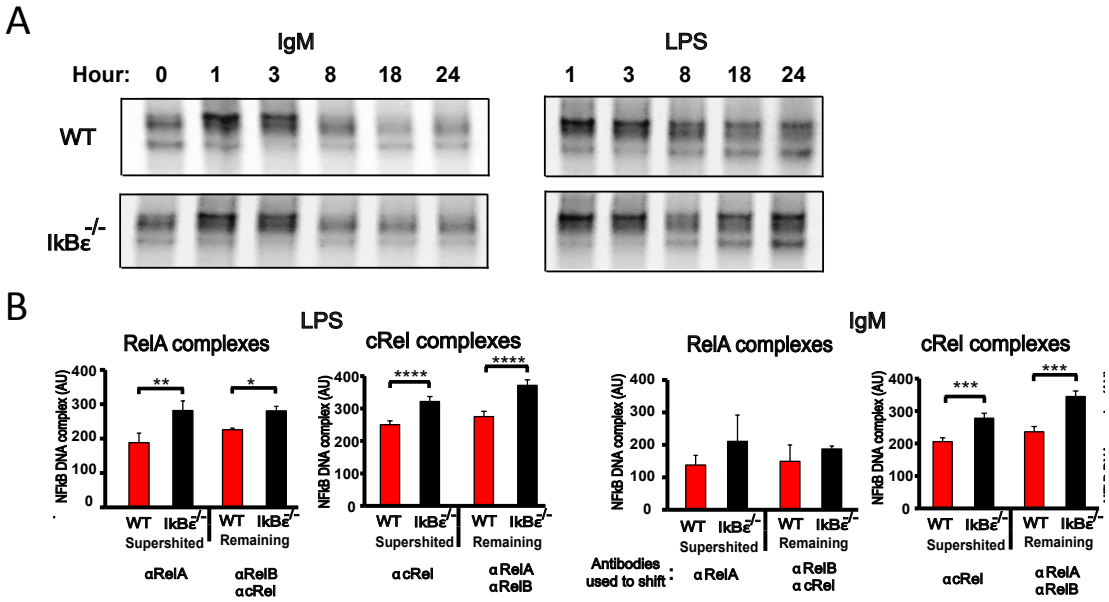

Figure 3.5: Experimental validation of IgM and LPS stimulated B cells show increased NFκB activity in IκBε-deficient B cells

A. Purified B cells were collected and extracted into cytoplasmic and nuclear fractions at indicated time points. Nuclear extracts were tested for total NFkB activity using EMSAs. IkBe-deficient B cells stimulated with either IgM or LPS exhibited increased NFkB activity at 18 and 24 hours following stimulation. B. The 24 hour nuclear extracts were supershifted to determine the specificity of the NFκB dimers formed. These samples were quantitated using IMageJ. Both IgM and LPS stimulation resulted in cRel:p50 activity in the IκBε-deficient B cell extracts compared with WT B cell extracts in the same condition. Additionally, LPS stimulated IκBε-deficient B cell extracts had increased RelA:p50 activity as compared to WT B cell extracts.

Chapter 4: BAFF engages distinct NFkB effectors in maturing and proliferating B cells

4.1 Introduction

In Chapter 3, we established the importance of the NFκB signaling system in B cell proliferation in survival. IκBε was shown to have a negative feedback effect on NFκB activity, and thus limiting B cell proliferation and survival when undergoing pathogenic (LPS) or antigenic (IgM) stimulation. Here we look at the importance of the NFκB signaling system in maturing and proliferating B cells, particularly mature follicular B cells. Two receptors are critical in the process of maintenance and activation/expansion of the follicular B cell pool, the B cell antigen receptor (BCR) and the B cell activating factor (BAFF) (Cancro, 2009; Khan, 2009; Lesley et al., 2004; Shinners et al., 2007; Stadanlick et al., 2008). Previous studies have shown that the BCR has a critical function in antigen-responsive B cell expansion and in maintaining the mature B cell pool (Lam et al., 1997). In contrast, deletion of the BAFF ligand or BAFF receptor results in a severe deficiency of mature B cells (Harless et al., 2001; Schiemann et al., 2001). Additionally, previous work has shown that upon antigenic stimulation of mature follicular B cells, co-stimulation of the BAFF receptor results in enhanced B cell expansion *in vitro* (Huang et al., 2004; Rickert et al., 2011; Schweighoffer et al., 2013).

NFκB signaling through these receptors in B cells is known to be mediated by two distinct pathways, the NEMO-dependent canonical pathway and the NEMO-independent non-canonical pathway. BCR activation results in the activation of the NEMO-IKK complex. This leads to degradation of the IκBs that sequester NFκB in the cytoplasm, allowing for the nuclear translocation of RelA- and cRel- containing NFκB dimers. Activation of the BAFF receptor results in the sequestration of TRAF3, allowing for the stabilization of NIK and subsequent activation of the NEMO-independent IKK1 complex. This complex triggers the processing of p100 to p52, resulting in the generation and nuclear accumulation of RelB:p52 NFκB dimers (Claudio et al., 2002).

Recent studies have begun to investigate how the interactions of the NFκB canonical and non-canonical pathways in order to understand the integration of BCR and BAFF receptor signaling. There is evidence for a dependency on the canonical NFκB signaling induced by BCR activation as a requirement for the BAFF receptor to transmit survival signals. That is, induction of the nfkb2 gene is required in order to provide a pool of p100 substrate for the activated non-canonical IKK1 complex to process and produce the non-canonical RelB:p52 NFκB effector (Cancro, 2009; Stadanlick et al., 2008). This dependency between canonical and non-canonical NFκB signaling was also found to be evident in MEFs in response to lymphotoxin beta (Basak et al., 2008).

This work focuses on the role of NFκB signaling in mediating BAFF's function in both maturing and proliferating B cells using quantitative cell biology, biochemistry, and mathematical modeling. In particular, we show here that BAFF co-stimulation enhances BCR-stimulated cRel activation and the fraction of B cells entering the proliferative program. Using quantitative analysis through a mathematical model of the NFκB signaling network, we show that cRel hyperactivation is mediated through the non-canonical pathway, through neutralization of p100 overexpression that leads to the formation of the multimeric IκBsome and its associated IκBδ activity. We are able to show through the mathematical model that these processes are sufficient to account for the experimental observations, and we develop predictions from the model that are then tested and confirmed experimentally.

4.2 Materials and Methods

Cell isolation and culture

Spleens were harvested from C57Bl6 mice *wild type* (Jackson Labs, Bar Harbor, MN). The collected spleens were homogenized using frosted glass slide grinding. For B cell isolation, homogenized splenocytes were incubated with anti-CD43 (Ly-48) microbeads for 15 minutes at room temperature. Following this incubation, the cells were washed with Hanks Buffered salt solution (HBSS) (Gibco 14170) containing 1% FCS, 10mM HEPES (Gibco 15630) and 1% FCS (Sigma F2442) and separated over a magnetic column (LS column MiltenyiBiotec 130-042-401). For B cells, purity was determined by flow cytometry using PE anti-B220 (eBioscience 12-0452-83). Purity was consistently found to be between 92% and 95% (data not shown). Complete media consisting of RPMI-1640 (Gibco 11875), 10mM HEPES (Gibco 15630), 1 mM Sodium Pyruvate (Gibco 11360), 1 mM non-essential amino acids (Gibco 11140), 0.055 mMb-mercaptoethanol (Gibco 21985), 100 units Penicillin/Streptomycin (Gibco 10378016) and .3 mg/ml glutamine was used to culture either B cells. B cells were stimulated with 5-10mg/ml of Fab Goat anti-mouse IgM, m-chain specific (Jackson Immunology Research#115-006-020) and / or 50ng/ml Recombinant Mouse BAFF / BLyS / TNFSF13B (R&D systems 2106BF).

Electrophoretic Mobility Shift Assay

Nuclear extracts were generated from B cells using high salt extraction. In brief, purified B cells were incubated with a low salt buffer (10mM HEPEs pH 7.9 (Gibco), 10mM KCl (Thermo Fisher Scientific P217), 0.1mM EGTA (Sigma E-4378), 0.1mM EDTA (Thermo Fisher Scientific S312), 1mM DTT (Thermo Fisher Scientific BP172-5), 1mM PMSF (Sigma P7626), 5mg/mL apoprotein (Sigma A1153), 5mg/ml leupeptin (Sigma L2884), 1mM pepstatin A (Sigma P5318) for 10 minutes on ice. Following this incubation, the cells were disrupted through the addition of NP-40 (US Biological N3500) to a final concentration of .5% and vortexing for 15 seconds. Nuclei were pelleted away from the cytoplasmic fraction by centrifugation at 15,000 rpm for 1 minute and the cytoplasmic fraction was pipetted into a separate tube. The remaining nuclei were disrupted by a 20 minute incubation at 4oC in a high salt buffer (20mM HEPES pH 7.9 (Gibco), 400mM NaCl (Thermo Fisher Scientific S671), 1mM EGTA (Thermo Fisher Scientific), 1mM EDTA (Thermo Fisher Scientific), 20% Glycerol (Thermo Fisher Scientific), 1mM DTT (Thermo Fisher Scientific), 1mM PMSF(Sigma). The nuclear fraction was collected following centrifugation at 15,000 rpm for 5 minutes. Equal amounts of nuclear extracts (1ug) were pre-incubated for 20 minutes on ice in the presence or absence of antibodies specific for RelA (Santa Cruz Biotechnology sc-372), RelB (Santa Cruz Biotechnology sc-226), and cRel (Santa Cruz Biotechnologies sc-71) or in combination. Following the pre-incubation with antibodies, [g-32P]ATP (GE health) radio-labeled probe derived from HIV-kB sequence:

5’-GCTACAAGGGACTTTCCGCTGGGGACTTTCCAGGGAGG-3’ was added and incubated at room temperature for an additional 15 minutes. The resulting DNA/protein/antibody complexes were resolved by electrophoresis on a 5% non-denaturing polyacrylamide gel and exposed to storage phosphor screen (GE healthcare) overnight before image development on at Typhoon 9200 Variable Mode Imager (GE healthcare). Images were analyzed and quantitated using ImageQuant™ (GE Health).

Western blot analysis

Whole cell lysates were prepared using RIPA buffer lysis of B cells. Cytoplasmic extracts and nuclear extracts were prepared as previously described. The resulting lysates and extracts were run on either 10% SDS-PAGE gels or 5%-14% Criterion Tris-HCl Gel (Bio Rad). The following antibodies were used to identify the protein of interest: p65, cRel, RelB, Ikba, Ikbe, actin, atubulin (Santa Cruz Biotechnology), nfkb1 and nfkb2 (Dr. Nancy Rice). The resulting proteins were detected using the Bio-Rad ChemiDoc XRS System and SuperSignal West Femto Substrate Maximum Sensitivity Substrate (Thermo Scientific) to detect chemiluminescense released by HRP-labeled secondary antibodies.

IKK kinase assays

Assays were performed as described(Werner et al., 2005). Briefly, cytoplasmic extracts were collected and the IKK complex was immunoprecipitated with anti-IKKγ antibody, followed by addition of protein G

sepharose beads. Beads were washed and subject to in vitro kinase assay containing ATPγ32, GST-IκBα(1-54). The reaction was stopped with SDS-sample buffer, and proteins were resolved by SDS-PAGE, and visualized by autoradiography or immunoblot.

Flow cytometry analysis of survival and B cell development

Purified B cells were stained with cultured in complete media with or without BAFF, at various time points B cells were collected and stained with 7AAD (Invitrogen A1310). The B cells were analyzed for survival using a C6 Accuri flow cytometer (BD Biosciences). Differences in cell viability were measured using FlowJo (Tree star inc.).

B cell development was obtained from single-cell suspensions of spleens incubated with fluorescently labeled antibodies for 30 min at 4°C in staining buffer (PBS with 0.5% BSA or 2.5% FCS). Data were collected on a FACSCalibur or LSR II flow cytometer (BD Biosciences) and analyzed using FlowJo software (Tree Star, Inc.) and FLOWmax(Shokhirev and Hoffmann, 2013)which determines maximum-likelihood cellular parameter sets for fraction of responding cells, times to division, and times to death for generations 0 to 10.

Computational modeling

This model is adapted from the previously published IκB – containing NFκB signaling models with the reactions that govern NF-κB dimer generation. The input to this model is a numerical curve for NEMO-IKK2 activity and the

outputs are free, nuclear RelA:p50, RelA:p52, RelB:p50, RelB:p52, cRel:p50, and cRel:p52 dimers. The association and dissociation rate constants between IkBs and NFkBs were adapted from a previous iteration of a B-cell version of the IkB – NFkB signaling model (Alves et al., 2014) and a previous iteration of a dendritic cell version of the IkB – NFkB signaling model (Shih et al., 2012).Parameterization of the model included the use of MEF and B-cell protein abundances.

This model represents the single-cell response of a population of B-cells, and the variability of NFkB responsive cells is assumed to be in the activation of NEMO-IKK2. This variability is assumed to be a lognormal distribution about the peak NEMO-IKK2 activity based on experimental data. Because the experimental data is an average of a population of cells, single-cell NEMO-IKK2 activity can have variability in the timing of its peak activity.

Based on population FACs experiments, a percentage of active responsive cells were assumed for each population in determining the output protein levels. We assume that cells that are responsive to BCR stimuli (divide and survive) are cells that have responsive NFkB activity while cells that are not responsive have basal levels of NFkB. Representative of the percentage of active B-cells are as follows: anti-IgM activation of wild type B-cells results in 20% active cells, while anti-IgM activation of *nfkb2*$^{+/-}$ B-cells results in 10% active cells. We defined a population of B-cells to include 1000 simulations of single B-cells, with a percentage of non BCR–responsive cells resulting from

basal levels of NEMO-IKK2 and NIK, while the active cells have a log-normal population distribution of NEMO-IKK2 activity and increased NIK accumulation as defined below. Additionally, we assume that all cells respond to BAFF stimulation, and have a lower BAFF-induced NEMO-IKK2 activity that also has a lognormal distribution. These BAFF stimulated cells also result in increased NIK accumulation as a result of activation of the non-canonical pathway. The co-stimulated cells have 20% BCR induced NEMO-IKK2 activity, with 80% BAFF-induced NEMO-IKK2 activity, while they all have increased NIK accumulation.

The ODEs were solved numerically using MATLAB version R2013a (The MathWorks, Inc.) with subroutine *ode15s*, a variable order, multi-step solver. Prior to stimulation, the system was allowed to equilibrate from starting conditions to a steady state, defined as showing no concentration changes greater than 1% over a period of 4000 minutes. Stimulus-induced perturbation from the steady state was accomplished by direct modulation of IKK activity via a numerical input curve representing anti-IgM and BAFF stimulation (adapted from (Werner et al., 2005)). Non-canonical activity was simulated by decreasing the NIK degradation rate constant by 30-fold at 5 hours, resulting in increased NIK accumulation. MATLAB model codes are available upon request.

Animal use.

The animal protocols for this study were approved by the University of California, San Diego Animal Care and Use Committee.

4.3 Results

Prior work has established that BCR and BAFF-R activate distinct NFκB signaling pathways, the so-called canonical, NEMO-dependent pathway, and the non-canonical, NEMO-independent pathway, respectively (Fig. 4.1A). Whereas the primary transcriptional effector of the former are cRel-containing NFκB dimers which may initiate the B cell proliferative program and enhance survival, the latter is known to activate RelB as well as other signaling pathways (e.g. PI3K) to enhance survival (Mackay et al., 2007; Ramakrishnan et al., 2004; Zarnegar et al., 2004).

We asked whether BAFF co-stimulation would enhance BCR-triggered B cell expansion via enhanced cell survival, or whether other signaling crosstalk mechanisms might be involved. Using the dye dilution with carboxyfluoresceinsuccinimidyl ester (CFSE), we monitored splenic B cell expansion following BCR cross-linking with anti-IgM [5-10 μg/ml, or molar equivalents of the F(ab′)2 fragment]. Co-stimulation with BAFF-R increased this B cell expansion, as first observed at 44 hrs and confirming previous reports (Craxton et al., 2007; Huang et al., 2004; Schweighoffer et al., 2013; Stadanlick et al., 2008) (Fig. 4.1B).

In order to determine the underlying molecular mechanism for BAFF's enhancement of B cell expansion, we examined the NFκB DNA binding activities using electrophoretic mobility shift assay coupled with antibodies to ablate all but the NFκB dimer of interest. Anti-IgM stimulation alone resulted in

a transient cRel NFκB activity in B cells, while BAFF stimulation was able to stimulate transient cRel NFκB activity in addition to long lasting RelB NFκB activity. Co-stimulation of the BAFF-R and BCR resulted in an increase in amplitude and duration of cRel NFκB activity, while RelB activity had little change from BAFF stimulation alone. Quantitation of the results (Fig 4.2) indicated that co-stimulation resulted in hyper-activation of cRel but not RelB NFκB activity.

To investigate the underlying molecular mechanism that allows BAFF to exert its physiological functions via distinct transcriptional effectors of the NFκB signaling system, we constructed a mathematical model of NFκB control in B cells in response to both canonical and non-canonical signals induced by BAFFR and BCR (Fig 4.3). The model was adapted from a previous version that recapitulates NFκB system control in murine embryonic fibroblasts (MEFs) in response to lymphotoxin-beta (LTβ) (Shih et al., 2012). A key mediator of signaling crosstalk is the NFκB responsive expression of p100 which not only functions as a substrate for p52 generation via processing (Basak et al., 2008; Stadanlick et al., 2008), but may also oligomerize to form the high molecular weight IκBsome, which presents a fraction of the C-terminal p100 ankyrin-repeat domain of p100 molecules as an IκB activity, termed IκBδ, capable of trapping latent NFκB dimers (Basak et al., 2007; Savinova et al., 2009). Thus cRel-driven p100 expression may not only potentiate RelB:p52 activation, but also lead to post-induction repression of

cRel:p50, akin to IκBδ-mediated repression of LPS-induced NFκB activity in MEFs (Shih et al., 2009). BAFF as a co-stimulus with IgM might thus neutralize the IκBδ-mediated negative feedback loop.

To examine the basic premise of the model, we first examined stimulus-responsive IκB dynamics in B cells. The three canonical IκBs, IκBα, -β, -ε, showed characteristic degradation at early time point and induction at late time points in response to anti-IgM, but this profile was unchanged when BAFF was applied as a co-stimulus (Fig. 4.4A). In contrast, p100 levels did not initially degrade but showed a huge induction beginning at 12hrs, and this induction was almost completely absent in co-stimulation conditions (Fig.4.4B) despite ample NFκB activity (Fig.4.2) and nfkb2 mRNA synthesis. These observations support a model in which p100 forms IκBδ-containing complex, which limit cRel activity during BCR-triggered B cell expansion.

Development of the mathematical model began with careful delineation of the model's topology, leveraging previously established models. We may distinguish between reactions that control IκB synthesis and degradation (Fig. 4.3A) and those that control NFκB monomer synthesis, dimerization, and interactions of dimers with IκBs (Fig. 4.3B). The former represents an extension of the previously published four IκB model (Basak et al., 2007; Shih et al., 2009) and the latter is an extension of a model of RelA and RelB dimers in dendritic cells (Shih et al., 2012) to include cRel as well. We thus account for all p50- and p52-containing dimers (8 of the 15), and the resulting 19

NFκB-IκB complexes. The two topologies are thus connected not only via protein-protein interactions but also via NFκB-dependent synthesis control, and the dual roles of nfkb2 in generating the NFκB dimerization partner p52 as well as an IκB family member. The aforementioned data contributed to an extensive training set described the Methods to achieve a B cell-specific parameterization. However, a major challenge in modeling B cell signaling is the cell-to-cell heterogeneity. While BAFF is thought to activate every B cell, while the BCR signal is more variable in whether there is activation of the B cell, and if activated, the variable dynamics of that activation. In order to address the heterogeneity, we didn't consider just a single B cell but a whole population of B cells and produced distributed kinase input profiles as follows. Anti-IgM alone activates the BCR response, and 20% of the B cell population are activated to proliferate, so we assume 20% undergo a NEMO-IKK activation input. Conversely, we assume BAFF activates all cells, while a co-stimulation has 20% of cells undergoing BCR responsive NEMO-IKK while the rest have a BAFF induced NEMO-IKK input. Additionally, we assume NIK activation is the same in all BAFF activated cells (Fig. 4.5). Simulations were produced with the aforementioned distributed kinase input profiles in recognition of the cell-to-cell heterogeneity of B cell responses; their average conforms to the measured profiles of IKK activity (Fig. 4.4C, Fig. 4.6, 1st row). Likewise, averaged simulations of IκB and NFκB dynamics show that cRel-containing dimers are transiently induced peaking at about 5 hrs before

returning to basal levels in response to BCR or BAFF-R stimulation alone (Fig. 4.6, 3rd row) whereas RelB-containing dimers are induced late and in a sustained and BAFF-R-dependent manner (Fig. 4.6, 4th row); these simulation outputs match our biochemical analysis (Fig. 4.2). Finally, simulation of the co-stimulation scenario (**Fig. 4d, 3rd column**) provides for RelB and cRel with the observed superactivation of cRel at late times (20-40 hrs). The fact that early cRel activity is relatively unchanged suggests that augmented NEMO-IKK2 activity may not account for the observed superactivation. Instead, it coincides with a BAFF and NIK-dependent reduction in p100/IκBδ abundance at late times, which neutralizes its IgM driven expression. In sum, mathematical modeling demonstrates that kinetic considerations alone are sufficient to account for context-specific transcriptional effectors of BAFF-R signaling, without the need to invoke context-specific molecular mechanisms.

The mathematical model encapsulates the key hypothesis that BAFF functions to relieve IκBδ-mediated termination of cRel activity. To examine this hypothesis further, we asked if a reduction in nfkb2 expression may be sufficient to phenocopy BAFF's co-stimulatory effect on B cell expansion. Mathematical modeling of a two-fold reduction in nfkb2 mRNA synthesis rate akin to nfkb2 heterozygosity, resulted in reduced p100 protein in both basal and IgM-stimulated condition in silico (**Fig. 5a**) and in cells (**Fig. 5b**), encouraging us to use the model to the experimental work. Importantly, we found that *nfkb2*$^{+/-}$ mice showed normal B cell populations (**Supplementary**

Fig. 5), unlike *nfkb2*$^{-/-}$ mice, which show severe deficiencies in B cell development, in particular in the mature follicular B cell population, which are the primary responders to anti-IgM(Allman et al., 2001; Meyer-Bahlburg et al., 2008; Rawlings et al., 2012).

Using the model we predicted that the amount of cRel-p100 complex following 24 hours of anti-IgM stimulation would be reduced in *nfkb2*$^{+/-}$B cells compared to the *wild type* controls (**Fig. 5c**). Quantitative co-immunoprecipitation experiments tracked well with the mathematical calculation (**Fig.5d**). Next, we simulated NFκB activation by IgM; model simulations predicted that nfkb2 heterozygosity would result in enhanced cRel activity, showing a dramatic effect at late times (24-48 hrs), when cRel activity is usually terminated in wild type cells (**Fig. 5e**). Biochemical analysis confirmed this prediction, showing slight enhancement of peak activity, but dramatic failure to terminate cRel DNA binding activity at late times (**Fig. 5f**). These studies establish the expression level of p100 as a remarkably sensitive parameter in terminating NFκB activity via the multimeric IκBδ.

4.4 Discussion

In this study, we demonstrated that BAFF plays a critical role in the co-stimulation of BCR-activated B cells through hyper-activation of cRel. Through a combination of experimental methods and mathematical modeling, our studies revealed p100/IκBδ as a key regulator of this cRel driven proliferative program in B cells. In fact, it is the BAFF activation of the non-canonical pathway which allows for the ablation of IκBδ activity, resulting in hyper-activation of cRel NFκB activity in the co-stimulated conditions.

We turned to mathematical modeling in order to delineate the mechanisms that result in the B cell expansion phenotype observed upon co-stimulation. The model was able to show that known molecular mechanisms and kinetic rate constants (both experimentally determined or inferred within a reasonable range) are sufficient to account for the observed molecular and genetic phenomena in maturing and proliferating B cells. Additionally, this model was used to develop the hypothesis that reduced p100 expression (through nfkb2 heterozygous B cells) result in elevated levels of nuclear cRel NFκB activity at late time points.

Our work thus illustrates why previous mathematical models of NFκB regulation by IκBs remain incomplete and that the mechanisms of dimer generation must be included; a key reason is that the nfkb1 and nfkb2 gene products p105 and p100 function both as precursors for the dimerization partners p50 and p52, as well as building blocks for IκBsome assembly.

Indeed, the multi-step IκBsome maturation process (Savinova et al., 2009) is a key determinant of the speed of the negative feedback loop and thus the duration of cRel activity. The present version of the kinetic model is not explicit about the underlying molecular mechanisms; indeed, mechanistic fine-graining of the model may require further experimental studies to determine the sequence of molecular interactions that result in IκBsome functions. A second, even greater challenge is to provide such quantitative experimental data at single cell resolution; it is well known that lymphocytes respond to activation stimuli with a high degree of cell-to-cell heterogeneity. Here we assumed that the phenotypic heterogeneity at the cell biological level is reflected in heterogeneity at the NFκB network level, as digital dose responses of NFκB had also been observed with TNF (Tay et al., 2010). As such we included a digital activation filter, as well as heterogeneity in the timing of activation that were based on the distributions obtained from the analysis of CFSE data. However, future studies may address the challenge of obtaining dynamic data from single primary B-cells in live cell microscopy experiments and refine the model formulation accordingly.

4.5 Acknowledgements

Chapter 4, in part, is a reprint of material being prepared for publication as “BAFF engages distinct NFkB effectors in maturing and proliferating B cells” by Almaden J, Tsui R, Birnbaum H, Shokhirev MN, Davis-Turak J, and Hoffmann A. Jon Almaden provided the experimental data supporting the phenotype seen in co-stimulation of B cells and the experimental validation of computational model predictions for this chapter. The dissertation author was a primary investigator and author of this work.

Table 4.1: Western blot data of wild type B cells and wild type fibroblasts for the basal levels of NFκB and IκB

Species	Molecules/Cell (MEFs)	Concentration in MEFs (nM)	Concentration in B-cells (nM)
RelA	~480,000	~340	~220
IkBa	~400,000	~220	~150
IkBb	~100,000	~70	~80
IkBe	~25,000	~20	~45
p50	~450,000	~374	~380

Table 4.2: Parameter Table and Reactions for B cell model with canonical and non-canonical NFκB signaling pathways

Reaction	Location	Param .No.	Parameter Value	Category	Source
Reaction rates determined by transcriptional programs and cytokine levels					
=>tIκBα (basal)	Nucleus	1	4.8e-3 nM/min	IκB Synth.	Parameter value chosen to fit mRNA and protein Expression profiles as measure by RNase Protection (RPA) and Western blot assays, reformulated from Werner et al. (2008) to fit a Hill function
=>tIκBβ (basal)	Nucleus	2	1.2e-3 nM/min	IκB Synth.	*Refer to #1*
=>tIκBε (basal)	Nucleus	3	1.2e-4 nM/min	IκB Synth.	*Refer to #1*
=>tRelA (basal)	Nucleus	4	3.6e-5 nM/min	NFκB Synth.	*Refer to #1*
=>tp50 (basal)	Nucleus	5	2.9e-5 nM/min	NFκB Synth.	*Refer to #1*
=>tRelB (basal)	Nucleus	6	4.2e-5 nM/min	NFκB Synth.	*Refer to #1/*Fitted
=>tp100 (basal)	Nucleus	7	8e-7 nM/min	NFκB Synth.	*Refer to #1*
=>cRel (basal)	Nucleus	8	3.6e-6 nM/min	NFκB Synth.	*Refer to #1/*Fitted
=> NIK	Cytoplasm	9	4.2e-2 nM/min	NIK Synth.	Set to yield measured abundance in conjunction with #10
NIK =>	Cytoplasm	10	4.6e-2	NIK Deg.	Based on estimated 15-minute half-life/ Fitted
IκB Reactions					
mRNA => mRNA + protein	Nuc ->Cyt	11	12 proteins/ mRNA/min	Translation	Derived from the elongation rate of the ribosome and corrected for the nucleotide spacing between adjacent ribosomes on the same transcript 1800 nt min^{-1} / 150 nt = 12 min^{-1}
=>tIκBα (A50/A52-induced)	Nucleus	12	200 Fold over consitutive	IκB Synth.	*Refer to #1*
Hill K_d (A50/A52-induced)	Nucleus	13	150 nM	IκB Synth.	*Refer to #1*
=>tIκBε (A50/A52-induced, 37 min. delay)	Nucleus	14	25 Fold over consitutive	IκB Synth.	*Refer to #1*
Hill K_d (A50/A52-induced)	Nucleus	15	150 nM	IκB Synth.	*Refer to #1*

Table 4.2: Parameter Table and Reactions for B cell model with canonical and non-canonical NFkB signaling pathways, Continued

Reaction	Location	Param. No.	Parameter Value	Category	Source
=>tIκBε (C50/C52-induced, 37 min. delay)	Nucleus	16	250 Fold over consitutive	IκB Synth.	*Refer to #1*
Hill K_d (C50/C52-induced)	Nucleus	17	150 nM	IκB Synth.	*Refer to #1*
p100 + p100 =>IκBδ	Cyt, Nuc	18	1.2e-2 nM^{-1} min^{-1}	IκB Synth.	Estimated a $K_d$of 10nM
IκBδ => p100 + p100	Cyt, Nuc	19	1.2e-2 min^{-1}	IκB Synth.	*Refer to #19*
IκBα(c) =>IκBα(n)	Cyt ->Nuc	20	6.0e-2 min^{-1}	Transport	Adapted from (Shih et al., 2009)
IκBβ(c) =>IκBβ(n)	Cyt ->Nuc	21	9.0-3 min^{-1}	Transport	(Shih et al., 2009)
IκBε(c) =>IκBε(n)	Cyt ->Nuc	22	4.5e-2 min^{-1}	Transport	(Shih et al., 2009)
IκBδ(c) =>IκBδ(n)	Cyt ->Nuc	23	4.5e-2 min^{-1}	Transport	(Shih et al., 2009)
IκB[α/β/ε/δ](n) =>IκB[α/β/ε/δ](c)	Nuc ->Cyt	24	1.2e-2 min^{-1}	Transport	(Shih et al., 2009)
tIκBα =>	Nucleus	25	2.9e-2 min^{-1}	IκB Deg.	mRNA half-life measurements using actinomycin-D treatment of cells and RPA (unpublished results)
tIκBβ =>	Nucleus	26	2.9e-3 min^{-1}	IκB Deg.	*Refer to #25*
tIκBε =>	Nucleus	27	3.8e-3 min^{-1}	IκB Deg.	*Refer to #25*
IκBα =>	Cyt, Nuc	28	0.12 min^{-1}	IκB Deg.	(Shih et al., 2009)
IκBβ =>	Cyt, Nuc	29	0.12 min^{-1}	IκB Deg.	(Shih et al., 2009)
IκBε =>	Cyt, Nuc	30	1.2e-2 min^{-1}	IκB Deg.	Based on estimated 1 hour half-life
IκBδ =>	Cyt, Nuc	31	3e-3 min^{-1}	IκB Deg.	Based on estimated 4 hour half-life
IκB[α/β/ε/δ]-NFκB =>NFκB	Cyt, Nuc	32	2.4e-4 min^{-1}	IκB Deg.	Based on estimated 48 hour half-life
IκBα => (NEMO-mediated)	Cytoplasm	33	1.4e-3 nM^{-1} min^{-1}	IκB Deg.	Based on measured IκB degradation timecourses given numerical input curves
IκBαNFκB =>NFκB (NEMO-mediated)	Cytoplasm	33	1.4e-3 nM^{-1} min^{-1}	IκB Deg.	
IκBβ => (NEMO-mediated)	Cytoplasm	34	4.5e-4 nM^{-1} min^{-1}	IκB Deg.	*Refer to # 33*
IκBβNFκB =>NFκB (NEMO-mediated)	Cytoplasm	34	4.5e-4 nM^{-1} min^{-1}	IκB Deg.	*Refer to # 33*

Table 4.2: Parameter Table and Reactions for B cell model with canonical and non-canonical NFkB signaling pathways, Continued

Reaction	Location	Param .No.	Parameter Value	Category	Source
IκBε => (NEMO-mediated)	Cytoplasm	35	3.4e-4 nM^{-1} min^{-1}	IκB Deg.	*Refer to # 33*
IκBεNFκB =>NFκB (NEMO-mediated)	Cytoplasm	35	3.4e-4 nM^{-1} min^{-1}	IκB Deg.	*Refer to # 33*
IκBδ => (NIK-mediated)	Cytoplasm	36	0.6 nM^{-1} min^{-1}	IκB Deg.	V_{max} and K_m of NIK-mediated reactions based on protein degradation and estimated NIK abundances.
IκBδNFκB =>NFκB (NIK-mediated)	Cytoplasm	36	0.6 nM^{-1} min^{-1}	IκB Deg.	
IκBδ => (NIK-mediated, K_m)	Cytoplasm	37	100 nM	IκB Deg.	*Refer to #36*
NF-κB reactions					
p100 => p52 (NIK-mediated)	Cytoplasm	38	5.0e-2 nM^{-1} min^{-1}	NFκB Synth.	*Refer to #36*
p100 => p52 (NIK-mediated, p100 K_m)	Cytoplasm	39	10 nM	NFκB Synth.	*Refer to #36*
=>cRel (A50/A52/C50/C52-induced, 1 hr delay)	Nucleus	40	200 Fold over consitutive	NFκB Synth.	*Refer to #1/Fitted*
Hill K_d (A50/A52/C50/C52-induced)	Nucleus	41	150 nM	NFκB Synth.	*Refer to #1/Fitted*
=>tp100 (A50/A52-induced, 4 hr delay)	Nucleus	42	1000 Fold over consitutive	NFκB Synth.	*Refer to #1/Fitted*
Hill K_d (A50/A52-induced)	Nucleus	43	50 nM	NFκB Synth.	*Refer to #1/Fitted*
=>tp100 (C50/C52-induced, 4 hr delay)	Nucleus	44	1500 Fold over consitutive	NFκB Synth.	*Refer to #1/Fitted*
Hill K_d (C50/C52-induced)	Nucleus	45	50 nM	NFκB Synth.	*Refer to #1/Fitted*
tRelA =>	Nucleus	46	2.9e-3 min^{-1}	NFκB Deg.	*Refer to #25*
tp50 =>	Nucleus	47	2.9e-3 min^{-1}	NFκB Deg.	*Refer to #25*
tRelB =>	Nucleus	48	2.9e-3 min^{-1}	NFκB Deg.	*Refer to #25*
tp100 =>	Nucleus	49	9.6e-4 min^{-1}	NFκB Deg.	*Refer to #25*
tcRel=>	Nucleus	50	9.6e-4 min^{-1}	NFκB Deg.	*Refer to #25*

Table 4.2: Parameter Table and Reactions for B cell model with canonical and non-canonical NFkB signaling pathways, Continued

Reaction	Location	Param .No.	Parameter Value	Category	Source
RelA =>	Cyt, Nuc	51	2.3e-2 min^{-1}	NFκB Deg.	Based on estimated 0.5 hour half-life of NF-κB monomers
p50 =>	Cyt, Nuc	51	2.3e-2 min^{-1}	NFκB Deg.	
RelB =>	Cyt, Nuc	51	2.3e-2 min^{-1}	NFκB Deg.	
p100 =>	Cyt, Nuc	51	2.3e-2 min^{-1}	NFκB Deg.	
cRel =>	Cyt, Nuc	51	2.3e-2 min^{-1}	NFκB Deg.	
p52 =>	Cyt, Nuc	51	2.3e-2 min^{-1}	NFκB Deg.	
RelA + p50 => RelAp50	Cyt, Nuc	52	1.9e-3 nM^{-1} min^{-1}	NFκB Synth.	Based on dimerization studies (unpublished results)
RelA + p52 => RelAp52	Cyt, Nuc	52	1.9e-3 nM^{-1} min^{-1}	NFκB Synth.	
RelB + p52 => RelBp52	Cyt, Nuc	53	9.6e-4 nM^{-1} min^{-1}	NFκB Synth.	
RelB + p50 => RelBp50	Cyt, Nuc	53	3e-4 nM^{-1} min^{-1}	NFκB Synth.	
cRel + p50 => cRelp50	Cyt, Nuc	54	9.6e-4 nM^{-1} min^{-1}	NFκB Synth.	
cRel + p52 => cRelp52	Cyt, Nuc	55	1.9e-3 nM^{-1} min^{-1}	NFκB Synth.	
p50 + p50 => p50p50	Cyt, Nuc	56	1.8e-3 nM^{-1} min^{-1}	NFκB Synth.	
p52+ p52 => p52p52	Cyt, Nuc	57	1.8e-3 nM^{-1} min^{-1}	NFκB Synth.	
RelAp50 => RelA + p50	Cyt	58	1.9e-2 min^{-1}	NFκB Synth.	Based on dimerization studies (unpublished results)
RelAp52 => RelA + p52	Cyt	59	3.8e-2min^{-1}	NFκB Synth.	
RelBp52 => RelB + p52	Cyt	60	1.4e-2 min^{-1}	NFκB Synth.	
RelBp50 => RelB + p50	Cyt	61	4.6e-3 min^{-1}	NFκB Synth.	
cRelp50 =>cRel + p50	Cyt	62	1.4e-3 min^{-1}	NFκB Synth.	
cRelp52 =>cRel + p52	Cyt	63	1.4e-3min^{-1}	NFκB Synth.	
RelAp50 => RelA + p50	Nuc	64	1.9e-3 min^{-1}	NFκB Synth.	Estimated 10 fold higher affinity due to DNA binding
RelAp52 => RelA + p52	Nuc	65	3.8e-3min^{-1}	NFκB Synth.	*Refer to #64*
RelBp52 => RelB + p52	Nuc	66	1.4e-3 min^{-1}	NFκB Synth.	*Refer to #64*
RelBp50 => RelB + p50	Nuc	67	4.6e-3 min^{-1}	NFκB Synth.	*Refer to #64*
cRelp50 =>cRel + p50	Nuc	68	1.4e-4 min^{-1}	NFκB Synth.	*Refer to #64*
cRelp52 =>cRel + p52	Nuc	69	1.4e-4min^{-1}	NFκB Synth.	*Refer to #64*
p50p50 => p50 + p50	Cyt, Nuc	70	5.4e-2min^{-1}	NFκB Synth.	Based on dimerization studies (unpublished results)

Table 4.2: Parameter Table and Reactions for B cell model with canonical and non-canonical NFkB signaling pathways, Continued

Reaction	Location	Param .No.	Parameter Value	Category	Source
p52p52 => p52+ p52	Cyt, Nuc	71	5.4e-2min^{-1}	NFκB Synth.	Based on dimerization studies (unpublished results)
RelAp50(c) =>RelAp50(n)	Cyt ->Nuc	72	5.4 min^{-1}	Transport	(Shih et al., 2009)
RelAp52(c) =>RelAp52(n)	Cyt ->Nuc	72	5.4 min^{-1}	Transport	(Shih et al., 2009)
RelBp52(c) =>RelBp52(n)	Cyt ->Nuc	72	5.4 min^{-1}	Transport	(Shih et al., 2009)
RelBp50(c) =>RelBp50(n)	Cyt ->Nuc	72	5.4 min^{-1}	Transport	(Shih et al., 2009)
cRelp50(c) => cRelp50(n)	Cyt ->Nuc	72	5.4 min^{-1}	Transport	(Shih et al., 2009)
cRelp52(c) => cRelp52(n)	Cyt ->Nuc	72	5.4 min^{-1}	Transport	(Shih et al., 2009)
p50p50(c) => p50p50(n)	Cyt ->Nuc	72	5.4 min^{-1}	Transport	(Shih et al., 2009)
p52p52(c) => p52p52(n)	Cyt ->Nuc	72	5.4 min^{-1}	Transport	(Shih et al., 2009)
NFκB(n) =>NFκB(c)	Nuc ->Cyt	73	4.8e-3 min^{-1}	Transport	(Shih et al., 2009)
RelAp50 =>	Cyt, Nuc	74	2.4e-4 min^{-1}	NFκB Deg.	Based on estimated 48 hour half-life
RelAp52 =>	Cyt, Nuc	74	2.4e-4 min^{-1}	NFκB Deg.	
RelBp50 =>	Cyt, Nuc	74	2.4e-4 min^{-1}	NFκB Deg.	
RelBp52 =>	Cyt, Nuc	74	2.4e-4 min^{-1}	NFκB Deg.	
cRelp50 =>	Cyt, Nuc	74	2.4e-4 min^{-1}	NFκB Deg.	
cRelp52 =>	Cyt, Nuc	74	2.4e-4 min^{-1}	NFκB Deg.	
p50p50 =>	Cyt, Nuc	74	2.4e-4 min^{-1}	NFκB Deg.	
p52p52 =>	Cyt, Nuc	74	2.4e-4 min^{-1}	NFκB Deg.	
IκB[α/β/ε/δ]-NFκB =>IκB[α/β/ε/δ]	Cyt, Nuc	75	2.4e-4 min^{-1}	NFκB Deg.	*Refer to #74*
IκB:NF-κB interactions					
IκBα + RelA:p50 =>IκBα:RelA:p50	Cyt, Nuc	76	3e-3 nM^{-1} min^{-1}	IκB-NFκB interaction	Adapted from *Alves et. al 2013*
IκBβ + RelA:p50 =>IκBβ:RelA:p50	Cyt, Nuc	77	2e-4 nM^{-1} min^{-1}	IκB-NFκB interaction	Adapted from *Alves et. al 2013*
IκBε + RelA:p50 => IκBε:RelA:p50	Cyt, Nuc	78	1.3e-3 nM^{-1} min^{-1}	IκB-NFκB interaction	Adapted from *Alves et. al 2013*
IκBδ + RelA:p50 => IκBδ:RelA:p50	Cyt, Nuc	79	6e-4 nM^{-1} min^{-1}	IκB-NFκB interaction	Adapted from *Alves et. al 2013*

Table 4.2: Parameter Table and Reactions for B cell model with canonical and non-canonical NFkB signaling pathways, Continued

Reaction	Location	Param .No.	Parameter Value	Category	Source
IκBα + RelA:p52 =>IκBα:RelA:p52	Cyt, Nuc	76	3e-3 nM^{-1} min^{-1}	IκB-NFκB interaction	Adapted from *Alves et. al 2013*
IκBβ + RelA:p52 =>IκBβ:RelA:p52	Cyt, Nuc	77	2e-4 nM^{-1} min^{-1}	IκB-NFκB interaction	Adapted from *Alves et. al 2013*
IκBε + RelA:p52 => IκBε:RelA:p52	Cyt, Nuc	78	1.3e-3 nM^{-1} min^{-1}	IκB-NFκB interaction	Adapted from *Alves et. al 2013*
IκBδ + RelA:p52 => IκBδ:RelA:p52	Cyt, Nuc	79	6e-4 nM^{-1} min^{-1}	IκB-NFκB interaction	Adapted from *Alves et. al 2013*
IκBα + RelB:p50 =>IκBα:RelB:p50	Cyt, Nuc	80	1.3e-3 nM^{-1} min^{-1}	IκB-NFκB interaction	Adapted from *Alves et. al 2013*
IκBε + RelB:p50 => IκBε:RelB:p50	Cyt, Nuc	81	1.3e-3 nM^{-1} min^{-1}	IκB-NFκB interaction	Adapted from *Alves et. al 2013*
IκBδ + RelB:p50 => IκBδ:RelB:p50	Cyt, Nuc	82	6e-4 nM^{-1} min^{-1}	IκB-NFκB interaction	Adapted from *Alves et. al 2013*
IκBα + cRel:p50 =>IκBα:cRel:p50	Cyt, Nuc	83	3e-3 nM^{-1} min^{-1}	IκB-NFκB interaction	Adapted from *Alves et. al 2013*
IκBβ +cRel:p50 =>IκBβ:cRel:p50	Cyt, Nuc	84	2.1e-4 nM^{-1} min^{-1}	IκB-NFκB interaction	Adapted from *Alves et. al 2013*
IκBε + cRel:p50 => IκBε:cRel:p50	Cyt, Nuc	85	1.3e-3 nM^{-1} min^{-1}	IκB-NFκB interaction	Adapted from *Alves et. al 2013*
IκBδ + cRel:p50 => IκBδ:cRel:p50	Cyt, Nuc	86	1.98e-2 nM^{-1} min^{-1}	IκB-NFκB interaction	Adapted from *Alves et. al 2013*
IκBα + cRel:p52 =>IκBα:RelA:p52	Cyt, Nuc	83	3e-3 nM^{-1} min^{-1}	IκB-NFκB interaction	Adapted from *Alves et. al 2013*
IκBβ + cRel:p52 =>IκBβ:cRel:p52	Cyt, Nuc	84	2.1e-4 nM^{-1} min^{-1}	IκB-NFκB interaction	Adapted from *Alves et. al 2013*
IκBε + cRel:p52 => IκBε:cRel:p52	Cyt, Nuc	85	1.3e-3 nM^{-1} min^{-1}	IκB-NFκB interaction	Adapted from *Alves et. al 2013*

Table 4.2: Parameter Table and Reactions for B cell model with canonical and non-canonical NFkB signaling pathways, Continued

Reaction	Location	Param .No.	Parameter Value	Category	Source
IκBδ + cRel:p52 => IκBδ:cRel:p52	Cyt, Nuc	86	1.98e-2 nM^{-1} min^{-1}	IκB-NFκB interaction	Adapted from *Alves et. al 2013* Fitted (dependent on 76-79)
IκBα:RelA:p50 =>IκBα + RelA:p50	Cyt, Nuc	87	6e-4 min^{-1}	IκB-NFκB interaction	
IκBβ:RelA:p50 =>IκBβ + RelA:p50	Cyt, Nuc	88	1.7e-2 min^{-1}	IκB-NFκB interaction	
IκBε:RelA:p50 =>IκBε + RelA:p50	Cyt, Nuc	89	6e-3 min^{-1}	IκB-NFκB interaction	
IκBδ:RelA:p50 =>IκBδ + RelA:p50	Cyt, Nuc	90	8.4e-4 min^{-1}	IκB-NFκB interaction	Fitted (dependent on 76-79)
IκBα:RelA:p52 =>IκBα + RelA:p52	Cyt, Nuc	91	6e-4 min^{-1}	IκB-NFκB interaction	Fitted (dependent on 76-79)
IκBβ:RelA:p52 =>IκBβ + RelA:p52	Cyt, Nuc	92	1.7e-2 min^{-1}	IκB-NFκB interaction	Fitted (dependent on 76-79)
IκBε:RelA:p52 =>IκBε + RelA:p52	Cyt, Nuc	93	6e-3 min^{-1}	IκB-NFκB interaction	
IκBδ:RelA:p52 =>IκBδ + RelA:p52	Cyt, Nuc	94	8.4e-4 min^{-1}	IκB-NFκB interaction	
IκBα:RelB:p50 =>IκBα + RelB:p50	Cyt, Nuc	95	3e-2 min^{-1}	IκB-NFκB interaction	Fitted (dependent on 80 -82)
IκBε:RelB:p50 =>IκBε + RelB:p50	Cyt, Nuc	96	3e-2 min^{-1}	IκB-NFκB interaction	
IκBδ:RelB:p50 =>IκBδ + RelB:p50	Cyt, Nuc	97	8.4e-4 min^{-1}	IκB-NFκB interaction	
IκBα:cRel:p50 =>IκBα + cRel:p50	Cyt, Nuc	98	4.8e-3 min^{-1}	IκB-NFκB interaction	Fitted (dependent on 83-86)
IκBβ:cRel:p50 =>IκBβ +cRel:p50	Cyt, Nuc	99	1.7e-2 min^{-1}	IκB-NFκB interaction	
IκBε:cRel:p50 =>IκBε + cRel:p50	Cyt, Nuc	100	2.7e-5 min^{-1}	IκB-NFκB interaction	
IκBδ:cRel:p50 =>IκBδ + cRel:p50	Cyt, Nuc	101	8.4e-4 min^{-1}	IκB-NFκB interaction	
IκBα:cRel:p52 =>IκBα + cRel:p52	Cyt, Nuc	98	4.8e-3 min^{-1}	IκB-NFκB interaction	Fitted (dependent on 83-86)

Table 4.2: Parameter Table and Reactions for B cell model with canonical and non-canonical NFkB signaling pathways, Continued

Reaction	Location	Param .No.	Parameter Value	Category	Source
IκBβ:cRel:p50 =>IκBβ +cRel:p50	Cyt, Nuc	99	1.7e-2 min^{-1}	IκB-NFκB interaction	Fitted (dependent on 83-86)
IκBε:cRel:p50 =>IκBε + cRel:p50	Cyt, Nuc	100	2.7e-5 min^{-1}	IκB-NFκB interaction	
IκBδ:cRel:p50 =>IκBδ + cRel:p50	Cyt, Nuc	101	8.4e-4 min^{-1}	IκB-NFκB interaction	
IκBα:cRel:p52 =>IκBα + cRel:p52	Cyt, Nuc	98	4.8e-3 min^{-1}	IκB-NFκB interaction	Fitted (dependent on 83-86)
IκBβ:cRel:p52 =>IκBβ + cRel:p52	Cyt, Nuc	99	1.7e-2 min^{-1}	IκB-NFκB interaction	
IκBε:cRel:p52 =>IκBε + cRelp52	Cyt, Nuc	100	2.7e-5 min^{-1}	IκB-NFκB interaction	
IκBδ:cRel:p52 =>IκBδ + cRel:p52	Cyt, Nuc	101	8.4e-4 min^{-1}	IκB-NFκB interaction	
IκBα:NFκB(c) =>IκBα:NFκB(n)	Cyt ->Nuc	102	0.28 min^{-1}	Transport	(Shih et al., 2009)
IκBβ:NFκB(c) =>IκBβ:NFκB(n)	Cyt ->Nuc	103	0.028 min^{-1}	Transport	(Shih et al., 2009)
IκBδ:NFκB(c) =>IκBδ:NFκB(n)	Cyt ->Nuc	104	0.028 min^{-1}	Transport	Based on slower import rate of IκBβ:NFκB
IκBε:NFκB(c) =>IκBε:NFκB(n)	Cyt ->Nuc	105	0.14 min^{-1}	Transport	(Shih et al., 2009)
IκBα:NFκB(n) =>IκBα:NFκB(c)	Nuc ->Cyt	106	0.84 min^{-1}	Transport	(Shih et al., 2009)
IκBβ:NFκB(n) =>IκBβ:NFκB(c)	Nuc ->Cyt	107	0.42 min^{-1}	Transport	(Shih et al., 2009)
IκBε:NFκB(n) =>IκBε:NFκB (c)	Nuc ->Cyt	108	0.42 min^{-1}	Transport	(Shih et al., 2009)
IκBδ:NFκB(n) =>IκBδ:NFκB(c)	Nuc ->Cyt	109	0.42 min^{-1}	Transport	(Shih et al., 2009)

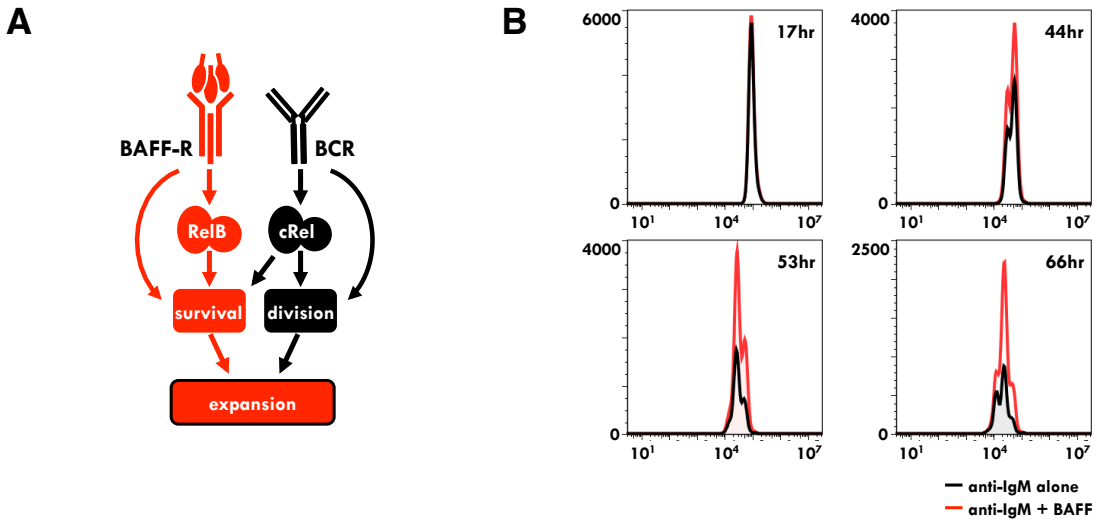

Figure 4.1: Activation of the both BAFF receptor and the BCR results in B cell expansion through activation of the canonical and non-canonical NFκB pathways

A. Schematic of the non-canonical and canonical NFkB pathways in B cells. Activation of the BAFF receptor is thought to activate the non-canonical NFkB pathway, resulting in RelB NFkB dimer activation which subsequently activates B cell survival, while activation of the BCR is thought to activate the canonical pathway, resulting in cRel NFkB dimer activation, enhancing the proliferation of B cells. This model suggests that co-stimulation results in B cell expansion as a result of BAFF enhancement of the survival of B cells. B. In vitro proliferation of wild type B cells labeled with CFSE and stimulated for three days with anti-IgM alone (black histogram) or anti-IgM + BAFF ligand (red histogram) and analyzed by flow cytometry. Live cell numbers gated by side- and forward-scatter profiles, followed by exclusion of 7AAD^{Hi} population representing dead cells.

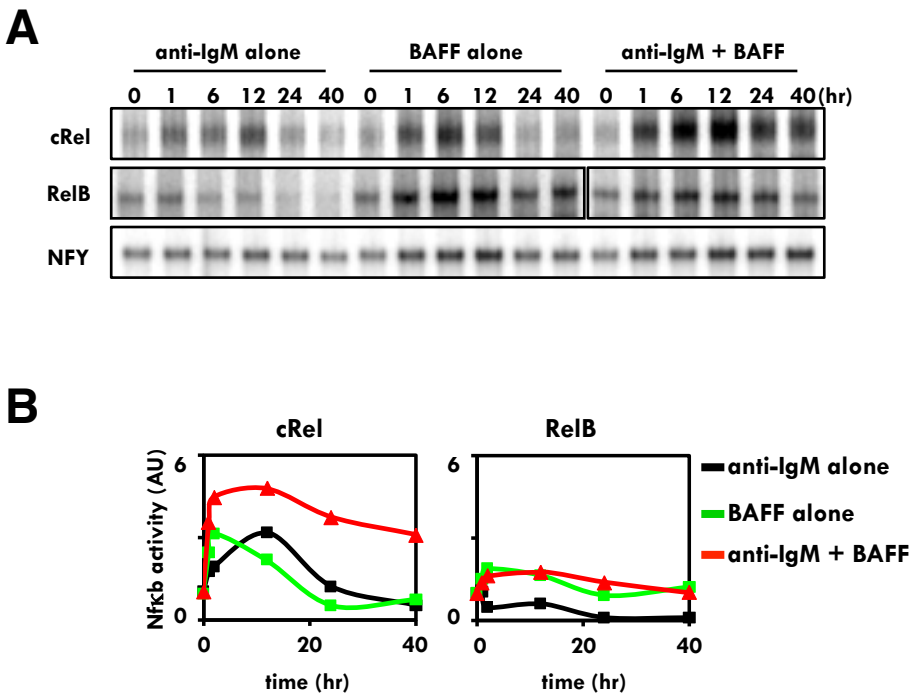

Figure 4.2: Co-stimulation of BCR and BAFF-R result in activation of cRel and RelB dimers, but enhanced expansion phenotype is dependent solely on cRel

A. Time course of NFκB cRel and RelB DNA binding activities monitored by EMSA. Nuclear extracts from wild-type B cells activated by indicated stimuli were collected and subjected to EMSA. NFY is used to ensure near-equal amounts of nuclear proteins were loaded onto gels. B. NFkB activity signals were quantified and graphed relative to their respective resting cell activities.

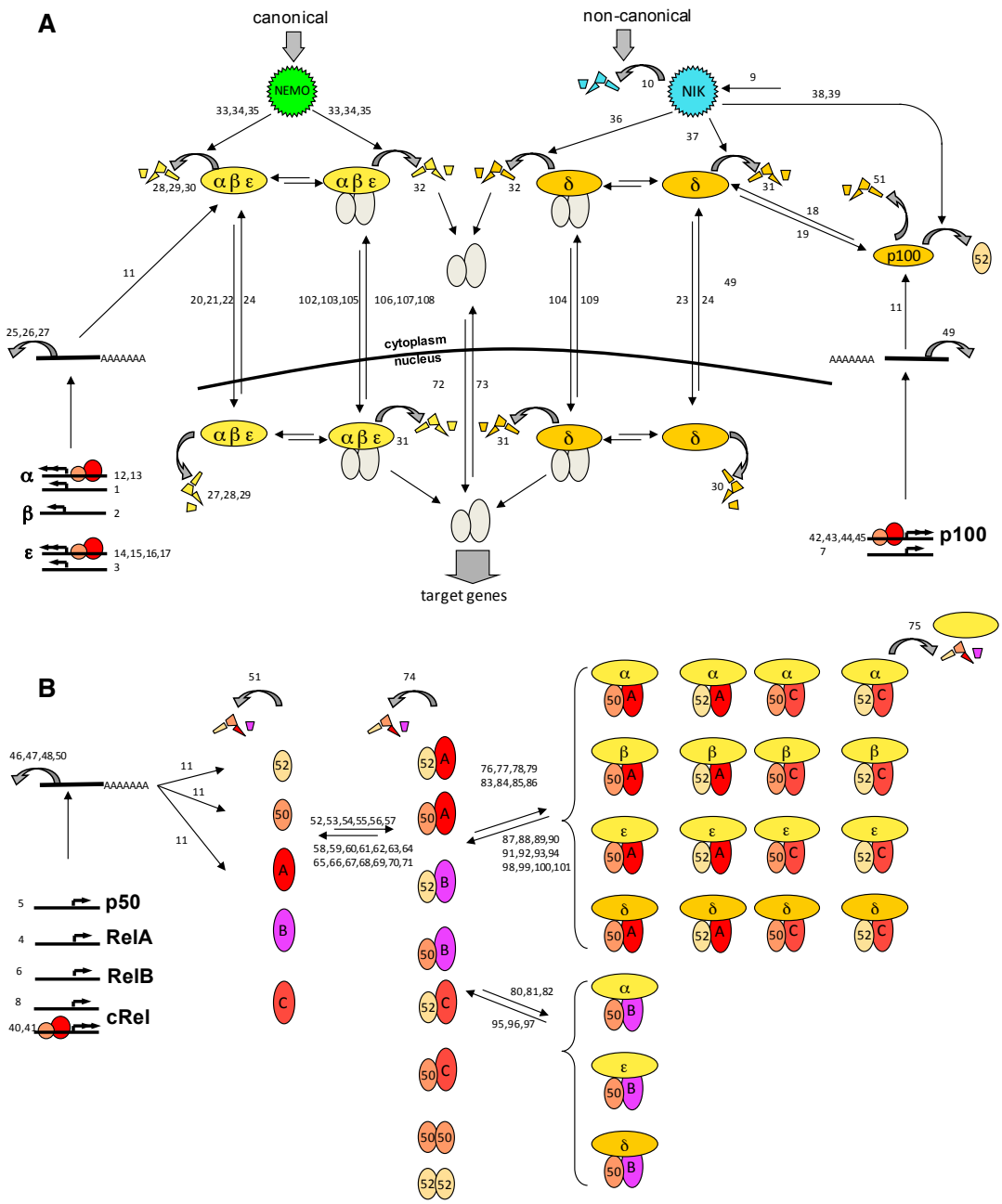

Figure 4.3: Wiring diagram depicting biochemical reactions described in the mathematical model

A. A schematic of the NFkB model that includes both the canonical stimulus through NEMO/IKK2 activity and the non-canonical stimulus through affecting the levels of NIK. A general NFkB is the grey dimer that is then further described in (B). B. A schematic of the NFkB monomers that are synthesized in the model and the dimer combinations included in the model. The IkB-NFkB complexes are also described here.

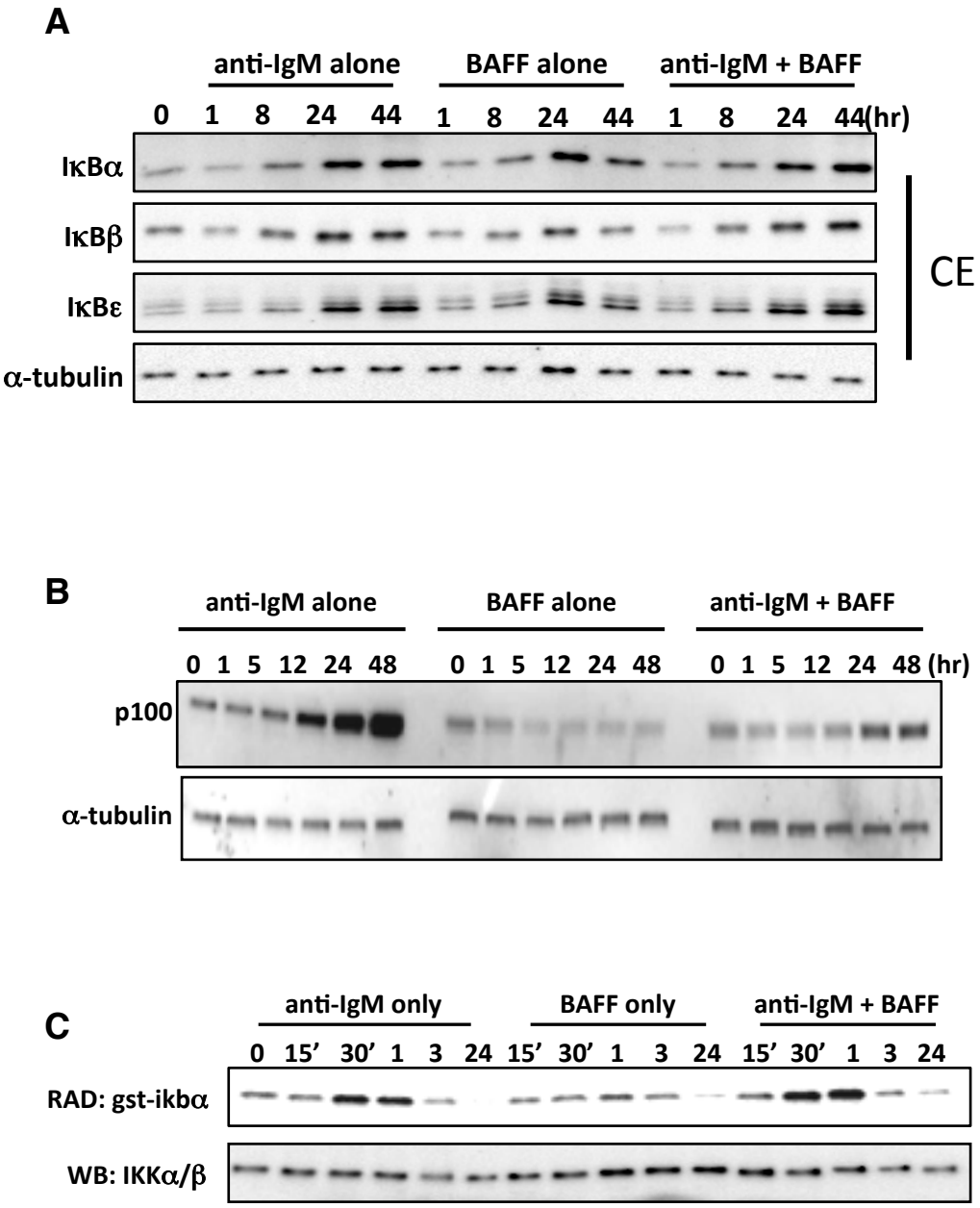

Figure 4.4: Canonical IκB protein levels and NEMO-IKK activity in BCR stimulated B cells are unchanged in BCR and BAFF co-stimulated B cells
A. Cytoplasmic protein levels of IκBα, IκBβ, and IκBε in stimulated *wild type* B cells were measured by Western blot. B. Cytoplasmic protein levels of p100 in stimulated *wild type* B cells as measured by Western blot. C. NEMO-associated kinase activity was determined in *wild type* B cells in an *in vitro* IP-kinase assay upon stimulation of anti-IgM alone, BAFF alone, or anti-IgM and BAFF.

Figure 4.5: Simulations of 1000 cells exposed to anti-IgM, BAFF, or both
Timecourses depicting canonical IKK and non-canonical NIK activities (model simulation input) in the top two rows and calculated timecourses in subsequent rows, specifically nuclear DNA binding activities of RelB and cRel, and abundances of IκBα, IκBε and IκBδ each with its indicated color scale. Each graph shows simulations of 1000 B cells for each condition (anti-IgM, BAFF, and co-stimulation). Cells vary in whether they activate IKK or not (20% do), and when it is activated, as the peak of the activity curve is normally distributed, as described in the methods.

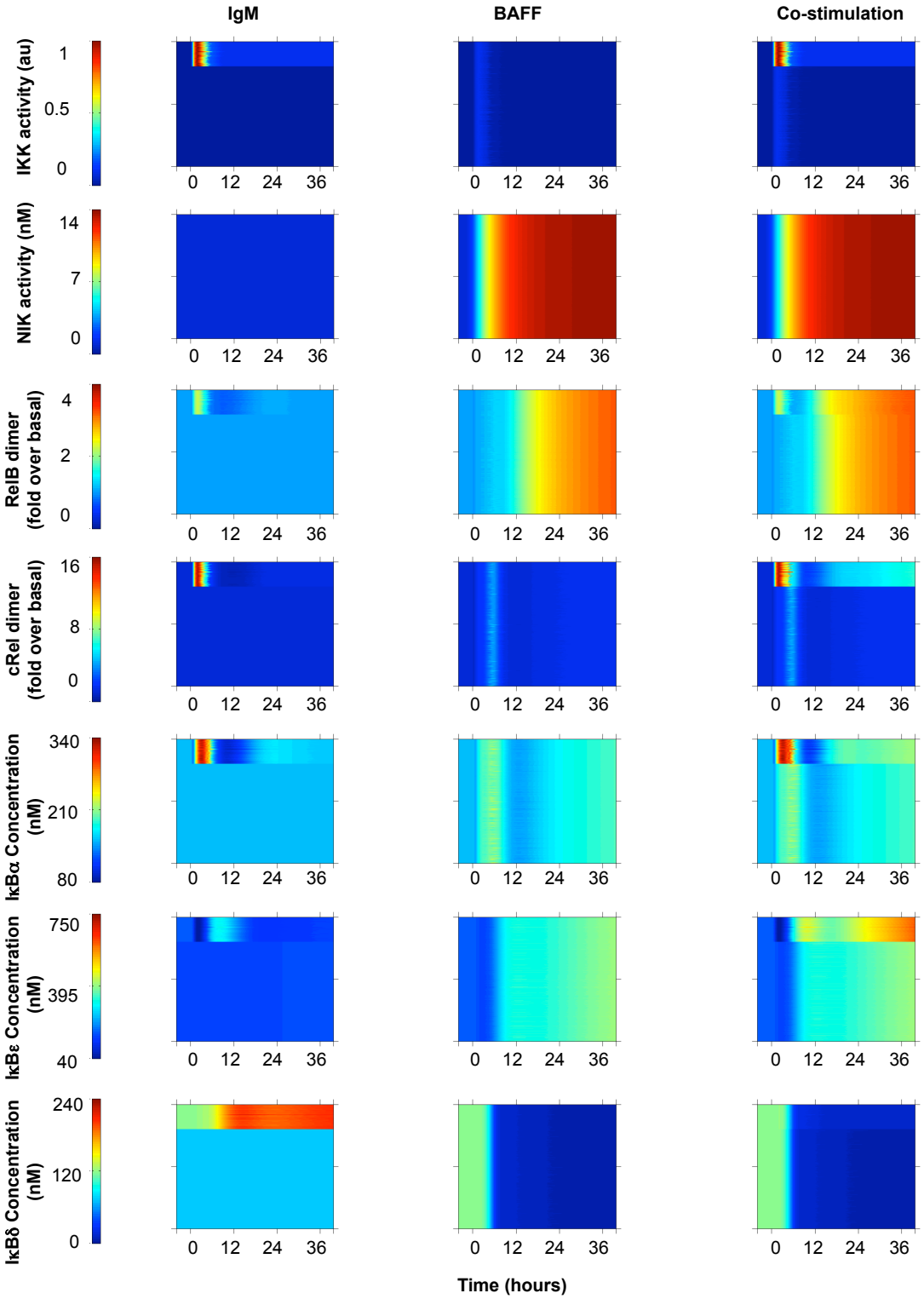
IgM
BAFF
Co-stimulation
IKK activity (au)
1
0.5
0
NIK activity (nM)
14
7
0
RelB dimer (fold over basal)
4
2
0
cRel dimer (fold over basal)
16
8
0
IκBα Concentration (nM)
340
210
80
IκBε Concentration (nM)
750
395
40
IκBδ Concentration (nM)
240
120
0
0 12 24 36
Time (hours)

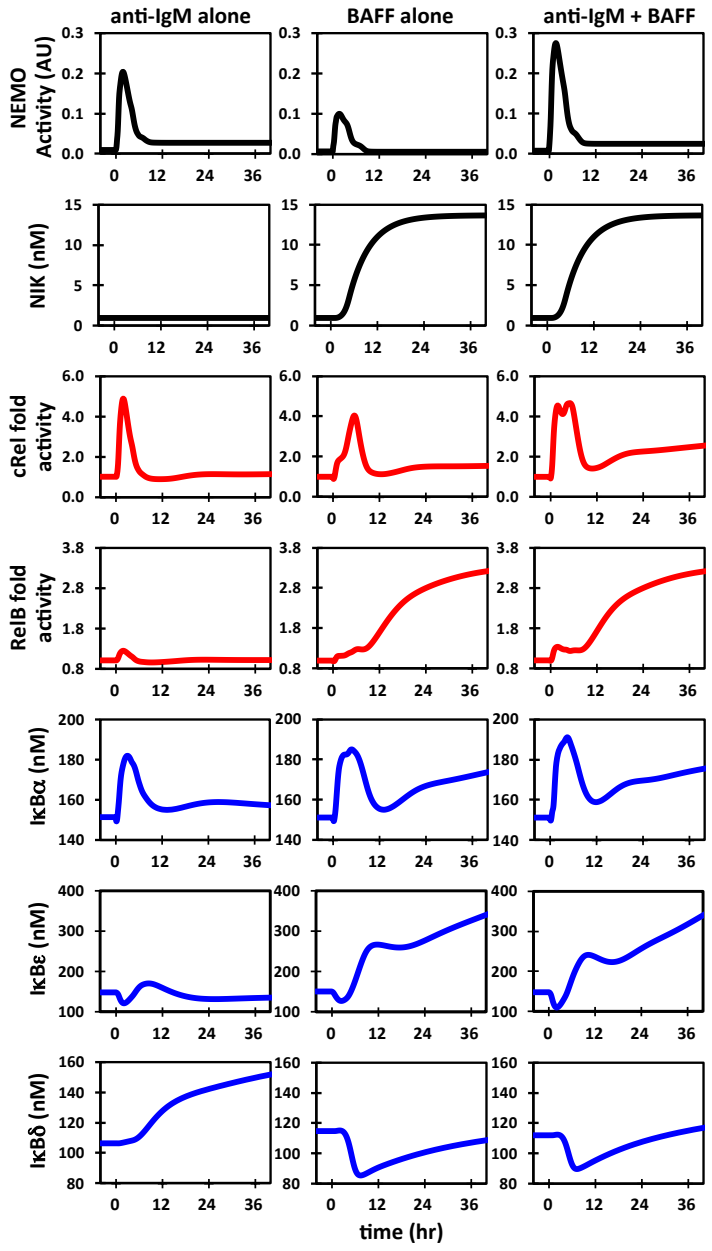

Figure 4.6: BAFF releases IκBδ inhibition of cRel in BCR stimulated B cells

Computational simulations are shown for the NEMO / IKK2-inducing stimuli anti-IgM (left column), NIK / IKK1-inducing survival signals mediated by BAFF ligand (middle column), and combined signals of anti-IgM plus BAFF ligand (left column). Simulation of NEMO/IKK2 and NIK/IKK1 activity profiles (top two panels, black), NFkB family members cRel, RelB, and p52 nuclear fold activities (middle three panels, red), and total cellular protein levels of IκBd substrate, p100 (bottom panel, blue).

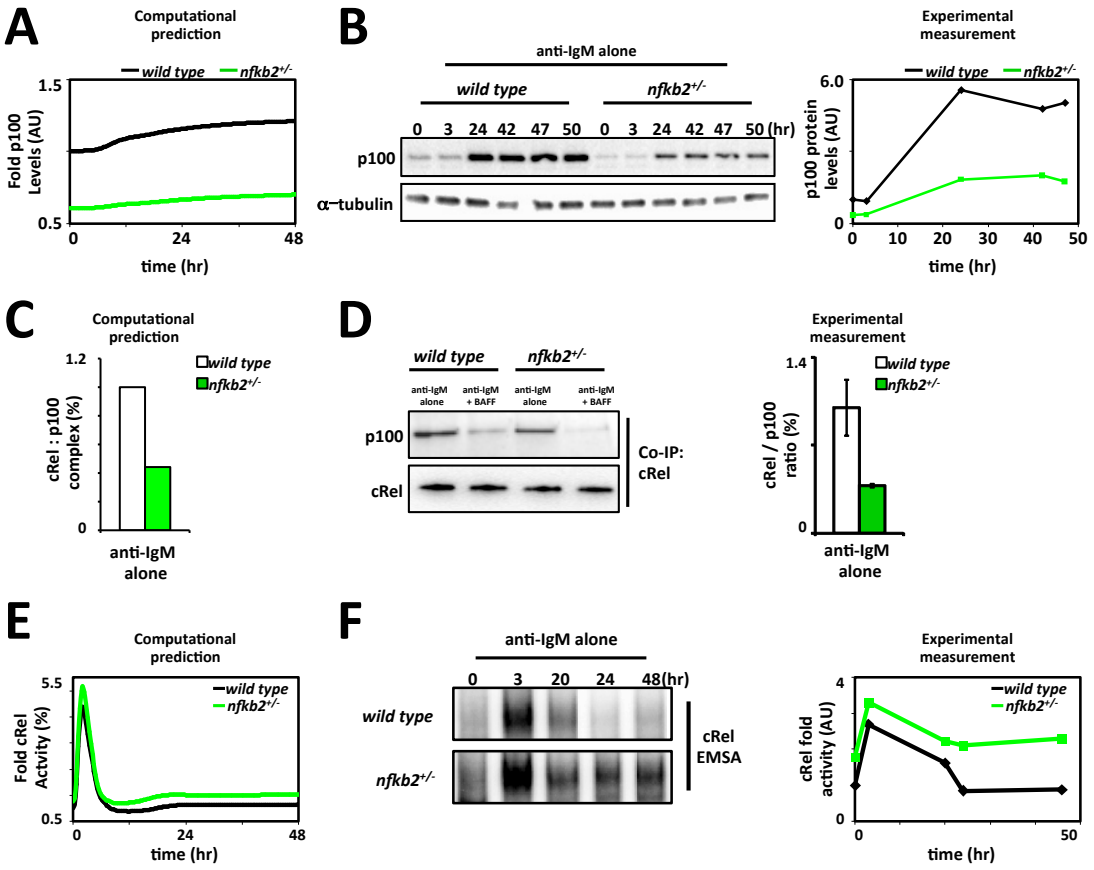

Figure 4.7: IκBδ limits the proliferative capacity of BCR-stimulated B cells

A. Model simulation of p100 protein levels in *wild type* and nfkb2 heterozygous B cells stimulated with anti-IgM alone. B. Immunoblot of p100 protein expression in *wild type* and *nfkb2*$^{+/-}$B cells stimulated with anti-IgM alone for two days. Blots were quantified and plotted in graph to the right. C. Computational prediction of Ikbd:cRel complex following 24 hours of anti-IgM stimulation in wild type (black bars) and *nfkb2*$^{+/-}$ (green bars) B cells. D. Representative western blot of co-immunoprecipitation of cRel - Ikbd from *wild type* and *nfkb2*$^{+/-}$B cells following 24 hours of stimulation with either anti-IgM alone or anti-IgM plus BAFF ligand (n=3). Samples were normalized to cRel protein levels (left panel). Immunoblots were quantified using Image Lab software and graphed (right panel). E. Model simulation of nuclear cRel protein levels in *wild type* and nfkb2 heterozygous B cells stimulated with anti-IgM alone. F. cRel DNA binding activities in wild type and nfkb2 heterozygous B cells induced by anti-IgM alone were monitored by EMSA. EMSA was qunatified and graphed in right panel.

Chapter 5: Canonical and non-canonical control of NFkB dimers in different cellular contexts

5.1 Abstract

NFκB is a transcription factor family that is critical in a variety of biological functions in numerous cell types, including inflammatory response, cell proliferation and survival, differentiation, and pathogenic responses. Its activation is dependent on a complex signaling pathway, and the activation of NFκB consists of potentially 15 dimers that can combinatorially form from 5 transcription factor monomers. Increased knowledge on downstream transcriptional effects have established the importance that specific NFκB dimers may play rather than general NFκB activation. Here we use *in silico* approaches to demonstrate that the balance of two upstream kinases (NEMO-IKK and NIK) can dictate the NFκB dimer repertoire as well as provide insights into various diseases that affect the complex NFκB signaling system.

5.2 Introduction

NFkB is a transcription factor family that plays a critical role in the regulation of inflammation, immunity, cell development, and cell survival and proliferation. While the activation of this transcription factor family has been extensively studied, the roles of the specific dimers are still largely unknown. This transcription factor family is comprised of 15 potential dimers that can be formed combinatorially from 5 different transcription factor monomers: RelA, RelB, cRel, p50, and p52. Latent NFkB activity is sequestered in the cytoplasm in resting cells by inhibitors of NFkB (IkBs), and is released upon (IkB kinase) IKK activation. The NFkB signaling pathway is comprised of two activation pathways, the canonical NEMO-containing pathway and the non-canonical NIK containing pathway (Fig. 5.1).

Activation of the canonical pathway occurs upon inflammatory or pathogenic stimuli, resulting in the activation of the NEMO-IKK complex. This activated kinase subsequently phosphorylates IκBs and targets them for proteasomal degradation. Upon IκB degradation, NFκB is released and able to translocate into the nucleus, and activate target genes for transcription. In contrast, activation of the non-canonical pathway typically occurs upon developmental signals, and results in the proteasomal degradation of TRAF3, allowing for NIK accumulation. This NIK accumulation results in the phosphorylation and subsequent activation of the IKK1 complex (a NEMO-independent IKK complex). Once activated, the IKK1 complex is then able to

phosphorylate p100 at serines 99, 108, 115, 123, and 872, which targets p100 for degradation of its C-terminal ankyin repeats domain (ARD). This allows for two activities to result from the non-canonical NFκB activation. First, p100 processing leads to the generation of p52, resulting in a major RelB containing dimer, the RelB:p52 dimer. Second, the degradation of the C-terminal ARD of p100 allows for the release of "canonical" NFκB dimers such as RelA:p50 and RelB:p50.

While the two NFκB pathways have been historically studied as two distinct and separate pathways, there are numerous interconnections between the two pathways. Studies have indicated that IκBδ, which is comprised of both p100 and p105, is capable of inhibiting RelA NFκB activity and thus allows for RelA control through non-canonical stimulation. These studies suggest that chronic inflammatory signals should not give rise to elevated RelA NFκB activity because IκBδ control. However, given an environment where there are tonic developmental signals in addition to chronic inflammatory signals, elevated and sustained RelA NFκB activity can result. Tonic developmental signals can then potentially exacerbate inflammatory signaling, and further studies can clarify the contribution of non-canonical activation on canonical NFκB activity in various inflammatory diseases and cancers.

Additionally, previous work has established the requirement for canonical NFκB activation in providing non-canonical NFκB activation. RelB

and p100 synthesis is dependent on RelA activity, and RelB reconstitution in RelA-deficient MEFs could restore non-canonical NFκB activation. However, p100 overexpression in RelA-deficient MEFs failed to restore non-canonical RelB activity. These studies suggest that while RelB activation is regulated by basal RelA activity, p100 synthesis induced by RelA activation is a critical determinant of non-canonical activation.

These studies have implicated p100 as an important mediator between the two activation pathways, with important functions in regulating basal and activated NFκB. However, these previous studies typically looked at either RelA:p50 or RelB:p52 as the primary NFκB dimers. With the rise of ChIP-seq technologies and knowledge on downstream transcriptional effects, there has been an increasing rise in the interest of specific NFκB dimers. While previous work has illustrated the importance of specific NFκB dimers in the regulation of NFκB signaling, the cell-dependent context of these dimers has not yet been delineated. Additionally, previous work have established the prevalence of specific NFκB dimers in specific cell types, including dendritic cells containing a high level of RelB:p50 (Shih et al., 2012), while MEFs primarily have RelA:p50 (Hoffmann et al., 2002), and B cells have cRel:p50 in addition to RelB:p52 as the predominant NFκB dimers (Gerondakis et al., 1998; Grumont and Gerondakis, 1994; Grumont et al., 1998).

Here, we focus on the analysis of canonical and non-canonical control of NFκB dimers in different cellular contexts. We show that the amount and

balance of tonic and/or activated kinase (NEMO-IKK or NIK) can dictate the level of NFκB responsiveness in addition to the specificity of the available activated NFκB dimers in the wild type cell. Using the mathematical model from previous work and adapting it to a “general cell” that can be modified for a particular cell-type, we illustrate multiple examples of how kinase levels affect NFκB activation and extend this analysis to known human diseases that have mutations in the NFκB signaling system.

5.3 Cell-type specificity determines the NFκB repertoire

Specific NFκB dimers have been shown to be prevalent in specific cell types, whether in various stages of B cell development, dendritic cells, or MEFs. B-lineage cells have shown differential expression of NFκB proteins, with RelA:p50 as a major inducible dimer in pre-B cells, cRel:p50 as a major dimer in mature B-cells, and RelB:p52 as a major dimer in plasma cells (Liou et al., 1994). Additionally, dendritic cells have reported an inducible RelB:p50 dimer(Shih et al., 2012), while MEFs have inducible RelA:RelA and RelA:p50 as the dominant dimers. Reports have also shown a RelA:cRel dimer that is prevalent in macrophages, which plays a role in the inflammatory response, upregulating pro-inflammatory genes such as TNF-α(Rao et al., 2010). However, the activation of these dimers is likely dependent on both the stimulus and the basal state of the cell, and most of the previous work on the activation of NFκB focuses on the mechanism of the signaling pathway rather than the specific dimers that are activated. While there can be many mechanisms involved in the abundance of specific NFκB dimers in the cell, such as the basal expression level of NFκB monomers or the activation pathways of the NFκB signaling system, we found that the basal expression levels of NFκB monomers in various cell types may not be the critical mechanism for the abundance of specific NFκB dimers. In fact, analysis of the expression levels of NFκB monomers in various cell types showed similar RelA expression, while RelB and cRel expression levels were more variable

(Fig. 5.2). RelB and cRel are known to be RelA-NFκB inducible, suggesting that it is still the activation pathway that affects expression, not the basal expression itself. Additionally, expression levels of nfkb1 and nfkb2 are also similar throughout various cell types, suggesting that basal expression of NFκB monomers is not the delineating factor in cell-type specific NFκB dimer abundance.

There are two pathways of NFκB activation, the canonical and non-canonical pathways. These pathways have been historically studied as distinct pathways, with major differences at the kinase level (NEMO-IKK and NIK) and in the resulting activated NFκB dimer output. Developmental signals often activate the non-canonical pathway while pathogen and inflammatory signals activate the canonical pathway (Shih et al., 2010). The activation of NFκB is often important for the immune response or inflammatory response to pathogenic or antigenic signals, while developmental signals activate NFκB to enhance cell survival, proliferation, and differentiation. However, misregulation of the NFκB activation pathways can cause inflammatory diseases such as arthritis and inflammatory bowel disease in addition to cancers such as leukemia and lymphomas. Both pathways have numerous interconnections, and previous work has established p100 as a primary mediator between these two pathways (Basak et al., 2007, 2008). However, while these studies have attempted to delineate the abundance and availability of specific NFκB dimers, it is still incomplete, and the majority of the previous work focused on the

mechanism of NFκB activation. While previous work sought to understand the mechanism of general NFκB activation, the multiple major players (kinases, inhibitors, 15 potential NFκB dimers) in the signaling pathway create a complexity that we want to understand further (Fig. 5.3). In order to determine the cell-type specific NFκB dimer repertoire, we use a mathematical model that encompasses the IKK-IκB-NFκB signaling system with both the canonical and non-canonical pathways. While there can be many methods for the activation of certain NFκB dimers in some cell types versus others, because of the major difference in the activated kinase of each pathway, we hypothesized that the tonic level of the upstream kinase in each pathway affects the downstream NFκB dimer repertoire. However, it is important to note that other mechanisms can play a role in the expression of the NFκB monomers, which can affect the NFκB dimer repertoire of specific cell types. However, we focus on the tonic levels of kinase because that is the major difference found in the two activation pathways found in all cell types.

We first considered an adaptation of a multi-dimer model that includes both pathways and the opportunity for combinatorial NFκB dimer generation (Fig. 5.4, Table 5.1). We then considered the effects of the non-canonical pathway on canonical activation of NFκB through varying basal levels of NIK in parallel simulations while allowing for NEMO-IKK induced NFκB responsiveness (Fig. 5.5A). Analysis of these simulations revealed three

different regimes of NEMO-IKK responsive NFκB dimers (Fig. 5.5B, Table 5.2). Low NIK abundance resulted in only RelA:p50 activation, while medium NIK levels included RelA:p50 and cRel:p50 activation, and high NIK levels allowed for RelA:p50, cRel:p50, and RelB:p50 activation.

The availability of specific NFκB dimers and the three regimes correspond to previous studies of specific cell types. MEFs are likely in the low NIK regime, where RelA:p50 is available as a primary NEMO-IKK responsive dimer. NIK is not needed for NEMO-IKK induced RelA:p50 activation in these cells. In contrast, the medium NIK regime has NEMO-IKK induced RelA:p50 and cRel:p50 dimers, which correspond to B cells. Dendritic cells show an increased availability of NEMO-IKK induced RelB:p50, corresponding to a high NIK regime in the cell. In fact, previous work has demonstrated that dendritic cells likely function in a higher NIK regime as compared to MEFs (Shih et al., 2012).

Conversely, we wanted to explore the effects of the canonical pathway on the non-canonical activation of NFκB dimer in a general wild type cell. We used the same model as before but varied the basal levels of NEMO-IKK and allowed for non-canonical NIK activation through protein abundance accumulation (Fig. 5.6). These simulations also revealed three regimes as listed in Table 3; the low NEMO-IKK regime has little to no NFκB dimer activation through the non-canonical pathway, which corresponds to previous work that found the canonical pathway critical for non-canonical NFκB

activation. The medium NEMO-IKK regime resulted in the availability of RelB:p52 dimers, while the high NEMO-IKK regime resulted in the availability of NIK induced RelA:p50 and cRel:p50 in addition to the already available RelB:p52 dimers. The medium NEMO-IKK regime allows for NIK to induce RelB:p52, which is seen in BAFF induced B cells. The high NEMO-IKK regime allows for the additional availability of cRel:p50, which corresponds to proliferating B cells that undergo BAFF enhanced BCR co-stimulation as previously observed (Grumont et al., 1998; Huang et al., 2004; Rickert et al., 2011; Schweighoffer et al., 2013).

These analyses indicate the importance of the kinase context of the cell in determining the NFκB repertoire. While there are potentially many other mechanisms that can affect the availability of particular NFκB dimers, the use of the mathematical model in this analysis illustrates that changing the kinase context is sufficient for the cell to have specific NFκB dimers available.

5.4 NFκB dimer repertoire in disease models

The balance of NFκB is important in the cell's response to extracellular signals. However, mutations that affect different species in the NFκB signaling system can result in a variety of diseases, including multiple types of cancer, atherosclerosis, lupus, and Hodgkin's disease. While our analysis was previously directed towards the cell-type specificity of NFκB dimers in wild type cells, we directed our efforts towards the activation of NFκB dimers in various disease types that have an impact on the NFκB signaling system. The mathematical model framework used for the wild type studies was adapted for the diseases in the following analysis.

MYD88 mutation

MYD88 is a signaling protein in the NFκB signaling system that transduces extracellular signals to the NFκB transcription factors that in turn regulate the production of cytokines and molecules that respond to the signals. Previous studies conducted in both mice and human show that have deletions in the *myd88* gene show an increase in susceptibility to bacterial infection due to an impaired immunity (Adachi et al., 1998; Bernuth et al., 2008). Additionally, recent reports have shown that mutations in MYD88 that cause a gain of function are found in a large number of diffuse large B cell lymphomas (DLBCL) (Davis et al., 2001; Jeelall and Horikawa, 2011). The gain of function mutation of MYD88 in DLBCLs causes high constitutive NFκB activity, but it is still unclear which of the specific NFκB dimers are activated.

Further understanding of which dimers are activated will provide insight into potential targets in developing therapies for DLBCL.

In order to mimic the effects of the MYD88 mutation resulting in its deletion in DLBCL, we assume that this gain of function results in high basal NEMO-IKK activity, and thus an increased basal level of canonical pathway strength as compared to wild type levels. Previous reports have reported about a 1% of the maximum NEMO-IKK activity at basal levels (Werner et al., 2005), and we use the same in our analysis of the wild type cell when comparing to the MYD88 mutant, which we assume has a much higher NEMO-IKK activity at 50%. We find that the increased basal NEMO-IKK activity results in increased non-canonical activation of RelB:p52 as compared to wild type (Fig. 5.7). We also see that there is a higher amount of basal RelA:p50, RelB:p50, and cRel:p50 in the mutant cells as compared to wild type cells. This analysis suggests that the basal dimers that are elevated in the mutant are the Rel-p50 dimers while the non-canonical activation results in higher RelB:p52 activation as compared to wild type. This corresponds to the high constitutive NFκB activity found in DLBCLs, and we show here that it is more than one type of NFκB dimer that is activated in this disease mutation.

Hodgkin's disease affects the canonical pathway and increases sensitivity to the non-canonical pathway

Hodgkin's disease is one of the most frequent lymphomas, resulting from tumor cells that are derived from B lymphocytes. The use of

Hodgkin/Reed-Strenberg (H/RS) cells of Hodgkin's disease has been crucial in the molecular analysis of Hodgkin's disease. While various signaling pathways show deregulation in the study of these H/RS cells, we focus on the studies that indicate mutations in the NFκB signaling pathway that result in the development of Hodgkin's disease. Numerous members of the NFκB signaling pathway are affected, suggesting a critical role of NFκB in Hodgkin's disease pathogenesis.

Previous work has shown high levels of nuclear NFκB in cultured H/RS cells (Bargou et al., 1996, 1997) as compared to wild type B cells. In fact, these studies show that unlike wild type B cells, which typically have cRel or RelB active dimers, the H/RS cells have high constitutive RelA:p50 activity. Because these studies show a high constitutive NFκB activity in the pathogenic cells, further work was done to determine the molecular causes of this hyperactivation. 10-15% of classical Hodgkin's disease cases have a mutation in the *nfkbia* gene that encodes IκBα, a primary inhibitor of NFκB in the canonical pathway (Lake et al., 2009; Schmitz et al., 2009a). Some cases of this disease also show a mutation in the *nfkbie*, the gene that encodes another canonical inhibitor, IκBε (Schmitz et al., 2009a). Other reports have shown that in 40% of Hodgkin's disease cases, mutations result in the inactivation of A20, which also functions as an inhibitor of NFκB (Kato et al., 2009; Schmitz et al., 2009b). Another mutation that contributes to the pathogenic disease as a result of high constitutive NFκB activity includes NIK,

causing a gain of function, which can contribute to higher non-canonical NFκB activation (Otto et al., 2012; Steidl et al., 2010). While most of these studies are done in separate cases of Hodgkin's disease, there is not much information on the combination of these mutations. However, many of the H/RS cell lines do show multiple mutations, suggesting that these mutations often coexist and strong NFκB activity results from these mutations, causing the pathogenesis of these cells (Küppers, 2012).

Most of these studies do not specify which of the various NFκB dimers are elevated in Hodgkin's disease as a result of the mutations in the NFκB signaling system. While some reports have shown that there is elevated RelA:p50, it is still unclear whether elevated abundances of other dimers affect the pathogenesis of this disease. Further understanding of the specific NFκB dimers involved can provide further insights into the pathogenesis of Hodgkin's disease and the outcome of the activated dimers.

In order to analyze the possible activated NFκB dimer repertoire of a particular mutation of Hodgkin's disease, we adapted the mathematical model with an IκBα deletion (Table 5.5). This mutation is prevalent in many cases of Hodgkin's disease, and was our candidate to mimic the cellular context in the mathematical model.

We find that the an IκBα deletion results in two responses as compared to wild type in the NFκB dimer repertoire that is canonically activated; that is, activated through NEMO-IKK. First, the deletion of this inhibitor results in an

increased duration of the NFκB response for RelA:p50, cRel:p50, and RelB:p50 at all levels of basal non-canonical strength as compared to wild type (Fig. 5.8A, Fig. 5.6B). In fact, there is a much stronger second wave of RelB:p50 activity in the IκBα-/- mutant, which suggests that increased RelB:p50 may play an important role in the pathogenesis of Hodgkin's disease cells that have the IκBα deletion. Second, the IκBα deletion results in an increased sensitivity of the NFκB response to the non-canonical pathway. Lower levels of tonic non-canonical activity (lower levels of tonic NIK) in the mutant cells result in higher levels of NFκB activity than their respective wild type cells (Fig. 5.8B). This suggests that the strength of non-canonical pathway on canonical activation is dependent on the balance of the canonical pathway.

Altered nfkb2 in lymphomas

Various lymphomas and leukemias, such as B cell chronic lymphocytic leukemia, multiple myeloma, and adult T cell leukemia/lymphoma have mutations in the *nfkb2* gene, which encodes the protein p100 (Rayet and Gélinas, 1999; Sun and Xiao, 2003; Xiao and Fu, 2010). p100 is not only a precursor to an NFκB monomer, p52, which is a binding partner for the Rel proteins, but it also acts as an inhibitor of NFκB in the form of IκBδ. Non-canonical activation is required to release NFκB dimers from IκBδ sequestration. In all the diseases studied, the mutation affecting the *nfkb2* gene resulted in gene rearrangement such that the C-terminal

processing-regulatory sequences along with some of the ankyrin repeats were deleted (Xiao et al., 2006). This deletion results in the truncation of the p100 protein that results in the constitutive generation of a p52-like protein that can bind to Rel-monomers and translocate to the nucleus (Qing et al., 2005, 2007; Xiao et al., 2001). Another consequence of this mutation causes the loss of IκBδ function, which results in increased nuclear NFκB activity (Qing et al., 2007). While the result of constitutive processing of p100 show strong oncogenesis, the mechanisms remains unclear. Deletion of the nfkb2 gene in mice result in the lack of both p100 and p52 proteins, yet the mice do not form tumors, suggesting that the simple loss of the IκBδ function is not sufficient to account for oncogenesis as a result of mutated p100 proteins (Franzoso et al., 1998). However, a previous study showed that p52 transgenic mice expressing wild type p100 did not develop tumors, but over 50% developed an autoimmune disease (Wang et al., 2008). These studies suggest that both the loss of IκBδ function and the gain of transcriptional p52 function contribute to the oncogenesis of these cells that contain the *nfkb2* gene rearrangement.

The aberrations in the *nfkb2* gene resulting in the loss of IκBδ function and constitutive processing of p100 to p52 leads to high nuclear NFκB activity in the tumors of these diseases. Some reports have suggested higher nuclear RelA:p52 dimer activity, while other reports have suggested a p52 homodimer that is capapble of binding κB sites on the DNA (Kim et al., 2000; Qing et al., 2007). The identities of the specific NFκB dimers that are activated in these

tumors as a result of the *nfkb2* gene rearrangement are still unclear. In order to predict what the activated dimers might be, we utilize the mathematical model and create the *nfkb2* gene rearrangement by preventing the formation of IκBδ activity and by removing the NIK dependence of p100 processing to p52, so that the processing is purely constitutive (Table 5.5).

In the ensuing simulations, we found that this mutation caused two responsive changes to the NFκB dimer repertoire. First, varying the non-canonical pathway strength no longer affects the canonical activation of the NFκB dimers, and the activation of these dimers solely depend on canonical activation (Fig. 5.9A). Second, varying the canonical pathway strength results in the presence of two distinct regimes, one with high tonic NFκB activity and one with low tonic NFκB activity (Fig. 5.9B). Further analysis of this disease cell type showed an increased sensitivity of the NFκB dimers to tonic NEMO-IKK activity as compared to wild type (Fig. 5.10). We found that all of the Rel-NFκB dimers displayed this pattern, and shows that while the non-canonical pathway no longer plays a role in the dynamics of activation, it does play a critical role in insulating the pathway from the digital effects of low versus high canonical activity. Without this insulation, hyper-activity of NFκB results in disease pathologies.

5.5 Conclusions

The canonical and non-canonical activation pathways of the NFκB signaling system has been historically studied as two distinct pathways. The canonical pathway results from inflammatory or pathogenic/antigenic signals that lead to the activation of a NEMO-IKK complex, which then leads to degradation of IκBα, IκBβ, and IκBε, resulting in the nuclear translocation of NFκB. In contrast, the non-canonical pathway is activated by developmental signals and results in the accumulation of NIK, resulting in the degradation of IκBδ and the processing of p100 to p52, allowing for the release of NFκB dimers bound by IκBδ and the generation of RelB:p52 dimers that can translocate into the nucleus to activate developmental genes. Recent work has established numerous interconnections between the two pathways, including the presence of p100 as critical mediator of both pathways. Additionally, the ubiquitous presence of NFκB in various cell types have enhanced our knowledge on the specific NFκB dimers available in specific cell types. By using a computational model that integrates both the canonical and non-canonical pathways with the multi-dimeric combinations of NFκB, our studies reveal that the kinase context of the cell is important in its NFκB dimer repertoire.

Previous work on delineating the NFκB signaling system led to our hypothesis that the kinase context of the cell is critical in the availability and activation of specific NFκB dimers. With the computational simulations and

varying the tonic basal levels of NEMO-IKK (canonical) or NIK (non-canonical), we were able to demonstrate that different levels would result in the availability of activated NFκB dimers. In fact, the regimes found when changing the tonic non-canonical signal, NIK, correspond to specific cell types, where a low NIK regime corresponds to the MEF NFκB repertoire in the availability of RelA:p50, while a high NIK regime corresponds to a dendritic cell NFκB repertoire with the availability of RelB:p50. In contrast, when exploring the regimes found while changing the tonic canonical signal, IKK, resulted in a medium IKK regime that corresponds to BAFF-induced B cells while a high IKK regime corresponds to proliferating B cells that have been co-stimulated by both BAFF and anti-IgM. We also found that mutations in the NFκB signaling system that result in various diseases can affect the responsiveness of these dimers when varying the tonic levels of the kinases in the cell. These computational simulations illustrate how the balance of the kinase levels is critical in the NFκB dimer repertoire of a cell type.

In addition to the aforementioned findings, we found that the disease mutations we chose to analyze demonstrated an opposition effect in the balance of the NFκB signaling system. That is, the IκBα-deficiency seen in Hodgkin's disease cells is a mutation in the canonical pathway, yet this deficiency affected the NFκB dimer sensitivity to the non-canonical pathway activation. In contrast, the *nfkb2* gene mutation seen in lymphomas is a mutation in the non-canonical pathway, yet its mutation increased the

sensitivity of NFκB to canonical activation. These oppositions suggest that therapies for diseases that are NFκB related should be targeted towards a pathway that is not directly affected by the disease; that is, non-canonical mutations can be targeted by therapies towards the canonical pathway and vice versa. This suggests that the interdependence between the two pathways is greater than previously anticipated, and that future studies should not delineate between the canonical and non-canonical pathways. Rather, future work should consider the NFκB signaling system as a whole complete system in order to gain predictive understanding of the effects a mutation may have on NFκB activation.

5.6 Acknowledgements

Chapter 5, in full, is a reprint of material being prepared for publication as “Controlling the NFκB dimer repertoire in different cellular contexts” by Tsui R and Hoffmann A. The dissertation author was the primary investigator and author of this material.

Table 5.1: Parameter Table and Reactions for the mathematical model with canonical and non-canonical NFκB signaling pathways

Reaction	Location	Param .No.	Parameter Value	Category	Source
Reaction rates determined by transcriptional programs and cytokine levels					
=>tIκBα (basal)	Nucleus	1	4.8e-3 nM/min	IκB Synth.	Parameter value chosen to fit mRNA and protein Expression profiles as measure by RNase Protection (RPA) and Western blot assays, reformulated from Werner et al. (2008) to fit a Hill function
=>tIκBβ (basal)	Nucleus	2	1.2e-3 nM/min	IκB Synth.	*Refer to #1*
=>tIκBε (basal)	Nucleus	3	1.2e-4 nM/min	IκB Synth.	*Refer to #1*
=>tRelA (basal)	Nucleus	4	3.6e-5 nM/min	NFκB Synth.	*Refer to #1*
=>tp50 (basal)	Nucleus	5	2.9e-5 nM/min	NFκB Synth.	*Refer to #1*
=>tRelB (basal)	Nucleus	6	4.2e-5 nM/min	NFκB Synth.	*Refer to #1/*Fitted
=>tp100 (basal)	Nucleus	7	8e-7 nM/min	NFκB Synth.	*Refer to #1*
=>cRel (basal)	Nucleus	8	3.6e-6 nM/min	NFκB Synth.	*Refer to #1/*Fitted
=> NIK	Cytoplasm	9	4.2e-2 nM/min	NIK Synth.	Set to yield measured abundance in conjunction with #10
NIK =>	Cytoplasm	10	4.6e-2	NIK Deg.	Based on estimated 15-minute half-life/ Fitted
IκB Reactions					
mRNA => mRNA + protein	Nuc ->Cyt	11	12 proteins/ mRNA/min	Translation	Derived from the elongation rate of the ribosome and corrected for the nucleotide spacing between adjacent ribosomes on the same transcript 1800 nt min^{-1} / 150 nt = 12 min^{-1}
=>tIκBα (A50/A52-induced)	Nucleus	12	200 Fold over consitutive	IκB Synth.	*Refer to #1*
Hill K_d (A50/A52-induced)	Nucleus	13	150 nM	IκB Synth.	*Refer to #1*
=>tIκBε (A50/A52-induced, 37 min. delay)	Nucleus	14	25 Fold over consitutive	IκB Synth.	*Refer to #1*
Hill K_d (A50/A52-induced)	Nucleus	15	150 nM	IκB Synth.	*Refer to #1*

Table 5.1: Parameter Table and Reactions for the mathematical model with canonical and non-canonical NFkB signaling pathways, Continued

Reaction	Location	Param .No.	Parameter Value	Category	Source
=>tIκBε (C50/C52-induced, 37 min. delay)	Nucleus	16	250 Fold over consitutive	IκB Synth.	*Refer to #1*
Hill K_d (C50/C52-induced)	Nucleus	17	150 nM	IκB Synth.	*Refer to #1*
p100 + p100 =>IκBδ	Cyt, Nuc	18	1.2e-2 nM^{-1} min^{-1}	IκB Synth.	Estimated a $K_d$of 10nM
IκBδ => p100 + p100	Cyt, Nuc	19	1.2e-2 min^{-1}	IκB Synth.	*Refer to #19*
IκBα(c) =>IκBα(n)	Cyt ->Nuc	20	6.0e-2 min^{-1}	Transport	Adapted from (Shih et al., 2009)
IκBβ(c) =>IκBβ(n)	Cyt ->Nuc	21	9.0-3 min^{-1}	Transport	(Shih et al., 2009)
IκBε(c) =>IκBε(n)	Cyt ->Nuc	22	4.5e-2 min^{-1}	Transport	(Shih et al., 2009)
IκBδ(c) =>IκBδ(n)	Cyt ->Nuc	23	4.5e-2 min^{-1}	Transport	(Shih et al., 2009)
IκB[α/β/ε/δ](n) =>IκB[α/β/ε/δ](c)	Nuc ->Cyt	24	1.2e-2 min^{-1}	Transport	(Shih et al., 2009)
tIκBα =>	Nucleus	25	2.9e-2 min^{-1}	IκB Deg.	mRNA half-life measurements using actinomycin-D treatment of cells and RPA (unpublished results)
tIκBβ =>	Nucleus	26	2.9e-3 min^{-1}	IκB Deg.	*Refer to #25*
tIκBε =>	Nucleus	27	3.8e-3 min^{-1}	IκB Deg.	*Refer to #25*
IκBα =>	Cyt, Nuc	28	0.12 min^{-1}	IκB Deg.	(Shih et al., 2009)
IκBβ =>	Cyt, Nuc	29	0.12 min^{-1}	IκB Deg.	(Shih et al., 2009)
IκBε =>	Cyt, Nuc	30	1.2e-2 min^{-1}	IκB Deg.	Based on estimated 1 hour half-life
IκBδ =>	Cyt, Nuc	31	3e-3 min^{-1}	IκB Deg.	Based on estimated 4 hour half-life
IκB[α/β/ε/δ]-NFκB =>NFκB	Cyt, Nuc	32	2.4e-4 min^{-1}	IκB Deg.	Based on estimated 48 hour half-life
IκBα => (NEMO-mediated)	Cytoplasm	33	1.4e-3 nM^{-1} min^{-1}	IκB Deg.	Based on measured IκB degradation timecourses given numerical input curves
IκBαNFκB =>NFκB (NEMO-mediated)	Cytoplasm	33	1.4e-3 nM^{-1} min^{-1}	IκB Deg.	
IκBβ => (NEMO-mediated)	Cytoplasm	34	4.5e-4 nM^{-1} min^{-1}	IκB Deg.	*Refer to # 33*
IκBβNFκB =>NFκB (NEMO-mediated)	Cytoplasm	34	4.5e-4 nM^{-1} min^{-1}	IκB Deg.	*Refer to # 33*

Table 5.1: Parameter Table and Reactions for the mathematical model with canonical and non-canonical NFkB signaling pathways, Continued

Reaction	Location	Param .No.	Parameter Value	Category	Source
IκBε => (NEMO-mediated)	Cytoplasm	35	3.4e-4 nM^{-1} min^{-1}	IκB Deg.	*Refer to # 33*
IκBεNFκB =>NFκB (NEMO-mediated)	Cytoplasm	35	3.4e-4 nM^{-1} min^{-1}	IκB Deg.	*Refer to # 33*
IκBδ => (NIK-mediated)	Cytoplasm	36	0.6 nM^{-1} min^{-1}	IκB Deg.	V_{max} and K_m of NIK-mediated reactions based on protein degradation and estimated NIK abundances.
IκBδNFκB =>NFκB (NIK-mediated)	Cytoplasm	36	0.6 nM^{-1} min^{-1}	IκB Deg.	
IκBδ => (NIK-mediated, K_m)	Cytoplasm	37	100 nM	IκB Deg.	*Refer to #36*
NF-κB reactions					
p100 => p52 (NIK-mediated)	Cytoplasm	38	5.0e-2 nM^{-1} min^{-1}	NFκB Synth.	*Refer to #36*
p100 => p52 (NIK-mediated, p100 K_m)	Cytoplasm	39	10 nM	NFκB Synth.	*Refer to #36*
=>cRel (A50/A52/C50/C52-induced, 1 hr delay)	Nucleus	40	200 Fold over consitutive	NFκB Synth.	*Refer to #1/Fitted*
Hill K_d (A50/A52/C50/C52-induced)	Nucleus	41	150 nM	NFκB Synth.	*Refer to #1/Fitted*
=>tp100 (A50/A52-induced, 4 hr delay)	Nucleus	42	1000 Fold over consitutive	NFκB Synth.	*Refer to #1/Fitted*
Hill K_d (A50/A52-induced)	Nucleus	43	50 nM	NFκB Synth.	*Refer to #1/Fitted*
=>tp100 (C50/C52-induced, 4 hr delay)	Nucleus	44	1500 Fold over consitutive	NFκB Synth.	*Refer to #1/Fitted*
Hill K_d (C50/C52-induced)	Nucleus	45	50 nM	NFκB Synth.	*Refer to #1/Fitted*
=>p50 (A50/A52/C50/C52-induced, 1 hr delay)	Nucleus	109	20 Fold over consitutive	NFκB Synth.	*Refer to #1/Fitted*

Table 5.1: Parameter Table and Reactions for the mathematical model with canonical and non-canonical NFkB signaling pathways, Continued

Reaction	Location	Param .No.	Parameter Value	Category	Source
Hill K_d (A50/A52/C50/ C52-induced)	Nucleus	110	150 nM	NFκB Synth.	*Refer to #1/Fitted*
=>RelB (A50/A52 - induced, 1 hr delay)	Nucleus	111	5 Fold over consitutive	NFκB Synth.	*Refer to #1/Fitted*
=>RelB (C50/C52 - induced, 1 hr delay)	Nucleus	112	100 Fold over consitutive	NFκB Synth.	*Refer to #1/Fitted*
Hill K_d (A50/A52/C50/ C52-induced)	Nucleus	113	50 nM	NFκB Synth.	*Refer to #1/Fitted*
tRelA =>	Nucleus	46	2.9e-3 min^{-1}	NFκB Deg.	*Refer to #25*
tp50 =>	Nucleus	47	2.9e-3 min^{-1}	NFκB Deg.	*Refer to #25*
tRelB =>	Nucleus	48	2.9e-3 min^{-1}	NFκB Deg.	*Refer to #25*
tp100 =>	Nucleus	49	9.6e-4 min^{-1}	NFκB Deg.	*Refer to #25*
tcRel=>	Nucleus	50	9.6e-4 min^{-1}	NFκB Deg.	*Refer to #25*
RelA =>	Cyt, Nuc	51	2.3e-2 min^{-1}	NFκB Deg.	Based on estimated 0.5 hour half-life of NF-κB monomers
p50 =>	Cyt, Nuc	51	2.3e-2 min^{-1}	NFκB Deg.	
RelB =>	Cyt, Nuc	51	2.3e-2 min^{-1}	NFκB Deg.	
p100 =>	Cyt, Nuc	51	2.3e-2 min^{-1}	NFκB Deg.	
cRel =>	Cyt, Nuc	51	2.3e-2 min^{-1}	NFκB Deg.	
p52 =>	Cyt, Nuc	51	2.3e-2 min^{-1}	NFκB Deg.	
RelA + p50 => RelAp50	Cyt, Nuc	52	1.9e-3 nM^{-1} min^{-1}	NFκB Synth.	Based on dimerization studies (unpublished results)
RelA + p52 => RelAp52	Cyt, Nuc	52	1.9e-3 nM^{-1} min^{-1}	NFκB Synth.	
RelB + p52 => RelBp52	Cyt, Nuc	53	9.6e-4 nM^{-1} min^{-1}	NFκB Synth.	
RelB + p50 => RelBp50	Cyt, Nuc	53	3e-4 nM^{-1} min^{-1}	NFκB Synth.	
cRel + p50 => cRelp50	Cyt, Nuc	54	9.6e-4 nM^{-1} min^{-1}	NFκB Synth.	
cRel + p52 => cRelp52	Cyt, Nuc	55	1.9e-3 nM^{-1} min^{-1}	NFκB Synth.	
p50 + p50 => p50p50	Cyt, Nuc	56	1.8e-3 nM^{-1} min^{-1}	NFκB Synth.	
p52+ p52 => p52p52	Cyt, Nuc	57	1.8e-3 nM^{-1} min^{-1}	NFκB Synth.	
RelAp50 => RelA + p50	Cyt	58	1.9e-2 min^{-1}	NFκB Synth.	Based on dimerization studies (unpublished results)
RelAp52 => RelA + p52	Cyt	59	3.8e-2min^{-1}	NFκB Synth.	
RelBp52 => RelB + p52	Cyt	60	1.4e-2 min^{-1}	NFκB Synth.	

Table 5.1: Parameter Table and Reactions for the mathematical model with canonical and non-canonical NFkB signaling pathways, Continued

Reaction	Location	Param .No.	Parameter Value	Category	Source
RelBp50 => RelB + p50	Cyt	61	4.6e-3 min^{-1}	NFκB Synth.	Based on dimerization studies (unpublished results)
cRelp50 =>cRel + p50	Cyt	62	1.4e-3 min^{-1}	NFκB Synth.	
cRelp52 =>cRel + p52	Cyt	63	1.4e-3min^{-1}	NFκB Synth.	
RelAp50 => RelA + p50	Nuc	64	1.9e-3 min^{-1}	NFκB Synth.	Estimated 10 fold higher affinity due to DNA binding
RelAp52 => RelA + p52	Nuc	65	3.8e-3min^{-1}	NFκB Synth.	*Refer to #64*
RelBp52 => RelB + p52	Nuc	66	1.4e-3 min^{-1}	NFκB Synth.	*Refer to #64*
RelBp50 => RelB + p50	Nuc	67	4.6e-3 min^{-1}	NFκB Synth.	*Refer to #64*
cRelp50 =>cRel + p50	Nuc	68	1.4e-4 min^{-1}	NFκB Synth.	*Refer to #64*
cRelp52 =>cRel + p52	Nuc	69	1.4e-4min^{-1}	NFκB Synth.	*Refer to #64*
p50p50 => p50 + p50	Cyt, Nuc	70	5.4e-2min^{-1}	NFκB Synth.	Based on dimerization studies (unpublished results)
p52p52 => p52+ p52	Cyt, Nuc	71	5.4e-2min^{-1}	NFκB Synth.	Based on dimerization studies (unpublished results)
RelAp50(c) =>RelAp50(n)	Cyt ->Nuc	72	5.4 min^{-1}	Transport	(Shih et al., 2009)
RelAp52(c) =>RelAp52(n)	Cyt ->Nuc	72	5.4 min^{-1}	Transport	(Shih et al., 2009)
RelBp52(c) =>RelBp52(n)	Cyt ->Nuc	72	5.4 min^{-1}	Transport	(Shih et al., 2009)
RelBp50(c) =>RelBp50(n)	Cyt ->Nuc	72	5.4 min^{-1}	Transport	(Shih et al., 2009)
cRelp50(c) => cRelp50(n)	Cyt ->Nuc	72	5.4 min^{-1}	Transport	(Shih et al., 2009)
cRelp52(c) => cRelp52(n)	Cyt ->Nuc	72	5.4 min^{-1}	Transport	(Shih et al., 2009)
p50p50(c) => p50p50(n)	Cyt ->Nuc	72	5.4 min^{-1}	Transport	(Shih et al., 2009)
p52p52(c) => p52p52(n)	Cyt ->Nuc	72	5.4 min^{-1}	Transport	(Shih et al., 2009)
NFκB(n) =>NFκB(c)	Nuc ->Cyt	73	4.8e-3 min^{-1}	Transport	(Shih et al., 2009)
RelAp50 =>	Cyt, Nuc	74	2.4e-4 min^{-1}	NFκB Deg.	Based on estimated 48 hour half-life
RelAp52 =>	Cyt, Nuc	74	2.4e-4 min^{-1}	NFκB Deg.	
RelBp50 =>	Cyt, Nuc	74	2.4e-4 min^{-1}	NFκB Deg.	
RelBp52 =>	Cyt, Nuc	74	2.4e-4 min^{-1}	NFκB Deg.	
cRelp50 =>	Cyt, Nuc	74	2.4e-4 min^{-1}	NFκB Deg.	
cRelp52 =>	Cyt, Nuc	74	2.4e-4 min^{-1}	NFκB Deg.	
p50p50 =>	Cyt, Nuc	74	2.4e-4 min^{-1}	NFκB Deg.	
p52p52 =>	Cyt, Nuc	74	2.4e-4 min^{-1}	NFκB Deg.	

Table 5.1: Parameter Table and Reactions for the mathematical model with canonical and non-canonical NFkB signaling pathways, Continued

Reaction	Location	Param .No.	Parameter Value	Category	Source
IκB[α/β/ε/δ]-NFκB =>IκB[α/β/ε/δ]	Cyt, Nuc	75	2.4e-4 min^{-1}	NFκB Deg.	*Refer to #74*
IκB:NF-κB interactions					
IκBα + RelA:p50 =>IκBα:RelA:p50	Cyt, Nuc	76	3e-3 nM^{-1} min^{-1}	IκB-NFκB interaction	Adapted from *Alves et. al 2013*
IκBβ + RelA:p50 =>IκBβ:RelA:p50	Cyt, Nuc	77	2e-4 nM^{-1} min^{-1}	IκB-NFκB interaction	Adapted from *Alves et. al 2013*
IκBε + RelA:p50 => IκBε:RelA:p50	Cyt, Nuc	78	1.3e-3 nM^{-1} min^{-1}	IκB-NFκB interaction	Adapted from *Alves et. al 2013*
IκBδ + RelA:p50 => IκBδ:RelA:p50	Cyt, Nuc	79	6e-4 nM^{-1} min^{-1}	IκB-NFκB interaction	Adapted from *Alves et. al 2013*
IκBα + RelA:p52 =>IκBα:RelA:p52	Cyt, Nuc	76	3e-3 nM^{-1} min^{-1}	IκB-NFκB interaction	Adapted from *Alves et. al 2013*
IκBβ + RelA:p52 =>IκBβ:RelA:p52	Cyt, Nuc	77	2e-4 nM^{-1} min^{-1}	IκB-NFκB interaction	Adapted from *Alves et. al 2013*
IκBε + RelA:p52 => IκBε:RelA:p52	Cyt, Nuc	78	1.3e-3 nM^{-1} min^{-1}	IκB-NFκB interaction	Adapted from *Alves et. al 2013*
IκBδ + RelA:p52 => IκBδ:RelA:p52	Cyt, Nuc	79	6e-4 nM^{-1} min^{-1}	IκB-NFκB interaction	Adapted from *Alves et. al 2013*
IκBα + RelB:p50 =>IκBα:RelB:p50	Cyt, Nuc	80	1.3e-3 nM^{-1} min^{-1}	IκB-NFκB interaction	Adapted from *Alves et. al 2013*
IκBε + RelB:p50 => IκBε:RelB:p50	Cyt, Nuc	81	1.3e-3 nM^{-1} min^{-1}	IκB-NFκB interaction	Adapted from *Alves et. al 2013*
IκBδ + RelB:p50 => IκBδ:RelB:p50	Cyt, Nuc	82	6e-4 nM^{-1} min^{-1}	IκB-NFκB interaction	Adapted from *Alves et. al 2013*
IκBα + cRel:p50 =>IκBα:cRel:p50	Cyt, Nuc	83	3e-3 nM^{-1} min^{-1}	IκB-NFκB interaction	Adapted from *Alves et. al 2013*
IκBβ +cRel:p50 =>IκBβ:cRel:p50	Cyt, Nuc	84	2.1e-4 nM^{-1} min^{-1}	IκB-NFκB interaction	Adapted from *Alves et. al 2013*

Table 5.1: Parameter Table and Reactions for the mathematical model with canonical and non-canonical NFkB signaling pathways, Continued

Reaction	Location	Param .No.	Parameter Value	Category	Source
IκBε + cRelp52 => IκBε:cRel:p52	Cyt, Nuc	85	1.3e-3 nM^{-1} min^{-1}	IκB-NFκB interaction	Adapted from *Alves et. al 2013*
IκBδ + cRel:p52 => IκBδ:cRel:p52	Cyt, Nuc	86	1.98e-2 nM^{-1} min^{-1}	IκB-NFκB interaction	Adapted from *Alves et. al 2013*
IκBα:RelA:p50 =>IκBα + RelA:p50	Cyt, Nuc	87	6e-4 min^{-1}	IκB-NFκB interaction	Fitted (dependent on 76-79)
IκBβ:RelA:p50 =>IκBβ + RelA:p50	Cyt, Nuc	88	1.7e-2 min^{-1}	IκB-NFκB interaction	
IκBε:RelA:p50 =>IκBε + RelA:p50	Cyt, Nuc	89	6e-3 min^{-1}	IκB-NFκB interaction	
IκBδ:RelA:p50 =>IκBδ + RelA:p50	Cyt, Nuc	90	8.4e-4 min^{-1}	IκB-NFκB interaction	
IκBα:RelA:p52 =>IκBα + RelA:p52	Cyt, Nuc	91	6e-4 min^{-1}	IκB-NFκB interaction	Fitted (dependent on 76-79)
IκBβ:RelA:p52 =>IκBβ + RelA:p52	Cyt, Nuc	92	1.7e-2 min^{-1}	IκB-NFκB interaction	
IκBε:RelA:p52 =>IκBε + RelA:p52	Cyt, Nuc	93	6e-3 min^{-1}	IκB-NFκB interaction	
IκBδ:RelA:p52 =>IκBδ + RelA:p52	Cyt, Nuc	94	8.4e-4 min^{-1}	IκB-NFκB interaction	
IκBα:RelB:p50 =>IκBα + RelB:p50	Cyt, Nuc	95	3e-2 min^{-1}	IκB-NFκB interaction	Fitted (dependent on 80 -82)
IκBε:RelB:p50 =>IκBε + RelB:p50	Cyt, Nuc	96	3e-2 min^{-1}	IκB-NFκB interaction	
IκBδ:RelB:p50 =>IκBδ + RelB:p50	Cyt, Nuc	97	8.4e-4 min^{-1}	IκB-NFκB interaction	
IκBα:cRel:p50 =>IκBα + cRel:p50	Cyt, Nuc	98	4.8e-3 min^{-1}	IκB-NFκB interaction	Fitted (dependent on 83-86)
IκBβ:cRel:p50 =>IκBβ +cRel:p50	Cyt, Nuc	99	1.7e-2 min^{-1}	IκB-NFκB interaction	
IκBε:cRel:p50 =>IκBε + cRel:p50	Cyt, Nuc	100	2.7e-5 min^{-1}	IκB-NFκB interaction	

Table 5.1: Parameter Table and Reactions for the mathematical model with canonical and non-canonical NFkB signaling pathways, Continued

Reaction	Location	Param .No.	Parameter Value	Category	Source
IκBδ:cRel:p50 =>IκBδ + cRel:p50	Cyt, Nuc	101	8.4e-4 min^{-1}	IκB-NFκB interaction	Fitted (dependent on 83-86)
IκBα:cRel:p52 =>IκBα + cRel:p52	Cyt, Nuc	98	4.8e-3 min^{-1}	IκB-NFκB interaction	Fitted (dependent on 83-86)
IκBβ:cRel:p52 =>IκBβ + cRel:p52	Cyt, Nuc	99	1.7e-2 min^{-1}	IκB-NFκB interaction	
IκBε:cRel:p52 =>IκBε + cRelp52	Cyt, Nuc	100	2.7e-5 min^{-1}	IκB-NFκB interaction	
IκBδ:cRel:p52 =>IκBδ + cRel:p52	Cyt, Nuc	101	8.4e-4 min^{-1}	IκB-NFκB interaction	
IκBα:NFκB(c) =>IκBα:NFκB(n)	Cyt ->Nuc	102	0.28 min^{-1}	Transport	(Shih et al., 2009)
IκBβ:NFκB(c) =>IκBβ:NFκB(n)	Cyt ->Nuc	103	0.028 min^{-1}	Transport	(Shih et al., 2009)
IκBδ:NFκB(c) =>IκBδ:NFκB(n)	Cyt ->Nuc	104	0.028 min^{-1}	Transport	Based on slower import rate of IκBβ:NFκB
IκBε:NFκB(c) =>IκBε:NFκB(n)	Cyt ->Nuc	105	0.14 min^{-1}	Transport	(Shih et al., 2009)
IκBα:NFκB(n) =>IκBα:NFκB(c)	Nuc ->Cyt	106	0.84 min^{-1}	Transport	(Shih et al., 2009)
IκBβ:NFκB(n) =>IκBβ:NFκB(c)	Nuc ->Cyt	107	0.42 min^{-1}	Transport	(Shih et al., 2009)
IκBε:NFκB(n) =>IκBε:NFκB(c)	Nuc ->Cyt	108	0.42 min^{-1}	Transport	(Shih et al., 2009)
IκBδ:NFκB(n) =>IκBδ:NFκB(c)	Nuc ->Cyt	109	0.42 min^{-1}	Transport	(Shih et al., 2009)

Table 5.2: Available NFκB dimers that are canonically activated in different NIK regimes

Regime	RelA:p50	cRel:p50	RelB:p50
Low NIK	+	-	-
Medium NIK	+	+	-
High NIK	+	+	+

Table 5.3: Available NFκB dimers that are non-canonically activated in different NEMO-IKK regimes

Regime	RelA:p50	cRel:p50	RelB:p52
Low NEMO-IKK	-	-	-
Medium NEMO-IKK	-	-	+
High IKK	-	-	+

Table 5.4: Parameters that are changed for Hodgkin's disease and T cell/B cell lymphoma

Reactions	Param No	Wild type value	Value in IκBα -/-	Value in lymphoma
=>tIκBα (basal)	1	4.8e-3 nM/min	0 nM/min	4.8e-3 nM/min
p100 + p100 =>IκBδ	18	1.2e-2 nM^{-1} min^{-1}	1.2e-2 nM^{-1} min^{-1}	0 nM^{-1} min^{-1}
p100 => p52 (NIK-mediated)	38	5.0e-2 nM^{-1} min^{-1}	5.0e-2 nM^{-1} min^{-1}	0 nM^{-1} min^{-1}

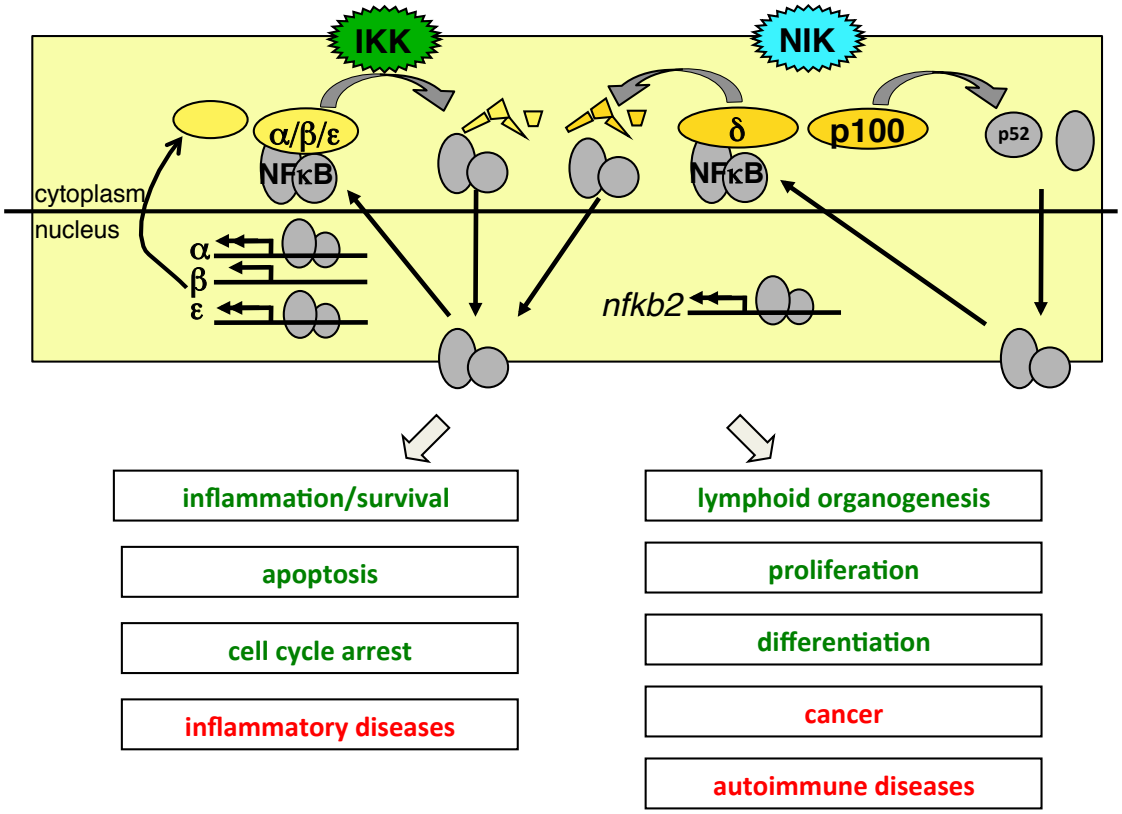

Figure 5.1: Overview of the NFkB activation pathways and its biological effects

Schematic illustrated the two canonical and non-canonical activation pathways of NFkB activation. NFkB activation regulates a variety of cellular functions including proliferation, differentiation, and inflammatory responses. Misregulation in this activity results in cancer, inflammatory diseases, and autoimmune diseases.

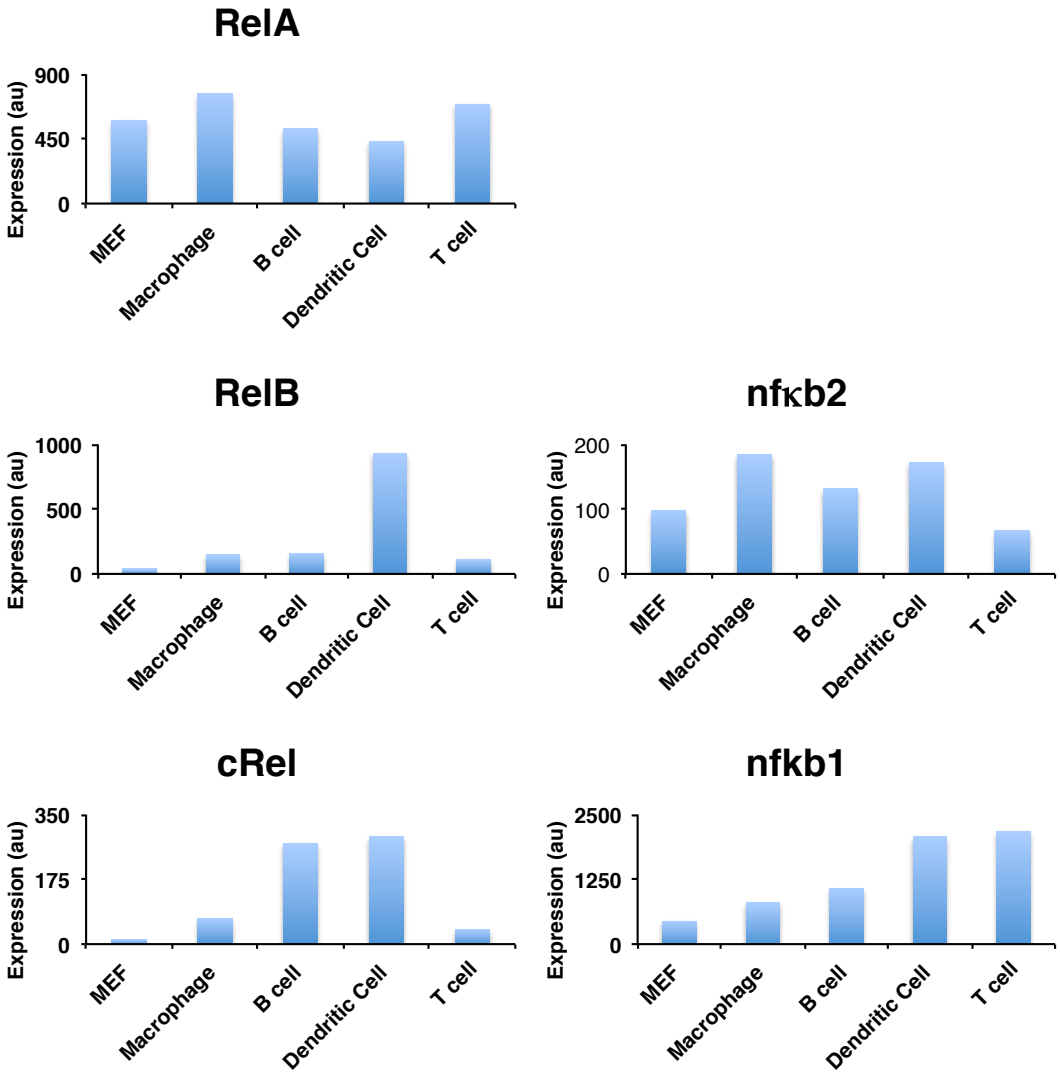

Figure 5.2: NFkB gene expression in various cell types
Gene expression data for the five NfkB monomers, RelA, RelB, cRel, nfkb1, and nfkb2, for various cell types were compared.

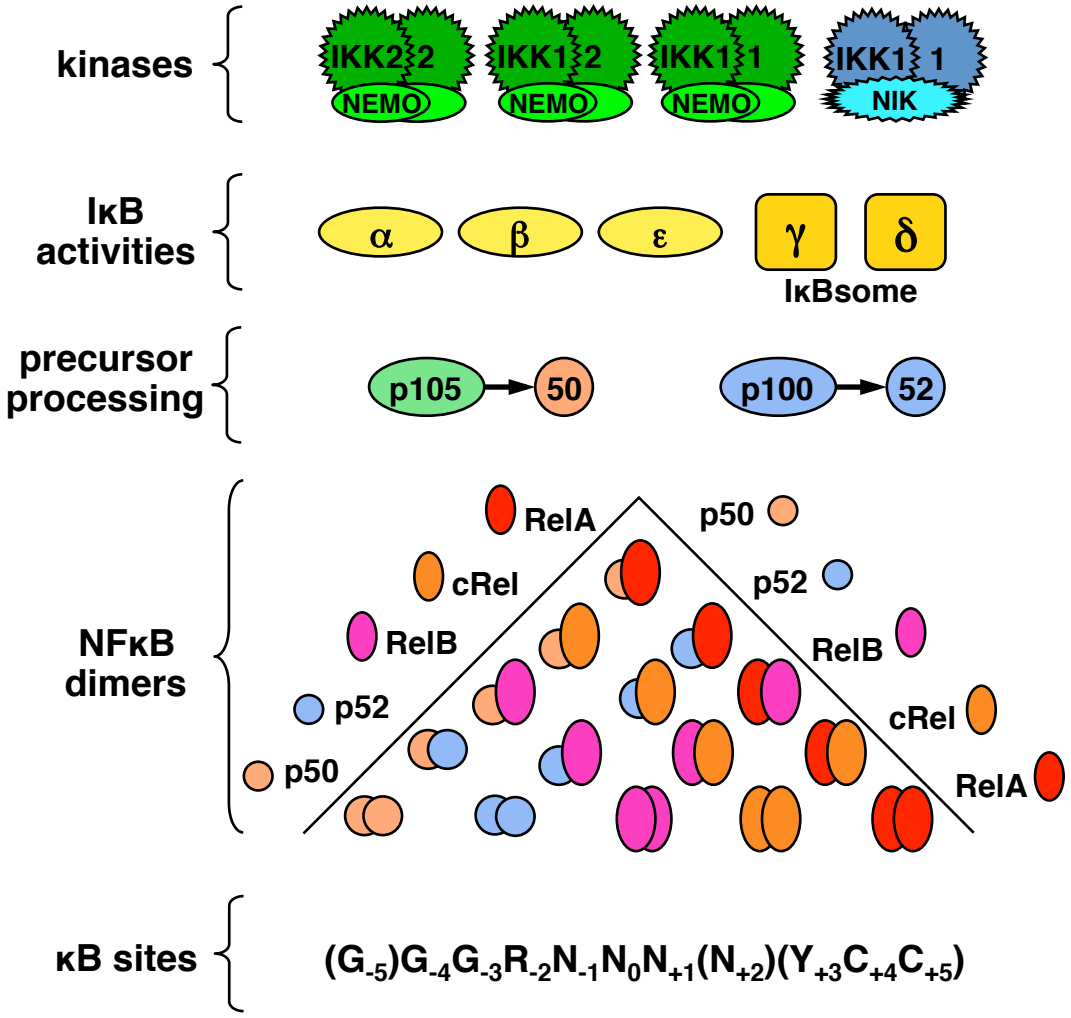

Figure 5.3: Scheme depicting the various players in the NFkB signaling system

While the NFkB signaling system has been previously studied in the context of both wild type and disease mutations, the NFkB signaling system contains a variety of players, including specific monomers that can combinatorially form specific NFkB dimers.

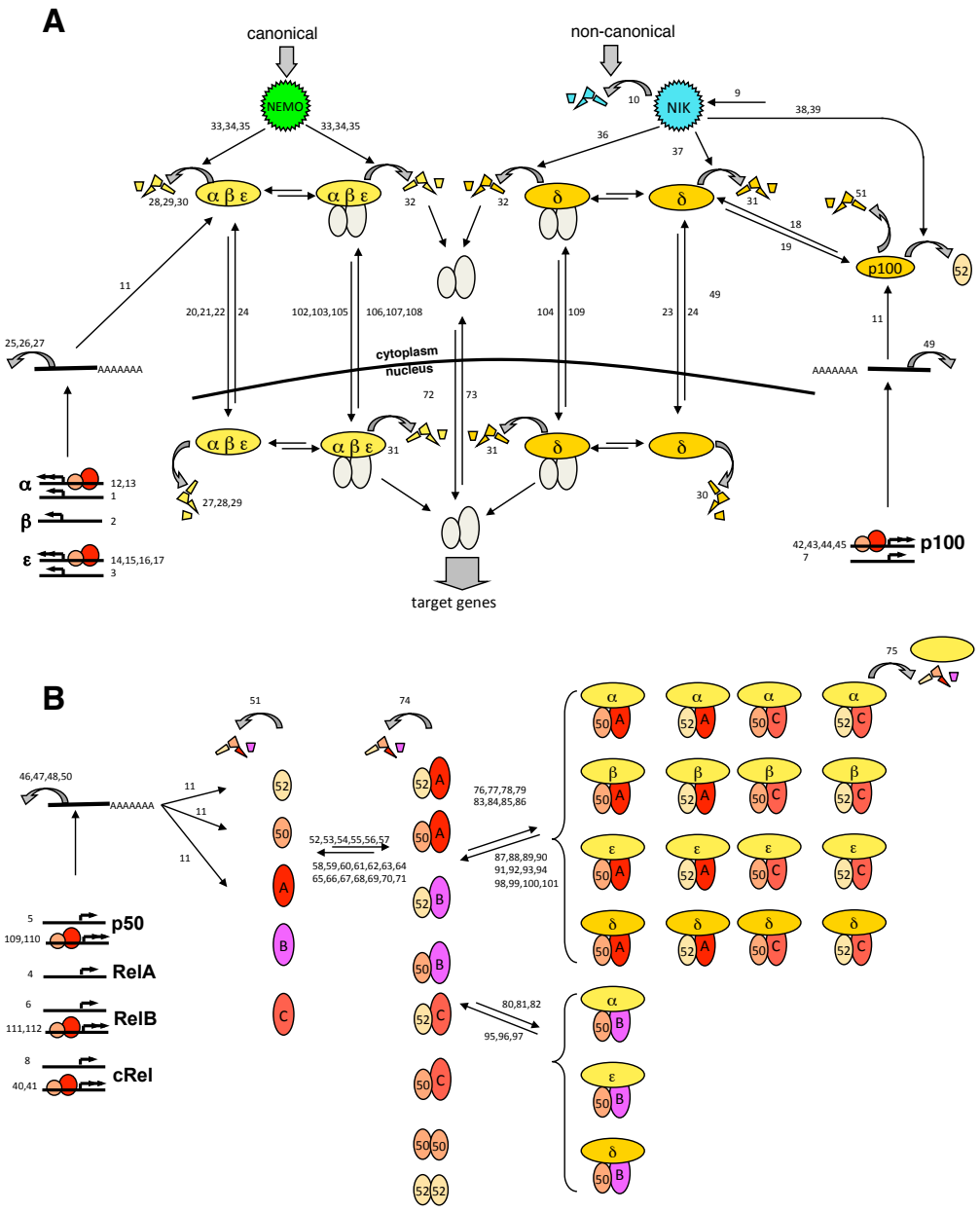

Figure 5.4: Wiring diagram depicting the biochemical reactions used in the mathematical model

A. A schematic of the NFkB model that includes both the canonical stimulus through NEMO/IKK2 activity and the non-canonical stimulus through affecting the levels of NIK. A general NFkB is the grey dimer that is then further described in (B). B. A schematic of the NFkB monomers that are synthesized in the model and the dimer combinations included in the model. The IkB-NFkB complexes are also described here.

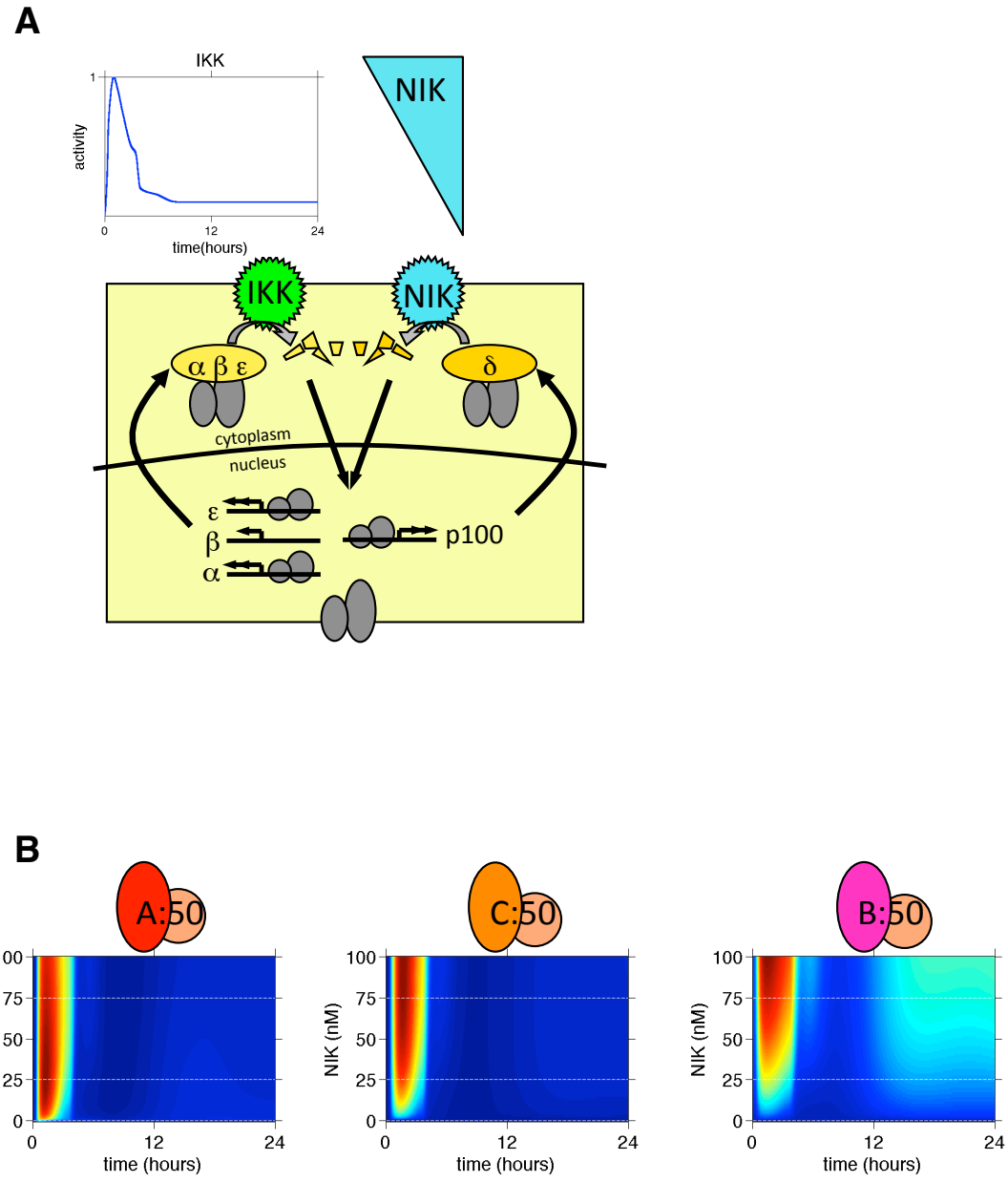

Figure 5.5: Basal levels of NIK determine specificity of NEMO-IKK responsive NFkB dimers in wild type cells

A. The non-canonical kinase, NIK, was varied while canonical stimulation of the NFkB pathway allowed for the activation of various NFkB dimers. This is a general scheme of the NFkB model while the more detailed wiring diagram is seen in Fig. 5.4. B. Heat maps of computational simulations of the specific NEMO-IKK responsive NFkB dimers (RelA:p50, cRel:p50, RelB:p50) upon varying tonic levels of NIK, from 0 – 100 nM.

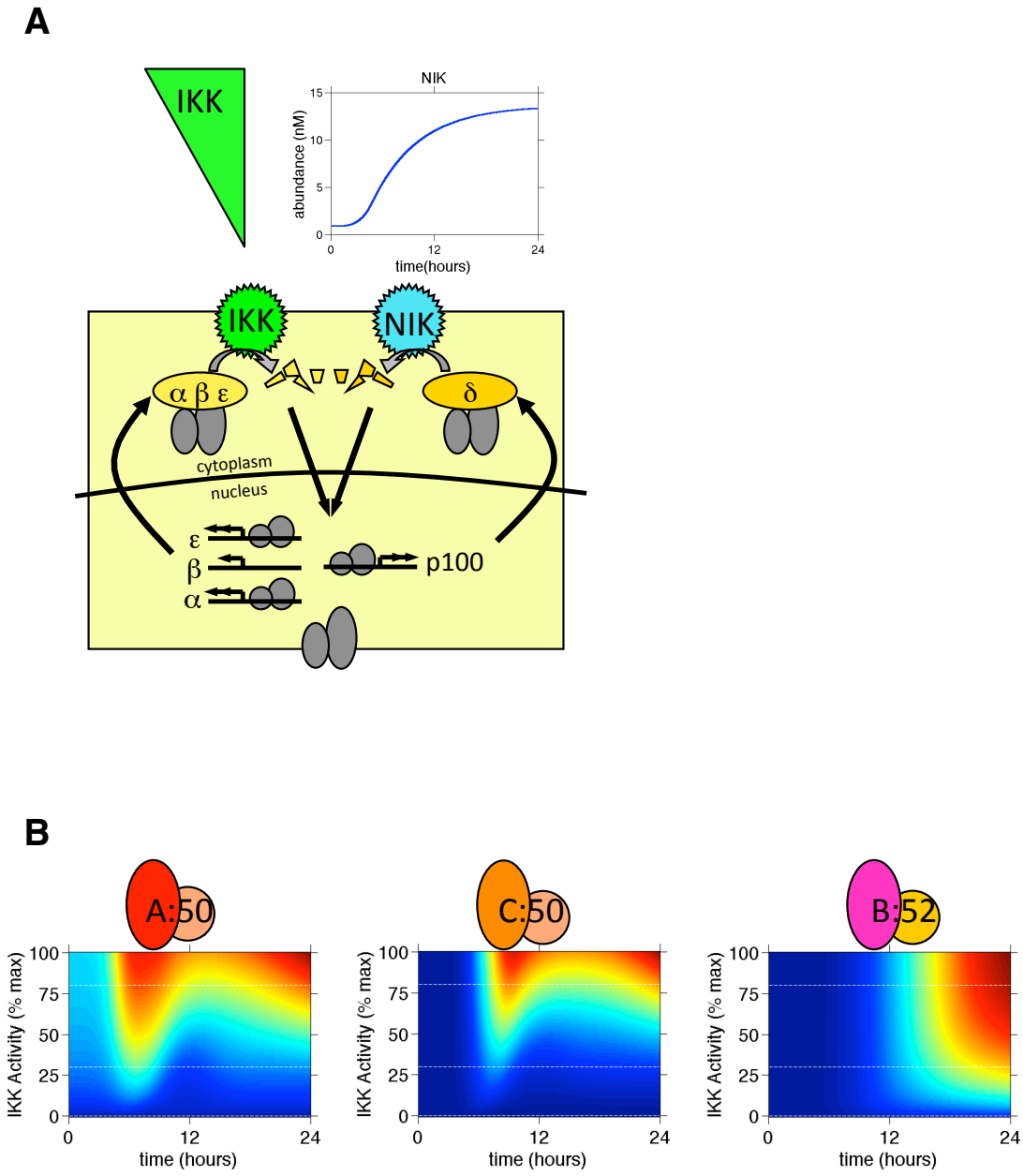

Figure 5.6: Basal levels of NEMO-IKK determine specificity of NIK responsive NFkB dimers in wild type cells

A. The canonical kinase activity, NEMO-IKK, was varied while non-canonical stimulation of the NFkB pathway allowed for the activation of various NFkB dimers. This is a general scheme of the NFkB model while the more detailed wiring diagram is seen in Fig. 5.4. B. Heat maps of computational simulations of the specific NIK responsive NFkB dimers (RelA:p50, cRel:p50, RelB:p52) upon varying tonic levels of NEMO-IKK activity, from 0 – 100%.

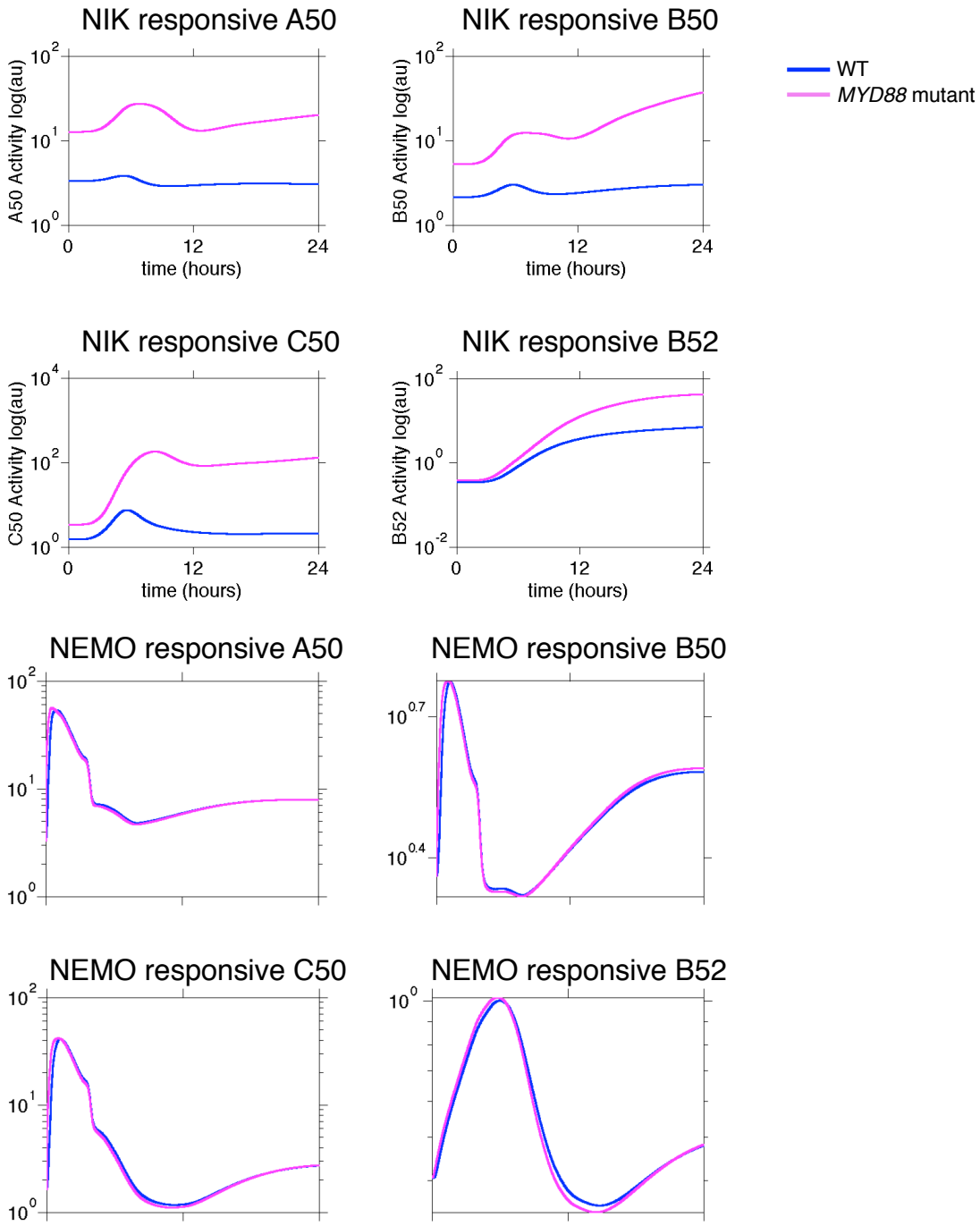

Figure 5.7: NIK responsive NFkB dimers in the WT vs. MYD88 mutant
WT activity of NFkB at basal NEMO-IKK activity (1%) is compared to a MYD88 mutant activity of NFkB (50% max NEMO-IKK activity).

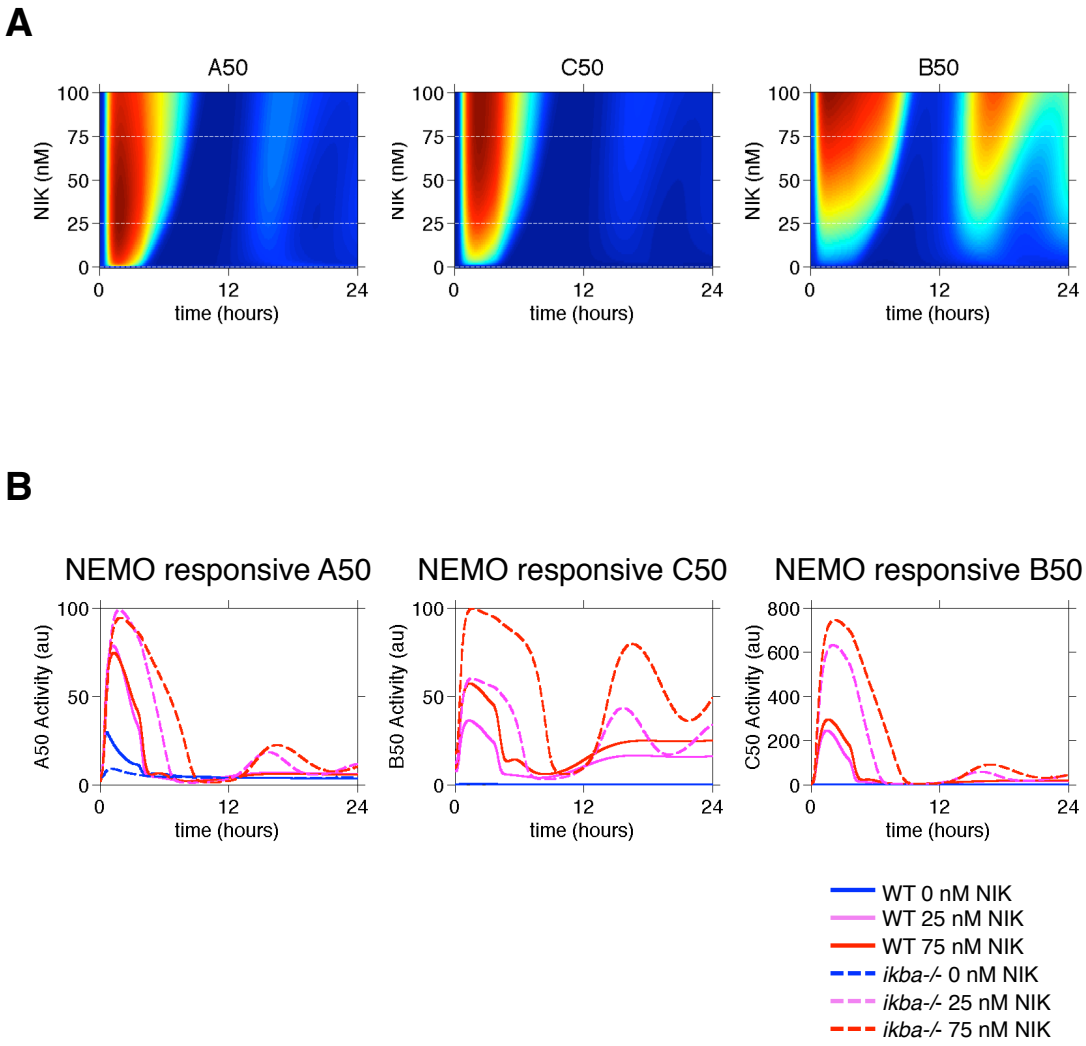

Figure 5.8: Basal levels of NIK determine specificity of NEMO-IKK responsive NFkB dimers in IkBa-deficient cells
A. Heat maps of computational simulations of NEMO-IKK responsive NFkB dimers (RelA:p50, cRel:p50, RelB:p50) with varying levels of NIK (1-100 nM) in an IkBa-deficient mathematical model. B. Line graphs of specific tonic levels of NIK (0, 25, 75 nM) NIK in both the wild type and the IkBa- deficient cells for the indicated NFkB dimers. IkBa deficiency results in increased activated NFkB at lower basal concentrations of NIK.

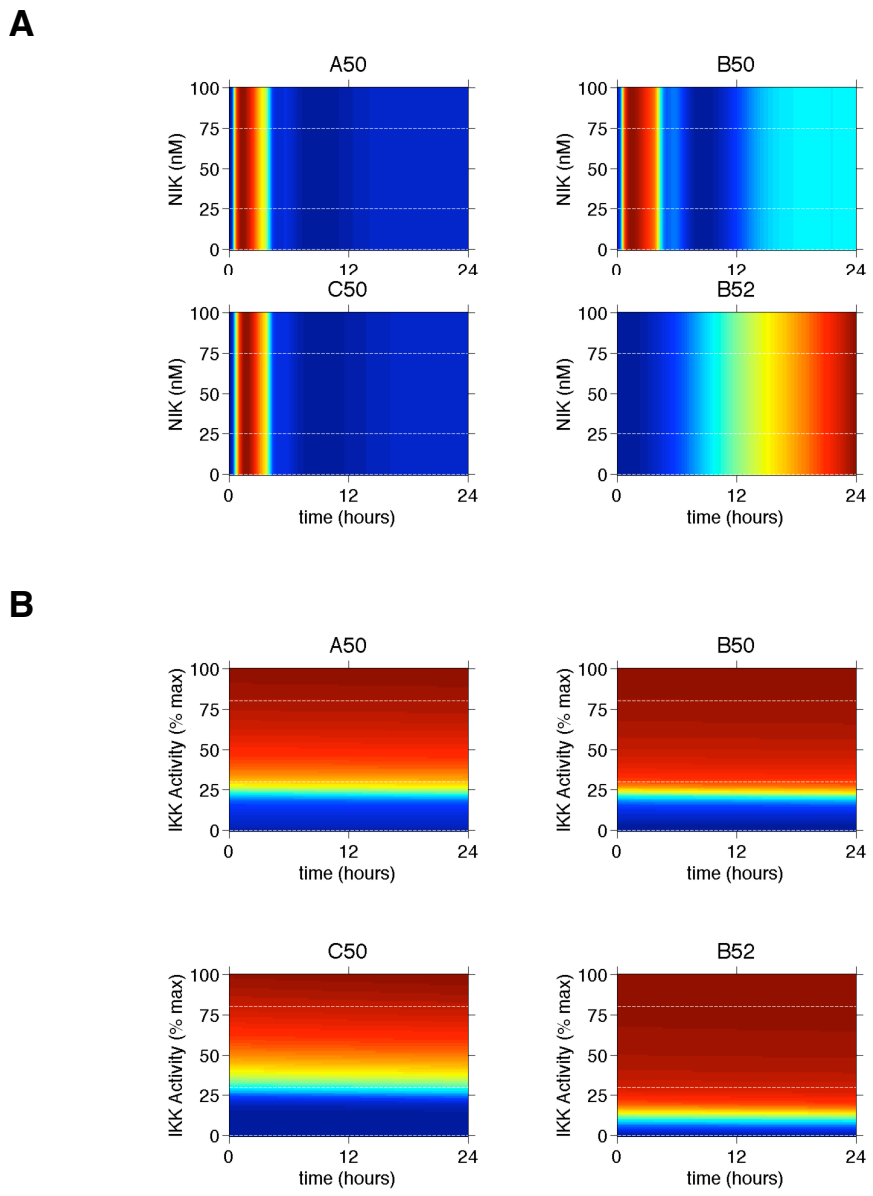

Figure 5.9: Basal levels of NEMO-IKK determine specificity of NIK responsive NFkB dimers in cells containing a mutation in the *nfkb2* gene
A. Heat maps of computational simulations of the specific NEMO-IKK responsive NFkB dimers (RelA:p50, cRel:p50, , RelB:p50RelB:p52) upon varying tonic levels of NIK activity, from 0 – 100 nM using a mathematical model that accounts for the *nfkb2* mutation that results in a constitutive truncation of the p100 protein. B. Heat maps of computational simulations of the specific NIK responsive NFkB dimers (RelA:p50, cRel:p50, RelB:p50 RelB:p52) upon varying tonic levels of NEMO-IKK activity, from 0 – 100% using a mathematical model that accounts for the *nfkb2* mutation that results in a constitutive truncation of the p100 protein.

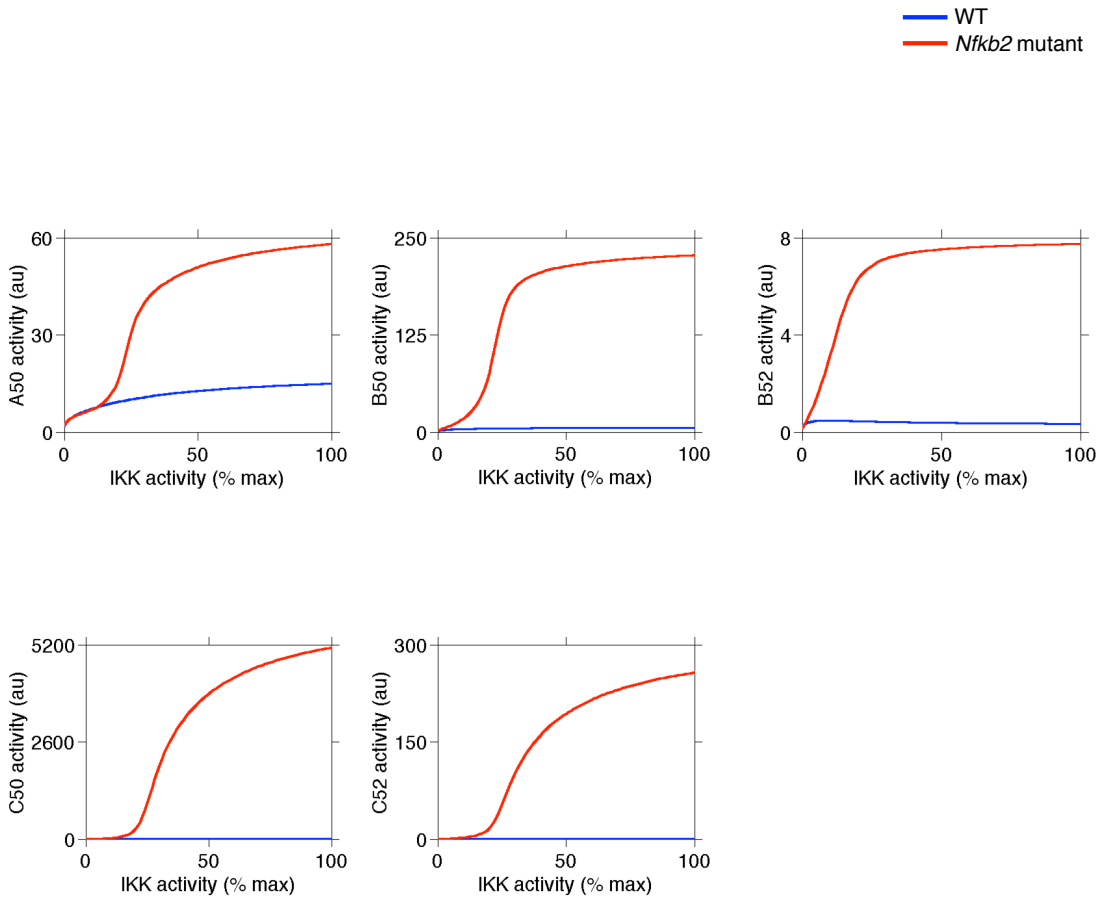

Figure 5.10: NFkB2 mutation results in an increased sensitivity of all NFkB dimers to tonic NEMO-IKK activity
The nfkb2 mutant that results in the lack of IkBd and the constitutive processing of p100 to p52 results in an increased sensitivity to any basal NEMO-IKK activity in the cell as compared to wild type.

Chapter 6: Concluding Remarks

In Chapter 2, we reveal a novel function for IkBb in the Rel-NFkB dimer generation module. Through our combined mathematical modeling and experimental efforts, we illustrate the importance of monomer competition and specific dimer generation on the abundance of available dimers in MEF cells. While IkBb has historically been labeled as an inhibitor of NFkB, we show its additional function as a chaperone for the RelA:RelA homodimer. We described the Rel-NFκB dimer generation module and the IκB-NFκB signaling module as distinct but there are of course numerous interactions. At a minimum, we may consider that IκBβ within the Rel-NFκB dimer generation module functions as a 'licensing factor' for subsequent dynamic control by IκBα. The distinct functions by these structurally homologous proteins are based on both their specific protein-interaction constants and their distinct dynamic degradation and synthesis control. Indeed, such 'hand-off' or 'relay control' network motifs based on kinetic differences between family members may be found in other regulatory systems.

We continue the adapting the IkB-NFkB signaling module with specific Rel-NFkB dimers for B cells in Chapter 3. While cRel does not play a dominant role in NFκB signaling in MEFs, in B cells cRel is an important NFκB effector. Here we observed the model's ability to demonstrate a kinetic difference as the basis for IkBe's stimulus specific regulatory effects on RelA and cRel containing NFkB dimers. We reveal that the kinetic considerations of the IKK

activity (transient for IgM, long-lived for LPS) resulted in a stimulus specific response for negative regulatory effects of IkBe on the specific dimers. Additionally, in an IkBe deficient mouse, we find that there is increased B cell expansion, showing a physiologically relevant role for IkBe in the regulation of the proliferative capacity for B cells. Here, the mathematical modeling efforts were able to reveal kinetic information that provided a mechanistic explanation for the observed phenotypes.

The adaptation of the multi-dimer NFkB signaling module was expanded to include the non-canonical activation pathway in Chapter 4 in order to further delineate the mechasism for B cell expansion in the presence of anti-IgM and BAFF co-stimulation. Here, specific NFκB dimers are important in the observed B cell phenotype upon canonical and non-canonical pathway activating co-stimulatory effects. Experimental observations showed an increase in B cell proliferation and survival for BAFF enhanced BCR activation, which resulted in hyper-cRel NFkB dimer activation. The mathematical model suggested p100/IkBd as the primary mediator of this phenotype, and that BAFF activation resulted in both the processing of p100 and the degradation of IkBd resulting in the release of cRel containing NFkB dimers upon co-stimulation. We were able to test this hypothesis by generating a predictive model in which *nfkb2* transcription was reduced, which subsequently reduced p100 protein expression, leading to increased cRel NFκB dimer activity upon BCR stimulation without the need for additional

BAFF co-stimulation. These computational predictions were confirmed with experimental analysis, showing that the hypothesis that p100 is a critical mediator in affecting BAFF enhanced BCR B cell expansion is supported.

Chapter 5 continues our analysis of the multi-dimer signaling module and the importance of the activation of specific NFκB dimers in distinct cell types. We hypothesized that the critical regulators of both the canonical and non-canonical activation pathways are at the kinase level (NEMO-IKK and NIK respectively), and we utilized the mathematical model to analyze the importance of the kinase activities for the availibity of specific NFκB dimer generation. We show that in fact the basal kinase levels are critical in the availability of the activation of specific NFκB dimers. Additional analysis of diseases that result in mutations in the NFκB signaling module also showed the importance of the effect of the canonical pathway on the non-canonical pathway and vice versa. This suggests that the interdependence between the two pathways is greater than previously anticipated, and that future studies should not delineate between the canonical and non-canonical pathways. Rather, future work should consider the NFκB signaling system as a whole complete system in order to gain predictive understanding of the effects a mutation may have on NFκB activation.

This dissertation work illustrates the importance of the cellular context on the NFκB dimer repertoire in various cell types. In fact, the basal kinase levels in a cell have a distinct effect on the activation of specific NFκB dimers.

Through the use of the mathematical model, we demonstrate the importance of kinetic parameters on the mechanism of NFκB activation, and reveal novel roles for the functions of three important NFκB signaling pathway species, IκBβ, IκBε, and p100/IκBδ. Overall, we show the importance of cellular context on the activation of specific NFκB dimers and the importance in considering the NFκB signaling system as a whole complete system rather than two distinctive activation pathways in order to gain understanding on the NFκB pathway mutations that cause diseases and cancers.

References

Adachi, O., Kawai, T., Takeda, K., Matsumoto, M., Tsutsui, H., Sakagami, M., Nakanishi, K., and Akira, S. (1998). Targeted Disruption of the MyD88 Gene Results in Loss of IL-1- and IL-18-Mediated Function. Immunity *9*, 143–150.

Alves, B.N., Tsui, R., Almaden, J., Shokhirev, M.N., Davis-Turak, J., Fujimoto, J., Birnbaum, H., Ponomarenko, J., and Hoffmann, A. (2014). IκB{varepsilon} Is a Key Regulator of B Cell Expansion by Providing Negative Feedback on cRel and RelA in a Stimulus-Specific Manner. J. Immunol. *192*, 3121–3132.

Baeuerle, P.A., and Baltimore, D. (1988). I kappa B: a specific inhibitor of the NF-kappa B transcription factor. Science *242*, 540–546.

Bargou, R.C., Leng, C., Krappmann, D., Emmerich, F., Mapara, M.Y., Bommert, K., Royer, H.D., Scheidereit, C., and Dörken, B. (1996). High-level nuclear NF-kappa B and Oct-2 is a common feature of cultured Hodgkin/Reed-Sternberg cells. Blood *87*, 4340–4347.

Bargou, R.C., Emmerich, F., Krappmann, D., Bommert, K., Mapara, M.Y., Arnold, W., Royer, H.D., Grinstein, E., Greiner, A., Scheidereit, C., and Dörken, B. (1997). Constitutive nuclear factor-kappaB-RelA activation is required for proliferation and survival of Hodgkin's disease tumor cells. Journal of Clinical Investigation *100*, 2961–2969.

Basak, S., Kim, H., Kearns, J.D., Tergaonkar, V., O'Dea, E., Werner, S.L., Benedict, C.A., Ware, C.F., Ghosh, G., Verma, I.M., and Hoffmann, A. (2007). A Fourth IκB Protein within the NF-κB Signaling Module. Cell *128*, 369–381.

Basak, S., Shih, V.F.-S., and Hoffmann, A. (2008). Generation and Activation of Multiple Dimeric Transcription Factors Within the NF-κB Signaling System. Mol. Cell. Biol. *28*, 3139–3150.

Basak, S., Behar, M., and Hoffmann, A. (2012). Lessons from mathematically modeling the NF-κB pathway. Immunol. Rev. *246*, 221–238.

Beg, A.A., Sha, W.C., Bronson, R.T., Ghosh, S., and Baltimore, D. (1995). Embryonic lethality and liver degeneration in mice lacking the RelA component of NF-kappa B. Nature *376*, 167–170.

Behar, M., Barken, D., Werner, S.L., and Hoffmann, A. (2013). The dynamics of signaling as a pharmacological target. Cell *155*, 448–461.

Bergqvist, S., Alverdi, V., Mengel, B., Hoffmann, A., Ghosh, G., and Komives, E.A. (2009). Kinetic enhancement of NF-κB·DNA dissociation by IκBα. Proceedings of the National Academy of Sciences *106*, 19328 –19333.

Bernuth, H. von, Picard, C., Jin, Z., Pankla, R., Xiao, H., Ku, C.-L., Chrabieh, M., Mustapha, I.B., Ghandil, P., Camcioglu, Y., Vasconcelos, J., Sirvent, N., Guedes, M., Vitor, A.B., Herrero-Mata, M.J., Aróstegui, J.I., Rodrigo, C., Alsina, L., Ruiz-Ortiz, E., Juan, M., Fortuny, C., Yagüe, J., Antón, J., Pascal, M., Chang, H.-H., Janniere, L., Rose, Y., Garty, B.-Z., Chapel, H., Issekutz, A., Maródi, L., Rodriguez-Gallego, C., Banchereau, J., Abel, L., Li, X., Chaussabel, D., Puel, A., and Casanova, J.-L. (2008). Pyogenic Bacterial Infections in Humans with MyD88 Deficiency. Science *321*, 691–696.

Cancro, M.P. (2009). Signalling crosstalk in B cells: managing worth and need. Nat. Rev. Immunol. *9*, 657–661.

Cariappa, A., Liou, H.C., Horwitz, B.H., and Pillai, S. (2000). Nuclear factor kappa B is required for the development of marginal zone B lymphocytes. J. Exp. Med. *192*, 1175–1182.

Claudio, E., Brown, K., Park, S., Wang, H., and Siebenlist, U. (2002). BAFF-induced NEMO-independent processing of NF-kappa B2 in maturing B cells. Nat. Immunol. *3*, 958–965.

Craxton, A., Draves, K.E., and Clark, E.A. (2007). Bim regulates BCR-induced entry of B cells into the cell cycle. Eur. J. Immunol. *37*, 2715–2722.

Davis, R.E., Brown, K.D., Siebenlist, U., and Staudt, L.M. (2001). Constitutive Nuclear Factor κB Activity Is Required for Survival of Activated B Cell–like Diffuse Large B Cell Lymphoma Cells. J Exp Med *194*, 1861–1874.

Doi, T.S., Takahashi, T., Taguchi, O., Azuma, T., and Obata, Y. (1997). NF-kappa B RelA-deficient lymphocytes: normal development of T cells and B cells, impaired production of IgA and IgG1 and reduced proliferative responses. J. Exp. Med. *185*, 953–961.

Franzoso, G., Carlson, L., Poljak, L., Shores, E.W., Epstein, S., Leonardi, A., Grinberg, A., Tran, T., Scharton-Kersten, T., Anver, M., Love, P., Brown, K., and Siebenlist, U. (1998). Mice deficient in nuclear factor (NF)-kappa B/p52 present with defects in humoral responses, germinal center reactions, and splenic microarchitecture. J. Exp. Med. *187*, 147–159.

Fusco, A.J., Savinova, O.V., Talwar, R., Kearns, J.D., Hoffmann, A., and Ghosh, G. (2008). Stabilization of RelB Requires Multidomain Interactions with p100/p52. Journal of Biological Chemistry *283*, 12324 –12332.

Gapuzan, M.-E.R., Schmah, O., Pollock, A.D., Hoffmann, A., and Gilmore, T.D. (2005). Immortalized fibroblasts from NF-κB RelA knockout mice show phenotypic heterogeneity and maintain increased sensitivity to tumor necrosis factor α after transformation by v-Ras. Oncogene *24*, 6574–6583.

Gerondakis, S., Grumont, R., Rourke, I., and Grossmann, M. (1998). The regulation and roles of Rel/NF-kappa B transcription factors during lymphocyte activation. Curr. Opin. Immunol. *10*, 353–359.

Gerondakis, S., Grumont, R., Gugasyan, R., Wong, L., Isomura, I., Ho, W., and Banerjee, A. (2006). Unravelling the complexities of the NF-kappaB signalling pathway using mouse knockout and transgenic models. Oncogene *25*, 6781–6799.

Ghosh, S., and Hayden, M.S. (2008). New regulators of NF-kappaB in inflammation. Nat. Rev. Immunol. *8*, 837–848.

Grumont, R.J., and Gerondakis, S. (1994). The subunit composition of NF-kappa B complexes changes during B-cell development. Cell Growth Differ. *5*, 1321–1331.

Grumont, R.J., Rourke, I.J., O'Reilly, L.A., Strasser, A., Miyake, K., Sha, W., and Gerondakis, S. (1998). B lymphocytes differentially use the Rel and nuclear factor kappaB1 (NF-kappaB1) transcription factors to regulate cell cycle progression and apoptosis in quiescent and mitogen-activated cells. J. Exp. Med. *187*, 663–674.

Harless, S.M., Lentz, V.M., Sah, A.P., Hsu, B.L., Clise-Dwyer, K., Hilbert, D.M., Hayes, C.E., and Cancro, M.P. (2001). Competition for BLyS-mediated signaling through Bcmd/BR3 regulates peripheral B lymphocyte numbers. Curr. Biol. *11*, 1986–1989.

Hertlein, E., Wang, J., Ladner, K.J., Bakkar, N., and Guttridge, D.C. (2005). RelA/p65 Regulation of IκBβ. Mol. Cell. Biol. *25*, 4956–4968.

Hoffmann, A., Levchenko, A., Scott, M.L., and Baltimore, D. (2002). The Ikappa B-NF-kappa B Signaling Module: Temporal Control and Selective Gene Activation. Science *298*, 1241–1245.

Hoffmann, A., Leung, T.H., and Baltimore, D. (2003). Genetic analysis of NF-kappaB/Rel transcription factors defines functional specificities. EMBO J. *22*, 5530–5539.

Hoffmann, A., Natoli, G., and Ghosh, G. (2006). Transcriptional regulation via the NF-kappaB signaling module. Oncogene *25*, 6706–6716.

Huang, X., Di Liberto, M., Cunningham, A.F., Kang, L., Cheng, S., Ely, S., Liou, H., Maclennan, I.C.M., and Chen-Kiang, S. (2004). Homeostatic cell-cycle control by BLyS: Induction of cell-cycle entry but not G1/S transition in opposition to p18INK4c and p27Kip1. Proc. Natl. Acad. Sci. U.S.A. *101*, 17789–17794.

Huxford, T., Huang, D.B., Malek, S., and Ghosh, G. (1998). The crystal structure of the IkappaBalpha/NF-kappaB complex reveals mechanisms of NF-kappaB inactivation. Cell *95*, 759–770.

Ishikawa, H., Claudio, E., Dambach, D., Raventós-Suárez, C., Ryan, C., and Bravo, R. (1998). Chronic Inflammation and Susceptibility to Bacterial Infections in Mice Lacking the Polypeptide (p)105 Precursor (NF-κB1) but Expressing p50. J Exp Med *187*, 985–996.

Jeelall, Y.S., and Horikawa, K. (2011). Oncogenic MYD88 mutation drives Toll pathway to lymphoma. Immunol Cell Biol *89*, 659–660.

Jones, S., and Thornton, J.M. (1996). Principles of protein-protein interactions. PNAS *93*, 13–20.

Kato, M., Sanada, M., Kato, I., Sato, Y., Takita, J., Takeuchi, K., Niwa, A., Chen, Y., Nakazaki, K., Nomoto, J., Asakura, Y., Muto, S., Tamura, A., Iio, M., Akatsuka, Y., Hayashi, Y., Mori, H., Igarashi, T., Kurokawa, M., Chiba, S., Mori, S., Ishikawa, Y., Okamoto, K., Tobinai, K., Nakagama, H., Nakahata, T., Yoshino, T., Kobayashi, Y., and Ogawa, S. (2009). Frequent inactivation of A20 in B-cell lymphomas. Nature *459*, 712–716.

Kearns, J.D., Basak, S., Werner, S.L., Huang, C.S., and Hoffmann, A. (2006). IκBε provides negative feedback to control NF-κB oscillations, signaling dynamics, and inflammatory gene expression. The Journal of Cell Biology *173*, 659 –664.

Khan, W.N. (2009). B cell receptor and BAFF receptor signaling regulation of B cell homeostasis. J. Immunol. *183*, 3561–3567.

Kim, K.E., Gu, C., Thakur, S., Vieira, E., Lin, J.C., and Rabson, A.B. (2000). Transcriptional regulatory effects of lymphoma-associated NFKB2/lyt10 protooncogenes. Oncogene *19*, 1334–1345.

Köntgen, F., Grumont, R.J., Strasser, A., Metcalf, D., Li, R., Tarlinton, D., and Gerondakis, S. (1995). Mice lacking the c-rel proto-oncogene exhibit defects in lymphocyte proliferation, humoral immunity, and interleukin-2 expression. Genes Dev. *9*, 1965–1977.

Küppers, R. (2012). New insights in the biology of Hodgkin lymphoma. Hematology Am Soc Hematol Educ Program *2012*, 328–334.

Lake, A., Shield, L.A., Cordano, P., Chui, D.T.Y., Osborne, J., Crae, S., Wilson, K.S., Tosi, S., Knight, S.J.L., Gesk, S., Siebert, R., Hay, R.T., and Jarrett, R.F. (2009). Mutations of NFKBIA, encoding IκBα, are a recurrent finding in classical Hodgkin lymphoma but are not a unifying feature of non-EBV-associated cases. Int. J. Cancer *125*, 1334–1342.

Lam, K.P., Kühn, R., and Rajewsky, K. (1997). In vivo ablation of surface immunoglobulin on mature B cells by inducible gene targeting results in rapid cell death. Cell *90*, 1073–1083.

Lesley, R., Xu, Y., Kalled, S.L., Hess, D.M., Schwab, S.R., Shu, H.-B., and Cyster, J.G. (2004). Reduced competitiveness of autoantigen-engaged B cells due to increased dependence on BAFF. Immunity *20*, 441–453.

Leung, T.H., Hoffmann, A., and Baltimore, D. (2004). One nucleotide in a kappaB site can determine cofactor specificity for NF-kappaB dimers. Cell *118*, 453–464.

Li, Z., and Nabel, G.J. (1997). A new member of the I kappaB protein family, I kappaB epsilon, inhibits RelA (p65)-mediated NF-kappaB transcription. Mol. Cell. Biol. *17*, 6184–6190.

Liao, G., Zhang, M., Harhaj, E.W., and Sun, S.-C. (2004). Regulation of the NF-κB-inducing Kinase by Tumor Necrosis Factor Receptor-associated Factor 3-induced Degradation. Journal of Biological Chemistry *279*, 26243 –26250.

Liou, H.C., Sha, W.C., Scott, M.L., and Baltimore, D. (1994). Sequential induction of NF-kappa B/Rel family proteins during B-cell terminal differentiation. Mol Cell Biol *14*, 5349–5359.

Mackay, F., Silveira, P.A., and Brink, R. (2007). B cells and the BAFF/APRIL axis: fast-forward on autoimmunity and signaling. Curr. Opin. Immunol. *19*, 327–336.

Maine, G.N., Mao, X., Komarck, C.M., and Burstein, E. (2007). COMMD1 promotes the ubiquitination of NF-kappaB subunits through a cullin-containing ubiquitin ligase. EMBO J. *26*, 436–447.

Mintseris, J., and Weng, Z. (2005). Structure, function, and evolution of transient and obligate protein–protein interactions. Proc Natl Acad Sci U S A *102*, 10930–10935.

O'Dea, E.L., Barken, D., Peralta, R.Q., Tran, K.T., Werner, S.L., Kearns, J.D., Levchenko, A., and Hoffmann, A. (2007). A homeostatic model of I[kappa]B metabolism to control constitutive NF-[kappa]B activity. Mol Syst Biol *3*.

Otto, C., Giefing, M., Massow, A., Vater, I., Gesk, S., Schlesner, M., Richter, J., Klapper, W., Hansmann, M.-L., Siebert, R., and Küppers, R. (2012). Genetic lesions of the TRAF3 and MAP3K14 genes in classical Hodgkin lymphoma. Br J Haematol *157*, 702–708.

Pando, M.P., and Verma, I.M. (2000). Signal-dependent and -independent Degradation of Free and NF-κB-bound IκBα. J. Biol. Chem. *275*, 21278–21286.

Phelps, C.B., Sengchanthalangsy, L.L., Huxford, T., and Ghosh, G. (2000). Mechanism of IκBα Binding to NF-κB Dimers. J. Biol. Chem. *275*, 29840–29846.

Qing, G., Qu, Z., and Xiao, G. (2005). Regulation of NF-kappa B2 p100 processing by its cis-acting domain. J. Biol. Chem. *280*, 18–27.

Qing, G., Qu, Z., and Xiao, G. (2007). Endoproteolytic processing of C-terminally truncated NF-kappaB2 precursors at kappaB-containing promoters. Proc. Natl. Acad. Sci. U.S.A. *104*, 5324–5329.

Ramakrishnan, P., Wang, W., and Wallach, D. (2004). Receptor-Specific Signaling for Both the Alternative and the Canonical NF-κB Activation Pathways by NF-κB-Inducing Kinase. Immunity *21*, 477–489.

Rao, P., Hayden, M.S., Long, M., Scott, M.L., West, A.P., Zhang, D., Oeckinghaus, A., Lynch, C., Hoffmann, A., Baltimore, D., and Ghosh, S. (2010). IκBβ acts to inhibit and activate gene expression during the inflammatory response. Nature *466*, 1115–1119.

Rayet, B., and Gélinas, C. (1999). Aberrant rel/nfkb genes and activity in human cancer. Oncogene *18*, 6938–6947.

Rickert, R.C., Jellusova, J., and Miletic, A.V. (2011). Signaling by the tumor necrosis factor receptor superfamily in B-cell biology and disease. Immunol. Rev. *244*, 115–133.

Salimi-Moosavi, H., Rathanaswami, P., Rajendran, S., Toupikov, M., and Hill, J. (2012). Rapid affinity measurement of protein–protein interactions in a microfluidic platform. Analytical Biochemistry *426*, 134–141.

Savinova, O.V., Hoffmann, A., and Ghosh, G. (2009). The Nfkb1 and Nfkb2 proteins p105 and p100 function as the core of high-molecular-weight heterogeneous complexes. Mol. Cell *34*, 591–602.

Scheibel, M., Klein, B., Merkle, H., Schulz, M., Fritsch, R., Greten, F.R., Arkan, M.C., Schneider, G., and Schmid, R.M. (2010). IκBβ is an essential co-activator for LPS-induced IL-1β transcription in vivo. J Exp Med *207*, 2621–2630.

Scheidereit, C. (2006). IkappaB kinase complexes: gateways to NF-kappaB activation and transcription. Oncogene *25*, 6685–6705.

Schiemann, B., Gommerman, J.L., Vora, K., Cachero, T.G., Shulga-Morskaya, S., Dobles, M., Frew, E., and Scott, M.L. (2001). An essential role for BAFF in the normal development of B cells through a BCMA-independent pathway. Science *293*, 2111–2114.

Schmitz, R., Stanelle, J., Hansmann, M.-L., and Küppers, R. (2009a). Pathogenesis of Classical and Lymphocyte-Predominant Hodgkin Lymphoma. Annual Review of Pathology: Mechanisms of Disease *4*, 151–174.

Schmitz, R., Hansmann, M.-L., Bohle, V., Martin-Subero, J.I., Hartmann, S., Mechtersheimer, G., Klapper, W., Vater, I., Giefing, M., Gesk, S., Stanelle, J., Siebert, R., and Küppers, R. (2009b). TNFAIP3 (A20) is a tumor suppressor gene in Hodgkin lymphoma and primary mediastinal B cell lymphoma. J Exp Med *206*, 981–989.

Schweighoffer, E., Vanes, L., Nys, J., Cantrell, D., McCleary, S., Smithers, N., and Tybulewicz, V.L.J. (2013). The BAFF receptor transduces survival signals by co-opting the B cell receptor signaling pathway. Immunity *38*, 475–488.

Senftleben, U., Cao, Y., Xiao, G., Greten, F.R., Krähn, G., Bonizzi, G., Chen, Y., Hu, Y., Fong, A., Sun, S.-C., and Karin, M. (2001). Activation by IKKα of a Second, Evolutionary Conserved, NF-κB Signaling Pathway. Science *293*, 1495–1499.

Sha, W.C., Liou, H.C., Tuomanen, E.I., and Baltimore, D. (1995). Targeted disruption of the p50 subunit of NF-kappa B leads to multifocal defects in immune responses. Cell *80*, 321–330.

Shih, V.F.-S., Kearns, J.D., Basak, S., Savinova, O.V., Ghosh, G., and Hoffmann, A. (2009). Kinetic control of negative feedback regulators of NF-κB/RelA determines their pathogen- and cytokine-receptor signaling specificity. Proceedings of the National Academy of Sciences *106*, 9619 – 9624.

Shih, V.F.-S., Tsui, R., Caldwell, A., and Hoffmann, A. (2010). A single NF|[kappa]|B system for both canonical and non-canonical signaling. Cell Research *21*, 86–102.

Shih, V.F.-S., Davis-Turak, J., Macal, M., Huang, J.Q., Ponomarenko, J., Kearns, J.D., Yu, T., Fagerlund, R., Asagiri, M., Zuniga, E.I., and Hoffmann, A. (2012). Control of RelB during dendritic cell activation integrates canonical and noncanonical NF-κB pathways. Nat Immunol *13*, 1162–1170.

Shinners, N.P., Carlesso, G., Castro, I., Hoek, K.L., Corn, R.A., Woodland, R.T., Woodland, R.L., Scott, M.L., Wang, D., and Khan, W.N. (2007). Bruton's tyrosine kinase mediates NF-kappa B activation and B cell survival by B cell-activating factor receptor of the TNF-R family. J. Immunol. *179*, 3872–3880.

Simeonidis, S., Liang, S., Chen, G., and Thanos, D. (1997). Cloning and functional characterization of mouse IkappaBepsilon. Proc. Natl. Acad. Sci. U.S.A. *94*, 14372–14377.

Sriskantharajah, S., Belich, M.P., Papoutsopoulou, S., Janzen, J., Tybulewicz, V., Seddon, B., and Ley, S.C. (2009). Proteolysis of NF-kappaB1 p105 is essential for T cell antigen receptor-induced proliferation. Nat. Immunol. *10*, 38–47.

Stadanlick, J.E., Kaileh, M., Karnell, F.G., Scholz, J.L., Miller, J.P., Quinn, W.J., 3rd, Brezski, R.J., Treml, L.S., Jordan, K.A., Monroe, J.G., Sen, R., and Cancro, M.P. (2008). Tonic B cell antigen receptor signals supply an NF-kappaB substrate for prosurvival BLyS signaling. Nat. Immunol. *9*, 1379–1387.

Steidl, C., Telenius, A., Shah, S.P., Farinha, P., Barclay, L., Boyle, M., Connors, J.M., Horsman, D.E., and Gascoyne, R.D. (2010). Genome-wide copy number analysis of Hodgkin Reed-Sternberg cells identifies recurrent imbalances with correlations to treatment outcome. Blood *116*, 418–427.

Sun, S.-C., and Xiao, G. (2003). Deregulation of NF-kappaB and its upstream kinases in cancer. Cancer Metastasis Rev. *22*, 405–422.

Suyang, H., Phillips, R., Douglas, I., and Ghosh, S. (1996). Role of unphosphorylated, newly synthesized I kappa B beta in persistent activation of NF-kappa B. Mol. Cell. Biol. *16*, 5444–5449.

Tay, S., Hughey, J.J., Lee, T.K., Lipniacki, T., Quake, S.R., and Covert, M.W. (2010). Single-cell NF-[kgr]B dynamics reveal digital activation and analogue information processing. Nature *466*, 267–271.

Tumang, J.R., Owyang, A., Andjelic, S., Jin, Z., Hardy, R.R., Liou, M.L., and Liou, H.C. (1998). c-Rel is essential for B lymphocyte survival and cell cycle progression. Eur. J. Immunol. *28*, 4299–4312.

Valovka, T., and Hottiger, M.O. (2011). p65 controls NF-κB activity by regulating cellular localization of IκBβ. Biochemical Journal *434*, 253–263.

Wang, Z., Zhang, B., Yang, L., Ding, J., and Ding, H.-F. (2008). Constitutive Production of NF-κB2 p52 Is Not Tumorigenic but Predisposes Mice to Inflammatory Autoimmune Disease by Repressing Bim Expression*. J Biol Chem *283*, 10698–10706.

Weih, D.S., Yilmaz, Z.B., and Weih, F. (2001). Essential role of RelB in germinal center and marginal zone formation and proper expression of homing chemokines. J. Immunol. *167*, 1909–1919.

Werner, S.L., Barken, D., and Hoffmann, A. (2005). Stimulus Specificity of Gene Expression Programs Determined by Temporal Control of IKK Activity. Science *309*, 1857–1861.

Werner, S.L., Kearns, J.D., Zadorozhnaya, V., Lynch, C., O'Dea, E., Boldin, M.P., Ma, A., Baltimore, D., and Hoffmann, A. (2008). Encoding NF-κB temporal control in response to TNF: distinct roles for the negative regulators IκBα and A20. Genes & Development *22*, 2093–2101.

Wertz, I.E., O'Rourke, K.M., Zhou, H., Eby, M., Aravind, L., Seshagiri, S., Wu, P., Wiesmann, C., Baker, R., Boone, D.L., Ma, A., Koonin, E.V., and Dixit, V.M. (2004). De-ubiquitination and ubiquitin ligase domains of A20 downregulate NF-kappaB signalling. Nature *430*, 694–699.

Whiteside, S.T., Epinat, J.C., Rice, N.R., and Israël, A. (1997). I kappa B epsilon, a novel member of the I kappa B family, controls RelA and cRel NF-kappa B activity. EMBO J. *16*, 1413–1426.

Xiao, G., and Fu, J. (2010). NF-?B and cancer: a paradigm of Yin-Yang. Am J Cancer Res *1*, 192–221.

Xiao, G., Harhaj, E.W., and Sun, S.C. (2001). NF-kappaB-inducing kinase regulates the processing of NF-kappaB2 p100. Mol. Cell *7*, 401–409.

Xiao, G., Fong, A., and Sun, S.-C. (2004). Induction of p100 Processing by NF-κB-inducing Kinase Involves Docking IκB Kinase α (IKKα) to p100 and IKKα-mediated Phosphorylation. J. Biol. Chem. *279*, 30099–30105.

Xiao, G., Rabson, A.B., Young, W., Qing, G., and Qu, Z. (2006). Alternative pathways of NF-kappaB activation: a double-edged sword in health and disease. Cytokine Growth Factor Rev. *17*, 281–293.

Yilmaz, Z.B., Weih, D.S., Sivakumar, V., and Weih, F. (2003). RelB is required for Peyer's patch development: differential regulation of p52-RelB by lymphotoxin and TNF. EMBO J. *22*, 121–130.

Zabel, U., and Baeuerle, P.A. (1990). Purified human I kappa B can rapidly dissociate the complex of the NF-kappa B transcription factor with its cognate DNA. Cell *61*, 255–265.

Zarnegar, B., He, J.Q., Oganesyan, G., Hoffmann, A., Baltimore, D., and Cheng, G. (2004). Unique CD40-mediated biological program in B cell activation requires both type 1 and type 2 NF-kappaB activation pathways. Proc. Natl. Acad. Sci. U.S.A. *101*, 8108–8113.